

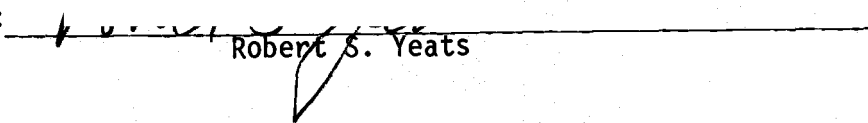
AN ABSTRACT OF THE THESIS OF

Sarah A. Barrow-Hurlbert for the degree of Master of Science in Geology  
presented on October 17, 1985.

Title: Geology and Neotectonics of the Upper Nevis Basin, South Island,  
New Zealand

Redacted for Privacy

Abstract approved:

  
Robert S. Yeats

The Upper Nevis Basin is a narrow, northeast-trending structurally controlled intermontane basin located along the Nevis-Cardrona Fault System in the Inland Range and Basin Terrain (Mutch, 1963) of Central Otago, South Island, New Zealand. The Inland Range and Basin Terrain lies in an east-west contractile regime where the ranges have been brought up along major reverse faults. Uplift in the region began in the Plio-Pleistocene and continued into the Holocene.

The Upper Nevis Basin is bounded on the northwest by a northwest-dipping reverse fault (Western Boundary Fault), along which schist is thrust over Tertiary sediments. The east side of the basin consists of an old erosional surface (Cretaceous peneplain) that has been downwarped towards the northwest by drag folding on the downthrown side of the Western Boundary Fault. The downwarping of the peneplain surface formed the basin.

A wedge of non-marine Tertiary sediments overlying the peneplain is unfaulted and preserved on the downthrown side of the Western Boundary

Fault. Quaternary sediments (fluvial gravels, alluvial fans, loess and floodplain deposits), deposited on top of the Tertiary sediments and schist have been folded and faulted during Quaternary tectonic deformation. In the middle of the basin there is an upthrown horst block (Linear Block) which is bounded on the southeast side by a northwest-dipping reverse fault (Nevis Fault) and on the northwest by a southeast-dipping reverse fault (Wrights Fault). The structural features of the Upper Nevis Basin can be explained by the basinward migration of thrust faulting (Ikeda, 1983) from a master boundary fault (Western Boundary Fault) to a frontal active fault (Nevis Fault). Between the frontal active fault and the master boundary fault, a tectonic bulge was formed and backtilted (the Linear Block). The tectonic bulge is bounded by a secondary antithetic fault (Wrights Fault) on the range side of the tectonic bulge. Complex faulting along the northern segment of the Nevis Fault may be due to restriction of basinward migration as the basin narrows to less than 0.5 km.

Field work, five trench excavations and a scarp morphology study of the active Nevis Fault and river-cut terrace scarps provide quantitative evidence of late Quaternary tectonic deformation. Progressive deformation of a sequence of faulted terraces along the Nevis Fault trace shows that the Nevis Fault may have moved five times in about 23,000 years, producing 1.0 m estimated dip-slip displacement with each movement. An average recurrence interval of 4,000-5,000 years is calculated, and the age of most recent movement is assessed to be 4,500 years based on scarp morphology.

GEOLOGY AND NEOTECTONICS  
OF THE  
UPPER NEVIS BASIN  
SOUTH ISLAND, NEW ZEALAND

by

Sarah A. Barrow-Hurlbert

A THESIS

submitted to

Oregon State University

in partial fulfillment of  
the requirements for the  
degree of

Master of Science

Completed October 17, 1985

Commencement June 1986

APPROVED:

Redacted for Privacy

Professor of Geology in charge of major

Redacted for Privacy

Head of department of Geology

Redacted for Privacy

Dean of Graduate School

Date thesis is presented October 17, 1985

Typed by Amerilis Foster for Sarah A. Barrow-Hurlbert

## ACKNOWLEDGMENTS

I would like to extend my sincerest thanks to Dr. Robert Yeats and the Earth Deformation Section of the New Zealand Geological Survey for giving me such a wonderful opportunity to travel to New Zealand and study the geology of the Upper Nevis Basin. I am very grateful to the Ministry of Works and Development for providing a 4-wheel-drive Land-rover and all the fuel necessary for transportation, a D-8 bulldozer for digging trenches, and office space in their headquarters in Cromwell. A very special thanks goes to Sarah Beanland for being such a great, perceptive field partner; for discussing many of the ideas held within this thesis with me; for helping me write and edit the text of this thesis; and for drafting many of the figures. I also want to thank Sarah for providing me with a horse to ride and a place to live in Cromwell. I greatly appreciate the help of Rod Anderson who surveyed and drafted the scarp profiles and drafted many of the figures. I want to thank Kelvin Berryman, Alan Hull and Les Basher for their help in doing a soil survey in the Lower and Upper Nevis Basins; and D.L. Homer for taking such great air photos. I deeply thank Bob and Sandy Brown for allowing us to live in their summer cottage in the Lower Nevis Basin and for giving us permission to dig trenches and map geology on their property. Finally, I would like to thank my husband, Dan Hurlbert, for being so supportive and loving through all of this. This project was funded by the Earthquake Hazards Reduction Program of the United States Geological Survey and by the New Zealand-United States Cooperative Scientific Exchange Program of the National Science Foundation.

## TABLE OF CONTENTS

	PAGE
1.0 BACKGROUND	1
1.1 Introduction	1
1.2 Objectives and Methods	5
1.3 Location, Access and Culture	6
1.4 Climate and Vegetation	7
1.5 Previous Work	7
2.0 REGIONAL TECTONIC AND GEOLOGIC SETTING	8
2.1 Regional Tectonic Setting	8
2.1.1 Plate Motions	8
2.1.2 Historical Seismicity	10
2.1.3 Tectonic Deformation in Central Otago	12
2.1.4 Nevis-Cardrona Fault System	14
2.2 Regional Geologic Setting	15
2.2.1 Rangitata Orogeny	15
2.2.2 Cretaceous Peneplain	16
2.2.3 Tertiary Sediments	16
2.2.4 Kaikoura Orogeny	16
3.0 GEOMORPHOLOGY	19
4.0 STRATIGRAPHY	24
4.1 Introduction	24
4.2 Haast Schist	24
4.3 Tertiary Sediments - Nevis Formation	24
4.3.1 Coal Measure Member	25
4.3.2 Oil Shale Member	27
4.4 Quaternary Deposits	29
4.4.1 Early Quaternary Weathered Gravels (Qwg1, Qwg2)	29
4.4.2 Late Quaternary Deposits	30
4.4.2.1 Alluvial Fan Surfaces (Qf1 to Qf5)	30
4.4.2.2 Alluvial Fan Deposits (Qf1 to Qf5)	33
4.4.2.3 Degraded Qf5 Surfaces	34
4.4.2.4 Loess Deposits	36
4.4.2.5 Floodplain Deposits (H)	36
4.5 Age of Late Quaternary Deposits and Landforms	37
4.5.1 Relative Ages	37
4.5.2 Soil Development	37
4.5.3 Morphologic Modification of River-cut Terrace Scarps with Time	38
4.5.4 Geologic Constraints	40
5.0 STRUCTURAL GEOLOGY AND NEOTECTONICS	43
5.1 Introduction	43
5.2 Western Boundary Fault	43
5.3 Topographic Depression (north)	45
5.4 Peneplain Surface	45
5.5 Linear Block	46
5.6 Wrights Fault	46

	PAGE
5.6.1 Fault Trace Location and Style of Deformation	46
5.6.2 Late Quaternary Tectonic Deformation	47
5.7 Nevis Fault	48
5.7.1 Northern Segment	48
5.7.1.1 Fault Trace Location and Style of Deformation	48
5.7.1.2 Late Quaternary Tectonic Deformation	51
5.7.2 Southern Segment	52
5.7.2.1 Fault Trace Location and Style of Deformation	52
5.7.2.2 Late Quaternary Tectonic Deformation	53
5.7.2.3 Fault Interaction with Geologic Units	57
5.7.2.4 Scarp Modification with Time	60
5.7.2.5 Displacement History	61
5.7.2.5.1 Evidence for Recurrent Movement	61
5.7.2.5.2 Recurrence Interval	65
5.7.2.5.3 Fault Activity	65
5.7.2.6 Maximum Credible Earthquake	65
5.8 Structural Evolution of the Basin	69
5.8.1 Model 1: Parallel, Northwest Dipping Reverse Faults	69
5.8.2 Model 2: Bending Moment Faults	71
5.8.3 Model 3: Thrust Front Migration	73
5.8.4 Model 4: Strike-slip Faulting	76
6.0 CENTRAL OTAGO MASTER FAULTS	77
6.1 Nevis-Cardrona Fault System	77
6.1.1 Style of Deformation	77
6.1.2 Fault Activity	79
6.2 Dunstan Fault	81
6.2.1 Style of Deformation	81
6.2.2 Fault Activity	82
6.3 Pisa Fault	83
6.3.1 Style of Deformation	83
6.3.2 Fault Activity	83
6.4 Comparison with the Upper Nevis Basin	84
7.0 SUMMARY AND CONCLUSIONS	85
8.0 REFERENCES CITED	89

## APPENDICES

	PAGE
APPENDIX A - TRENCHING INVESTIGATIONS	94
A-1.0 Introduction	94
A-2.0 Detailed Trench Descriptions	96
A-2.1.0 Trench Description: DC-5	96
A-2.1.1 Introduction	96
A-2.1.2 Stratigraphy	97
A-2.1.3 Structural Description	102
A-2.2.0 Trench Description: DC-6	103
A-2.2.1 Introduction	103
A-2.2.2 Stratigraphy	107
A-2.2.3 Structural Description	108
A-2.3.0 Trench Description: DC-7	109
A-2.3.1 Introduction	109
A-2.3.2 Stratigraphy	109
A-2.3.3 Structural Description	114
A-2.4.0 Trench Description: DC-8	116
A-2.4.1 Introduction	116
A-2.4.2 Stratigraphy	116
A-2.4.3 Structural Description	116
A-2.5.0 Trench Description: DC-9	119
A-2.5.1 Introduction	119
A-2.5.2 Stratigraphy	119
A-2.5.3 Structural Description	122
A-3.0 Conclusions from Trenching	122
Appendix B - SCARP MORPHOLOGY	124
B-1.0 Introduction	124
B-2.0 Fundamentals of Scarp Degradation	124
B-3.0 Degradation of Reverse Fault Scarps and River-cut Terrace Scarps	126
B-3.1 Reverse Fault Scarps	126
B-3.2 River-cut Terrace Scarps	129
B-4.0 Comparison of Upper Nevis Basin with Western United States	130
B-5.0 Scarp Morphometric Parameters	131
B-6.0 Method of Data Collection	134
B-7.0 $\theta$ versus Log H Model	141
B-7.1 Results from the Upper Nevis Basin	145
B-8.0 Diffusion Equation Model	147
B-8.1 Results from the Upper Nevis Basin	152
B-9.0 Conclusions	154
Appendix C - SOIL DEVELOPMENT	156
C-1.0 Introduction	156
C-2.0 Upper Nevis Soil Profiles	156



## LIST OF PLATES

### PLATE

### POCKET

- 1 Geologic Map, Upper Nevis Basin
- 2 Structural Features Map, Upper Nevis Basin

1  
1

## LIST OF FIGURES

FIGURE	PAGE
1 Location Map, Central Otago Region, South Island, New Zealand	2
2 Major Physiographic and Structural Features of the Central Otago Region	3
3 Location Diagram, Nevis-Cardrona Fault System	4
4 Tectonic Setting of New Zealand	9
5 Seismicity of New Zealand	11
6 Structural cross section through Cardrona, Cromwell-Tarras and Manuherikia Basins	13
7 Photo of downwarped peneplain surface, Upper Nevis Basin	21
8 Photo of Linear Block	21
9 Photo of Linear Block showing details	22
10 Photo of Hector Mountains showing Western Boundary Fault, Nevis Fault and topographic depression (north)	22
11 Stratigraphic column of Tertiary sediments	26
12 Oblique aerial photo of Nevis Fault zone and oil shale ridge, south of Whittens Creek	28
13 Vertical aerial photo of Nevis Fault zone and oil shale ridge, south of Whittens Creek	28
14 Photo of steeply dipping Qwg1 gravels	31
15 Geologic map, DC-5 area	35
16 Structural cross sections, Upper Nevis Basin	44
17 Oblique aerial photo of Nevis Fault Zone, south of Whittens Creek	49
18 Close-up photo of Tertiary sediments faulted over Qf4 gravels	49
19 Photo of schist thrust over Qwg1 gravels	50
20 Photo of late Quaternary fault scarp at DC-9 locality	54
21 Photo of fault splay on Nevis Fault, south of DC-8 locality	54
22 Photo of graben feature on Nevis Fault	55
23 Photo of Nevis Fault scarp, DC-9 locality	55
24 Photo of Nevis Fault scarp, DC-7 locality	56
25 Geologic map, DC-7 area	59
26 A sequence of faulting and degradational events on the Nevis Fault, DC-5 locality	62
27 Possible recurrence intervals for the Nevis Fault	66
28 Structural models of the Upper Nevis Basin	70
29 Diagram of Ikeda's (1983) model of thrust front migration	74
30 Schematic cross sections through basins along the Nevis-Cardrona Fault System	78
31 Trench log of DC-5	98
32 Photo of deformed schist and Tertiary sediments in DC-5	99
33 Photo of trench floor and southwest wall, DC-5	99
34 Photo of subtle fault zone in DC-5	100
35 Trench log of DC-6	104
36 Photo of southwest wall of DC-6 showing deformation	105
37 Bent sand layer and fault zone, DC-6	105
38 Close up photo of Tertiary sediments in DC-6	106
39 Trench log of DC-7	110

FIGURE	PAGE
40 Photo of southwest wall of DC-7	111
41 Close up photo of southwest wall of DC-7	112
42 Photo of northeast wall of DC-7	113
43 Photo of northeast wall of DC-7	113
44 Trench log of DC-8	117
45 Photo of northeast wall of DC-8	118
46 Photo of southwest wall of DC-8	118
47 Trench log of DC-9	120
48 Photo of northeast wall of DC-9	121
49 Photo of southwest wall of DC-9	121
50 Sequence of steps in scarp degradation	125
51 Initial configurations of a reverse faulting event	128
52 Scarp morphometric parameters	133
53 Representative fault scarp profiles, Upper Nevis Basin	135
54 Representative terrace scarp profiles, Upper Nevis Basin	136
55 Graph of $\theta$ versus $\log H$ from Machette (1982)	142
56 Graph of $\theta$ versus $\log H_s$ and $\log H_m$ for Upper Nevis Basin fault scarps	143
57 Graph of $\theta$ versus $\log H$ for Upper Nevis Basin terrace scarps	144
58 Scarp morphology progression of forms	149
59 Soil profiles, Upper Nevis Basin	157

## LIST OF TABLES

TABLE	PAGE
1 Estimated ages of faulted surfaces and their surface and subsurface vertical offsets	58
2 Quaternary fault activity in Central Otago	80
3 Summary of trench details	95
4 Scarp morphology data for single event fault scarps	137
5 Scarp morphology data for multiple event fault scarps	138
6 Scarp morphology data for river-cut terrace scarps	139
7 Regression equations of scarp-slope angle ( $\theta$ ) on the logarithm of scarp height (H)	140
8 Soil profile descriptions, Upper Nevis Basin	158
9 Soils of the Upper Clutha Valley from Leamy and Saunders (1967)	160

# GEOLOGY AND NEOTECTONICS OF THE UPPER NEVIS BASIN SOUTH ISLAND, NEW ZEALAND

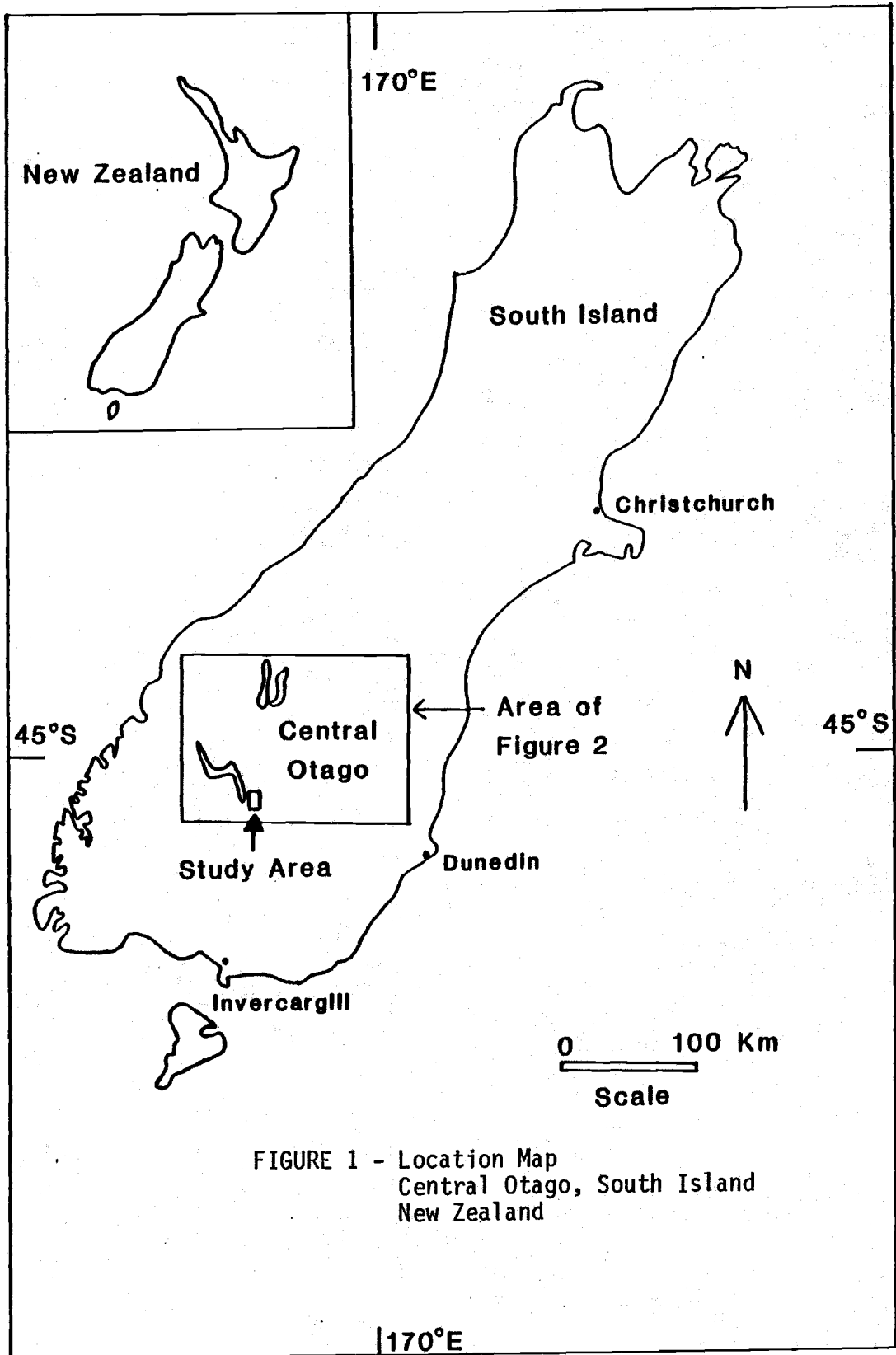
## 1.0 BACKGROUND

### 1.1 Introduction

Many papers have been published in recent years documenting the late Quaternary activity of faults throughout the world to evaluate seismic risk and to possibly predict future earthquakes. Allen (1975) pointed out that the record of historic and instrumental seismicity is not enough to predict future earthquake activity for a given region. One must examine the late Quaternary geological record to get a more representative account of activity over the past few thousand years.

Until recently, most of the work on late Quaternary faulting has concentrated on strike-slip and normal faults (Bonilla, 1979). This is probably due to the fact that such faults have good geomorphic expression and are easily recognized from LANDSAT imagery and aerial photographs as distinct linear features. In contrast, reverse faults have not been as intensively studied. This may be because they are not as easily recognized since their traces tend to be lobate rather than linear, and they are commonly obscured by landslides.

The Central Otago region of South Island, New Zealand (Figures 1 and 2) is an excellent area to study late Quaternary reverse faults. The region consists predominantly of northeast-trending ranges and basins which comprise part of the Inland Range and Basin Terrain of Mutch (1963). The region lies in an east-west contractile regime, and the faults bounding the ranges are reverse. The block-faulted Range and



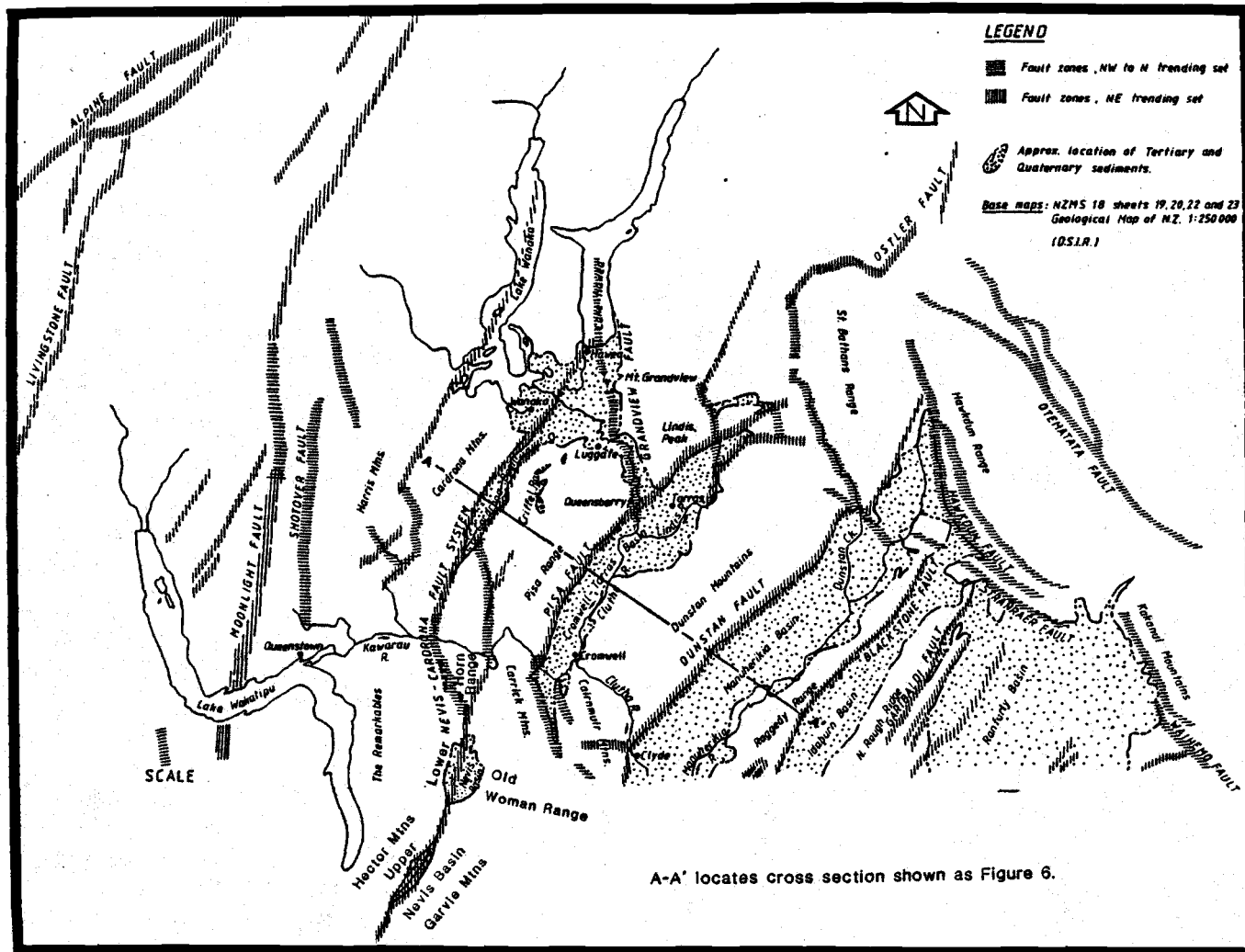
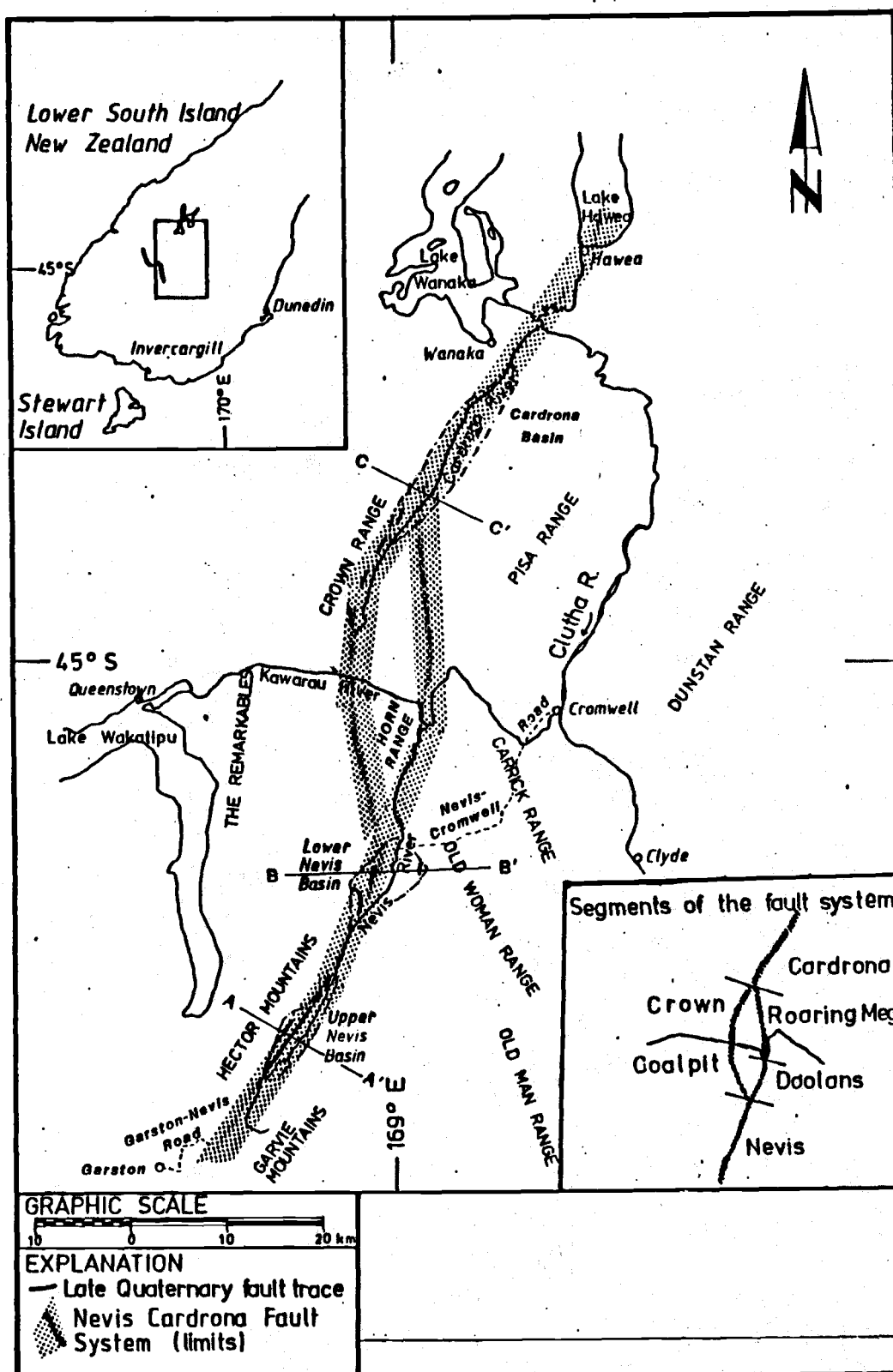


FIGURE 2 - Major physiographic and structural features of the Central Otago Region. Faults shown are known to be active or are potentially active. Figure is modified from Officers of the New Zealand Geological Survey, 1984, Fig. 4.



A-A', B-B', C-C' are cross sections shown in Figure 30.  
**FIGURE 3 - Location Diagram, Nevis-Cardrona Fault System, Central Otago.**



Basin topography began to develop in the Plio-Pleistocene, and deformation has continued into the Holocene (Officers of the New Zealand Geological Survey, 1983, 1984). In the last few years, an intensive study has been undertaken by the New Zealand Geological Survey and the Ministry of Works and Development to assess the late Quaternary activity of several of the range and basin boundary faults (Dunstan, Pisa, Nevis and Cardrona Faults; see Figure 2) to evaluate the seismic risk posed by these faults with respect to hydrodevelopment in the region.

The purpose of this study is to map the southern part of the Nevis Fault Segment (see inset on Figure 3) of the Nevis-Cardrona Fault System (Macfarlane, et al. 1982; Halliday, 1982) as a contribution to the seismotectonic hazard assessment currently underway for hydrodevelopment proposals on the Kawarau River. In particular, the study concentrates on the geology and late Quaternary tectonic deformation of the Upper Nevis Basin (Figures 2, 3 and Plate 1).

## 1.2 Objectives and Methods

The main objective of this project is to determine the geology and structural evolution of the Upper Nevis Basin, to study in detail the late Quaternary deformation, and to compare the style and rate of activity of the Nevis Segment of the Nevis-Cardrona Fault system to other major faults of the Central Otago region.

Field work was accomplished from October through December, 1983. A geologic map was produced (Plate 1) from field mapping and detailed aerial photograph interpretation. Scarps and lineaments presumed to be related to active structures were located. Trenches were excavated

across suspected active fault traces to gain information on the style of deformation, the age of the fault and/or the age of the rocks being faulted, the number of faulting events in the late Quaternary and the size of an individual displacement. Topographic profiles were drawn across fault scarps and river-cut terrace scarps to analyze the relative ages of scarps based on their degree of scarp degradation. A soil profile survey was undertaken to determine the relative ages of faulted surfaces based on their degree of soil development. A radiocarbon date obtained from a buried peat provides the only absolute age control in the Upper Nevis Basin. An average recurrence interval of faulting and maximum credible earthquake magnitude were calculated for the Nevis Fault.

### 1.3 Location, Access and Culture

The Upper Nevis Basin is located at latitude  $45^{\circ} 27' S$  and longitude  $168^{\circ} 50' E$  in the Central Otago region of South Island, New Zealand (see Figures 1, 2, 3 and Plate 1). It is the southern of two basins which occur along the Nevis River Valley.

The closest large town to the Upper Nevis Basin is Cromwell, 25 km to the northeast (Figures 2, 3). Access to the Upper Nevis Basin from Cromwell is along the Nevis-Cromwell Road. Access can also be gained from Garston, 15 km to the southwest, along the Garston-Nevis Road. Both of these routes require a four-wheel drive vehicle or a horse. There is a small airstrip at the northern end of the basin.

No one presently lives in the Upper Nevis Basin year round. There are a few abandoned shepherd and miner huts and several summer cottages

throughout the basin. The land is used for grazing sheep and cattle. The closest homestead is at Ben Nevis Station in the Lower Nevis Basin.

#### 1.4 Climate and Vegetation

The Central Otago region lies in the rain shadow of the Southern Alps of western New Zealand and therefore has a very dry climate. The average rainfall for the Central Otago region is 50 cm per year. The Upper Nevis Basin probably has a slightly higher average rainfall because it is located at a higher elevation. Vegetation is sparse in the Upper Nevis Basin and consists of tussock grasses, speargrass and sphagnum moss (the moss occurs only in marshy areas). A few willow trees were introduced by man.

#### 1.5 Previous Work

Gold was first discovered in the Nevis watershed in 1862. By 1865, 250 miners lived and worked the gold in the Upper and Lower Nevis Basins (Williams, 1974). Several papers were subsequently published which describe the rocks and structural deformation in the Lower Nevis Basin (McKay, 1897; Henderson, 1923; Willett, 1943; Williams, 1974) and in the basement schists along the Horn and Carrick Ranges (Turnbull, 1981). Prior to this investigation, there were no geologic maps or rock descriptions available for the Upper Nevis Basin except for the 1:250,000 regional geologic map of Wood (1962). Thomson (1983) described the nature and distribution of late Quaternary fault traces in the Upper Nevis Basin.

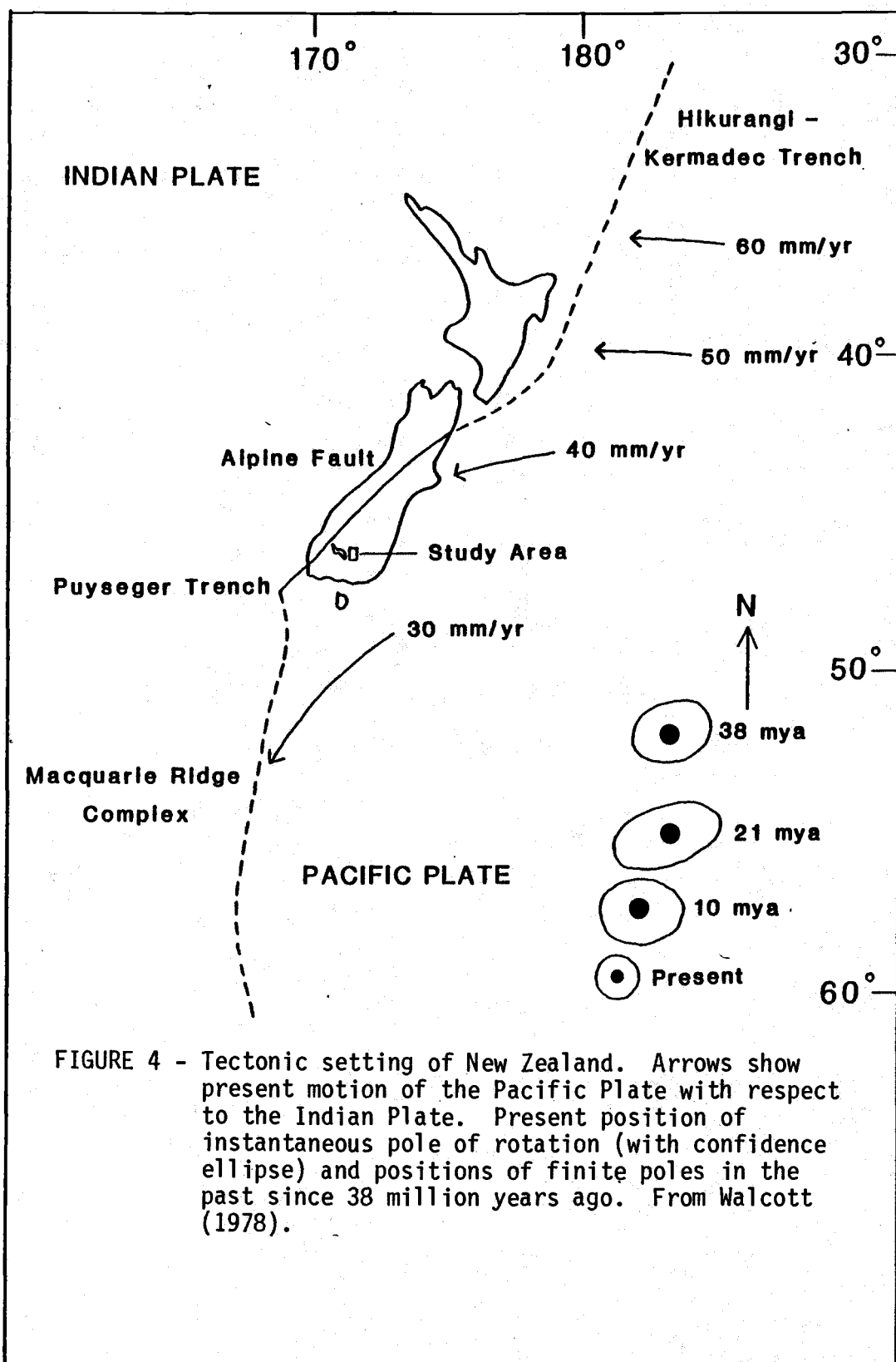
## 2.0 REGIONAL TECTONIC AND GEOLOGIC SETTING

### 2.1 Regional Tectonic Setting

#### 2.1.1 Plate Motions

The boundary between the Pacific Plate and the Indian Plate (located on Figure 4) crosses New Zealand along a northeast trending, 70-200 km wide zone of deformation (Walcott, 1978; 1984) that includes the Alpine Fault as the major crustal fracture. Northeast of New Zealand, the plate boundary is marked by the Hikurangi-Kermadec Trench system. To the southwest, the boundary becomes the Puysegur Trench and the Macquarie Ridge Complex. It continues southward to the present day triple junction with the Antarctic Plate at 60° S latitude and 165° E longitude. The history of movement along this plate boundary is important in understanding the geologic and structural development of New Zealand.

From studies of magnetic anomaly and bathymetric data, Molnar et al. (1975) and Weissel et al. (1977) reconstructed the history of plate motions in the South Pacific. Their histories differ with regard to the number of plates and their positions prior to 38 million years ago. From 38 my to the present, however, their histories are in good agreement. A brief summary of the major tectonic events occurring across the Indian-Pacific Plate boundary in the South Pacific since 38 my is as follows: 1) In the late Eocene (38 my ago), deformation across the plate boundary began in New Zealand. At that time, the finite pole of rotation between the Pacific and Indian Plates was very near the plate



boundary. Since then, it has been moving away from the region. 2) From late Eocene to early Miocene (38-21 my ago), an extensional transform boundary was formed across New Zealand by oblique separation (possibly oblique right lateral; Weissen, et al., 1977). 3) In the early Miocene (21 my ago), the sense of motion changed to oblique compression. Weissen et al. (1977) suggested that the motion was dominantly right lateral from 21 to 10 my ago. Since 10 my ago, late Miocene to the present, the motion has been obliquely compressional.

The present day plate motion is shown by arrows on Figure 4. To the east and north of New Zealand, the Pacific Plate is actively subducting beneath the Indian Plate along the Hikurangi-Kermadec Trench system (Adams and Ware, 1977). There is oblique convergence across the Alpine Fault which has uplifted the Southern Alps 5-10 km in the Cenozoic (Hurley, 1962; Adams, 1979). To the southwest, the Indian Plate is subducting beneath the Pacific Plate along the Puysegur Trench (Smith, 1971). There is right-lateral deformation and slow oblique spreading occurring along the Macquarie Ridge Complex to the south.

### 2.1.2 Historical Seismicity

Figure 5 is a map showing the location of crustal earthquake epicenters in New Zealand from 1956-1974. The seismicity is mainly concentrated in the southwest South Island and the southeast North Island but it is relatively diffuse across the country and is especially low across the Central Otago region. Both historic and instrumental records show that in the period from 1942-1982 the Central Otago region did not experience an earthquake greater than M5 (Officers of the New

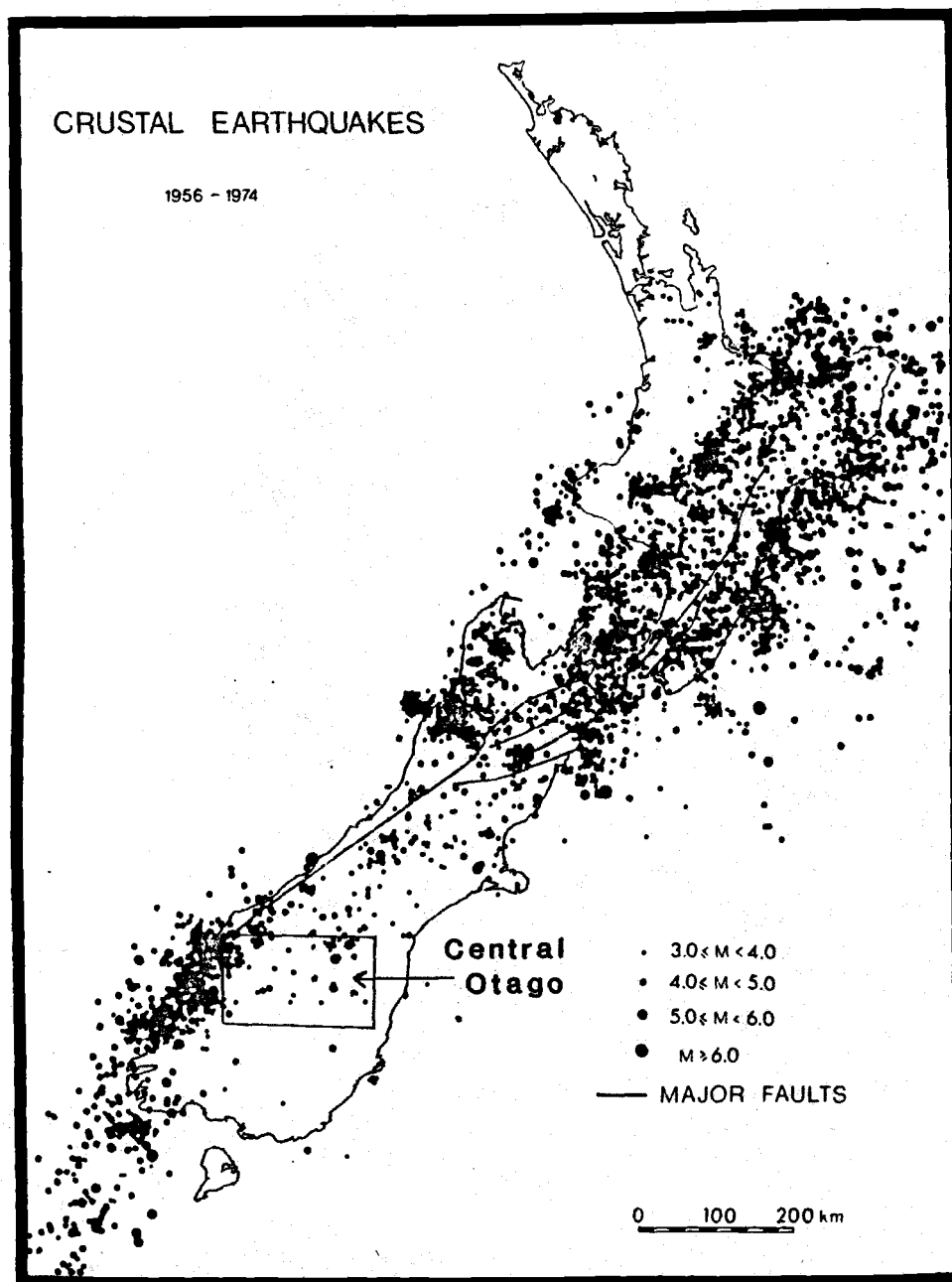


FIGURE 5 - Seismicity of New Zealand.  
Crustal earthquakes, 33 km in depth  
and less, for the period 1956-1974.  
Figure is from Walcott, 1978, Fig. 3.

Zealand Geological Survey, 1983; 1984). Although there is relatively low seismicity in this region, the Officers of the New Zealand Geological Survey (1983, 1984) have described two faults (Dunstan and Pisa Faults) in the Central Otago region that have undergone repeated deformation in the late Quaternary. This study describes part of a third suspected active fault system in Central Otago, the Nevis-Cardrona Fault System.

### 2.1.3 Tectonic Deformation in Central Otago

The Central Otago region is located southeast of the Alpine Fault (Figure 2). The region consists predominantly of northeast-trending ranges and basins. The northeast-trending ranges are composed of schist and are asymmetric with steep southeast facing slopes and gently dipping northwest facing slopes (Figure 6). The range fronts are bounded on the southeast by northwest-dipping reverse faults (ie. Pisa and Dunstan Faults) except in the Cardrona Basin and the Lower Nevis Basin where both the southeast and northwest sides of the valleys are bounded by outward dipping reverse faults. Drag folding associated with movement along these faults produced large antiforms in the schist on the upthrown side where the foliation in the schist is folded down from subhorizontal at the crest of the range to steeply southeast dipping and/or overturned adjacent to the fault. Tertiary fluvio-lacustrine sediments are preserved only on the downthrown side of the faults in the basins, where they are folded by drag into asymmetric synclines. Quaternary deposits are folded and faulted within 3 km of the master range-front faults, often forming uplifted horst blocks in



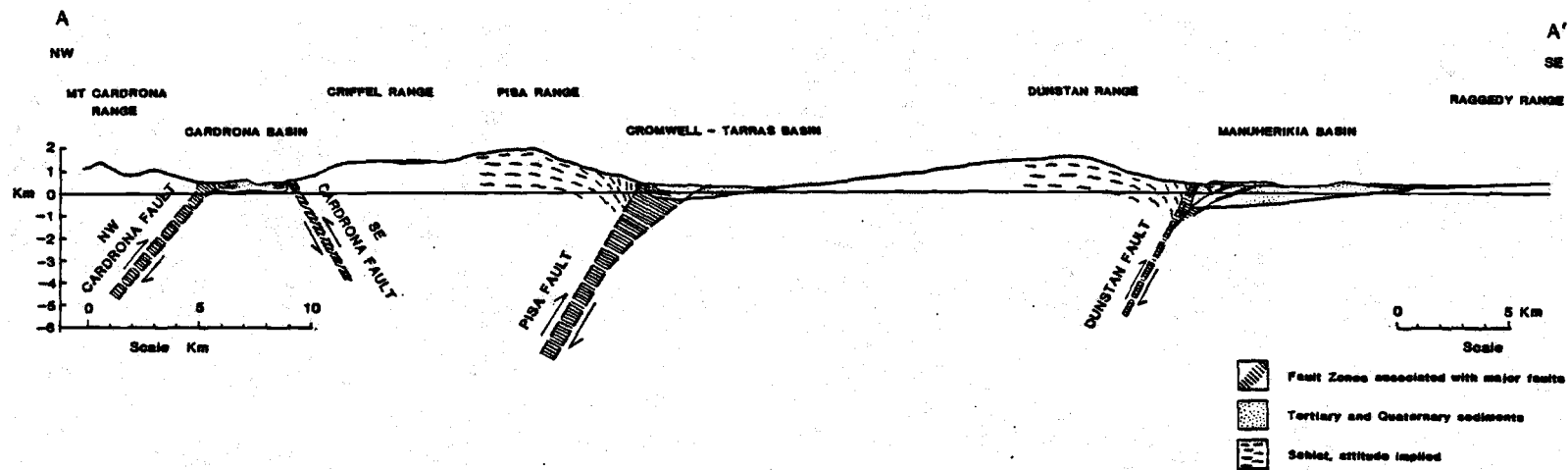


FIGURE 6 - Structural cross section through the Cardrona, Cromwell-Tarras and Manuherikia Basins, Central Otago. From Officers of the New Zealand Geological Survey, 1983; 1984. Cross section is located on Figure 2.

the basins. In southeast Central Otago, the ranges are low in elevation and the basins are broad (ie, Ranfurly Basin, Fig. 2). The ranges are increasingly higher and the basins narrower towards the northwest (ie, Cardrona Basin) which may indicate an increase in intensity of deformation closer to the Alpine Fault (Officers of the New Zealand Geological Survey, 1983; 1984).

The Central Otago region also contains a second system of north-to northwest-trending reverse faults. These faults are located mainly in northeast Central Otago (ie, Hawkdun Fault). The northwest-trending Hawkdun Range (Figure 2) is composed predominantly of greywacke.

The existence of northeast-trending and northwest-trending reverse faults may indicate conjugate faulting in an east-west contractile regime. This model would require a component of strike-slip faulting. Evidence for strike-slip faulting has only been documented at one locality in Central Otago, on the Blackmans Creek trace, Northwest Cardrona Fault (Beanland, 1984). This model is consistent with present day plate motions as shown by the 40 mm/yr arrow on Figure 4. An alternative model is that the northwest-trending reverse faults may be rejuvenated basement faults that are possibly of Rangitata (Jurassic to Cretaceous) or Miocene age (Officers of the New Zealand Geological Survey, 1984).

#### 2.1.4 Nevis-Cardrona Fault System

The Nevis-Cardrona Fault system (Figure 3) consists of two north-east-trending fault segments that step left in relation to each other and bifurcate across the region of stepover. South of the Kawarau

River, the Nevis Fault Segment diverges into the Coalpit and Doolans Segments (see inset on Figure 3). North of the Kawarau River, the Cardrona Fault Segment diverges into the Crown and Roaring Meg Segments. The system is characterized by three basins that contain in-faulted Tertiary sediments and Quaternary deposits that have undergone late Quaternary tectonic deformation. This study addresses the southern part of the Nevis Fault Segment located in the Upper Nevis Basin.

## 2.2 Regional Geologic Setting

### 2.2.1 Rangitata Orogeny

The basement rock of the Central Otago region is Haast Schist (Suggate, 1961, 1978; Wood, 1962). The schists are dominantly quartzofeldspathic and within the greenschist facies of metamorphism. Greenschist, metachert, and metavolcanic bodies occur locally (Wood, 1978; Turnbull, 1981). The schist is presumably derived from argillaceous sediment, siliceous sandstone, siliceous mudstone, greywacke and volcanics (Turnbull, 1981) that were originally deposited during the Carboniferous to Jurassic (Norris, et al., 1978; Norris and Carter, 1982). The sediments and volcanics were deformed and metamorphosed during several phases of metamorphism (Turnbull, 1981) occurring in the Rangitata Orogeny from the Jurassic to Cretaceous (Norris, et al., 1978; Wood, 1978; Norris and Carter, 1982). They have subsequently been faulted and folded into a gigantic oroclinal bend accompanying movement along the Alpine Fault.

### 2.2.2 Cretaceous Peneplain

During the late Cretaceous to Eocene, the schistose basement was raised to form part of the subaerial landmass of New Zealand. This basement uplift was subsequently eroded to a topographically subdued peneplain that was widespread across the Central Otago region. While marine transgression and regression occurred to the east and west of the tectonically stable landmass, the peneplain was intensely weathered to a depth of approximately 50 m.

### 2.2.3 Tertiary Sediments

In the early to middle Miocene (20-15 my ago: Williams, 1974; Officers of the New Zealand Geological Survey, 1983; 1984) non-marine fluvio-lacustrine sediments of the Manuherikia Group and Nevis Formation were deposited across the peneplain surface. These deposits consist of quartz-schist gravel, sandstone, siltstone, carbonaceous mudstone, oil shale and coal seams. Basal sediments of fluvial quartz conglomerate and sandstone are locally silica cemented and form resistant "sarsen stones" or "chinamen stones" on the ground surface. The occurrence of these stones indicates proximity to the original peneplain surface.

### 2.2.4 Kaikoura Orogeny

The Maori Bottom Formation and the Schoolhouse Fanglomerate are deposits which mark the beginning of the Kaikoura Orogeny. In the

Manuherikia and Cromwell-Tarras basins, the Pliocene to early Pleistocene Maori Bottom Formation (Officers of the New Zealand Geological Survey, 1983; 1984) is a highly weathered fluvial deposit composed of greywacke sand and gravel which conformably overlies the Manuherikia Group. The occurrence of this thick deposit of greywacke gravel indicates the beginning of tectonic deformation in the Central Otago region because it indicates that the greywacke ranges in the northeast of Central Otago (ie. Hawkdun Range, Figure 2) were being exposed by faulting. In the Lower Nevis Basin, Schoolhouse Fanglomerate of Plio-Pleistocene age (Williams, 1974) unconformably overlies the Nevis Formation. The fanglomerate is highly weathered and is composed of coarse schist and quartz gravels. This deposit indicates that the adjacent schist mountains were beginning to rise.

The compressional deformation that occurred throughout the Central Otago region during the Kaikoura Orogeny began in the north with initial deformation along northwest-trending reverse faults. The tectonic activity formed the greywacke ranges producing the source area for the Maori Bottom Formation. Later in the Plio-Pleistocene (Williams, 1974), uplift of the northeast-trending schist ranges began in the central and southern part of Central Otago producing the source area for schist fan gravels (ie. Schoolhouse Fanglomerate). Where the basement has been upfaulted, the Tertiary sediments have been stripped off, leaving an exhumed peneplain surface in the highlands of the region. Remnants of the Tertiary sequence are preserved in fault-angle depressions in the basins and as slivers along major faults.

In the Quaternary, thick sequences of fluvial and glacial sediments have been deposited unconformably on top of the schist and Ter-

tiary sediments. Thick sequences of glacial outwash have been deposited in the Clutha, Manuherikia and Kawarau River catchments (rivers are located on Figure 2). Major pulses of alluvial fan aggradation accompanying the glacial events occurred in subsidiary catchments (ie. Upper Nevis Basin). Late Quaternary tectonic deformation has both folded and faulted the schist, Tertiary sediments and Quaternary deposits. Periglacial processes and landslides have further modified the topography.

### 3.0 GEOMORPHOLOGY

From its headwaters, the Nevis River (Figure 3) flows northeast for 50 km between the Hector, Remarkable, and Horn Ranges to the west and the Garvie, Old Woman and Carrick Mountains to the east. It flows through the Upper Nevis Basin then passes through a gorge before it reaches the Lower Nevis Basin. From the Lower Nevis Basin, it passes through another steep gorge until it reaches its confluence with the Kawarau River between Queenstown and Cromwell.

The Upper Nevis Basin (Figure 3 and Plate 1) is a northeast-trending basin, 13 km long and 3 km wide, located at 850 m (2800 ft) elevation. It is widest near its midpoint and narrows to gorges at its northern and southern ends. The Hector Mountains in the west rise up to 2072 m (6797 ft) and the Garvie Mountains in the east rise up to 1867 m (6125 ft).

The Hector Mountains on the northwest side of the basin are rugged and rocky above 1524 m (5000 ft). Four well-developed nivation cirques are recognized on aerial photos and topographic maps. These scallop-shaped cirques occur between 1554-1676 m (5100-5500 ft) in altitude. Below this altitude, the mountains are rounded and slope gently into the basin. Where the Hector Mountains meet the basin, the intersection is broadly arcuate in plan view. This is because they are deeply dissected by six streams which have deposited coalescing alluvial fans where they enter the basin. The Nevis River has been forced to the southeast side of the valley because of alluvial fans building from the northwest.

East of the ridgecrest of the Garvie Mountains, there is a broad

plateau which extends for 30 km east to the Clutha River. This plateau is a dissected remnant of the Cretaceous peneplain surface (discussed in section 2.2.2 and 2.2.4). West of the ridgecrest of the Garvie Mountains, the peneplain is downwarped into the Upper Nevis Basin (see Figure 7). Where the base of the Garvie Mountains meets the basin, the intersection is a pronounced linear feature. Only one stream, Roaring Lion Creek cuts deeply into these mountains. It has deposited the only alluvial fan emanating from the Garvie Mountains (see Plate 1). The mountains on both sides of the basin are subject to landsliding. The hummocky topography characteristic of slumped terrain is evident on the photographs in Figures 7 and 10.

In the middle of the basin, trending in a northeast-southwest direction, there is a series of hills that are remnants of a dissected, elongate ridge (see photos in Figures 8, 9). The ridge is referred to as the Linear Block (Beanland and Barrow, 1984a). The hill remnants within the Linear Block are separated by coalescing alluvial fans and floodplains deposited by the streams flowing out of the Hector Mountains (see photo in Figure 9). The southeastern boundary of the Linear Block is sharply defined along the whole length of the basin by active traces of the Nevis Fault (Plates 1,2). The northwest boundary of the Linear Block is also distinct and linear and is the trace of the late Quaternary Wrights Fault (Figure 9).

Extensive gold workings (sluicing and dredging) carried out during the past 100 years have greatly modified some of the landforms in the Upper Nevis Basin. The floodplains of the Nevis River and its tributary streams are commonly covered with dredge tailings. Large rock exposures have been excavated throughout the basin. Small alluvial





FIGURE 7 - View looking southeast at the Garvie Mountains. The surface of the mountains sloping towards the Upper Nevis Basin is the exhumed Cretaceous peneplain surface that has been downwarped. Note slumped topography, and the Nevis Fault Zone in lower right corner. Photo by D.L. Homer, New Zealand Geological Survey (CN3447b).

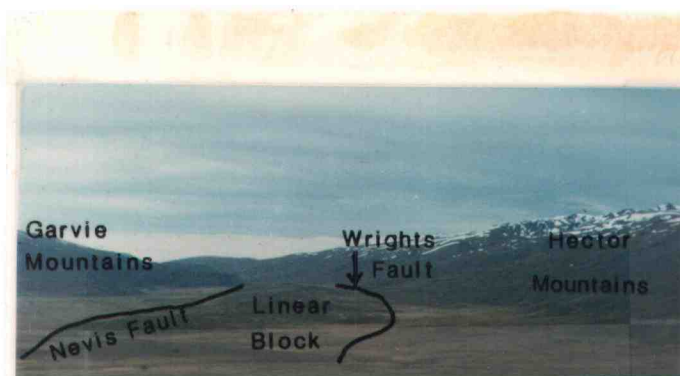


FIGURE 8 - View looking south at the Upper Nevis Basin. The Linear Block is the topographic ridge in the middle of the basin, bounded on the southeast by the Nevis Fault and the northwest by Wrights Fault. Photo by Kelvin Berryman, New Zealand Geological Survey.

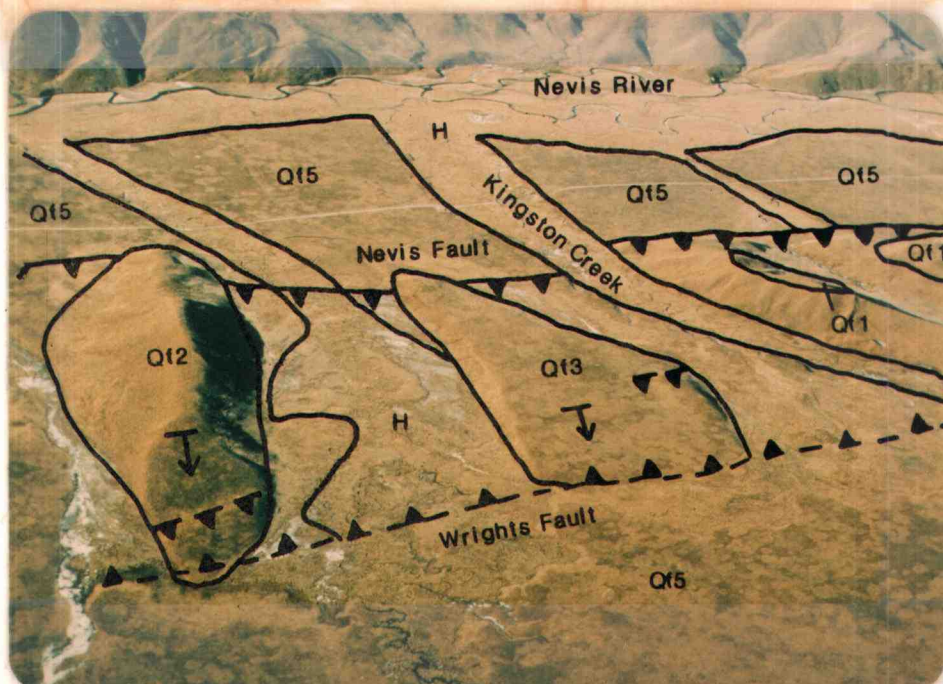


FIGURE 9 - Close up view of the Linear Block between Drummond Creek and Wrights Creek showing Qf1, Qf2, and Qf3 fan remnants (note backtilting of the surfaces towards the viewer), the extensive Qf5 alluvial piedmont (made up of several coalescing alluvial fans), the floodplain surfaces of tributary streams (labelled H), Nevis Fault, Wrights Fault, and the late Quaternary fault scarps crossing the Qf2 and Qf3 surfaces (possible splay faults off of Wrights Fault). View is to the south-east. Photo by D.L. Homer, New Zealand Geological Survey (CN3447a).

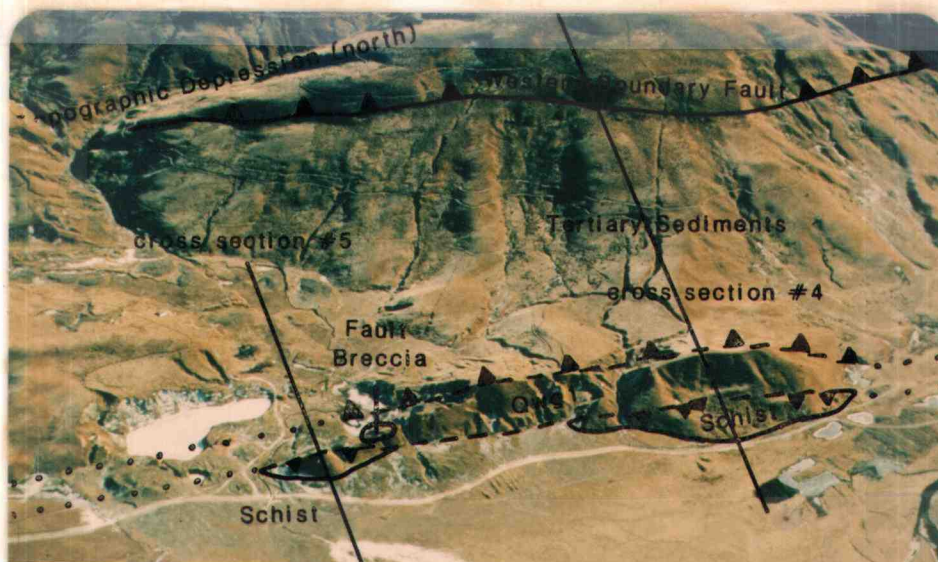


FIGURE 10 - View looking northwest at the Western Boundary Fault, north of Drummond Creek (note the resistant schist above a slumped terrain composed of Tertiary sediments), the northern topographic depression, and the complexly faulted northern segment of the Nevis Fault Zone. Cross sections are located in Figure 16. Photo by D.L. Homer, New Zealand Geological Survey (3445b).

fans which emanate from these man-made rock exposures have been built out onto the Nevis River floodplain and may well mask some natural geomorphologic features. Several water races (drainage ditches) built to bring water down from higher elevations scar the landscape on the lower slopes of the mountains and across the floor of the basin (see Figure 10).



## 4.0 STRATIGRAPHY

### 4.1 Introduction

The stratigraphic sequence of the Upper Nevis Basin is presented on the geologic map (Plate 1) and in the stratigraphic column (Figure 11). The stratigraphy consists of schist overlain unconformably by Tertiary non-marine sediments and Quaternary schist-derived gravels.

### 4.2 Haast Schist

The schist basement is the Otago Schist of the Haast Schist Group (Suggate, 1961; Wood, 1962; 1978). It comprises the high mountains surrounding the Upper Nevis Basin, and it is exposed on the basin floor north of Drummond Creek and in trenches DC-5 and DC-7 (see Plate 1).

The schist is dominantly quartzofeldspathic and composed of varying proportions of the mineral assemblage quartz-albite-muscovite-chlorite + epidote-actinolite-sphene-calcite-biotite-garnet-opaques (Turnbull, 1981). Most of the Otago Schists are within the chlorite zone of the greenschist facies (Turnbull, 1981). In the Upper Nevis Basin, the schists are strongly foliated with thick quartz laminae (Textural Zone IV of Bishop, 1972). Lower grade, finely laminated schist (Textural Zone III of Bishop, 1972) is present at the southern end of the basin but it is not differentiated on the geologic map (Plate 1). A brief history of the Haast Schist is presented in section 2.2.1.

### 4.3 Tertiary Sediments - Nevis Formation

The basement schist is unconformably overlain by strata correlated with the Tertiary Nevis Formation in the Lower Nevis Basin as described by Williams (1974). The correlation is based upon similar lithology. Throughout this paper the sediments comprising the Nevis Formation are informally referred to as "Tertiary Sediments".

#### 4.3.1 Coal Measure Member

The Coal Measure Member is the basal member of the Nevis Formation (Williams, 1974). In the Upper Nevis Basin, it is exposed throughout the Linear Block and on the west side of the basin at the north end (see Plate 1). The Coal Measure Member crops out poorly and is usually only exposed in landslide scarps or exposures excavated by gold sluicing. It is characteristically expressed as hummocky, slumped topography (see photo in Figure 10).

The Coal Measure Member in the Upper Nevis Basin comprises a sequence of interbedded clay, silt, sand, very coarse granular sand ("quartz grit"), schist-quartz gravel and lignite seams. It locally contains carbonized wood fragments and carbonaceous sediments. Figure 11 presents a composite section measured through 75 m of the Coal Measure Member at the north end of the basin where the sediments rest directly on weathered schist basement (Plate 1, Grid Reference (GR) 277 500 E, 338 300 N). The thickness of the Coal Measure Member is difficult to determine because it is extensively slumped and is commonly bounded by faults. The greatest thickness exposed is 75 m. In the adjacent Lower Nevis Basin, the Coal Measure Member attains a thickness of 107 m (Williams, 1974).

# Stratigraphic Column of Tertiary Sediments, Upper Nevis Basin

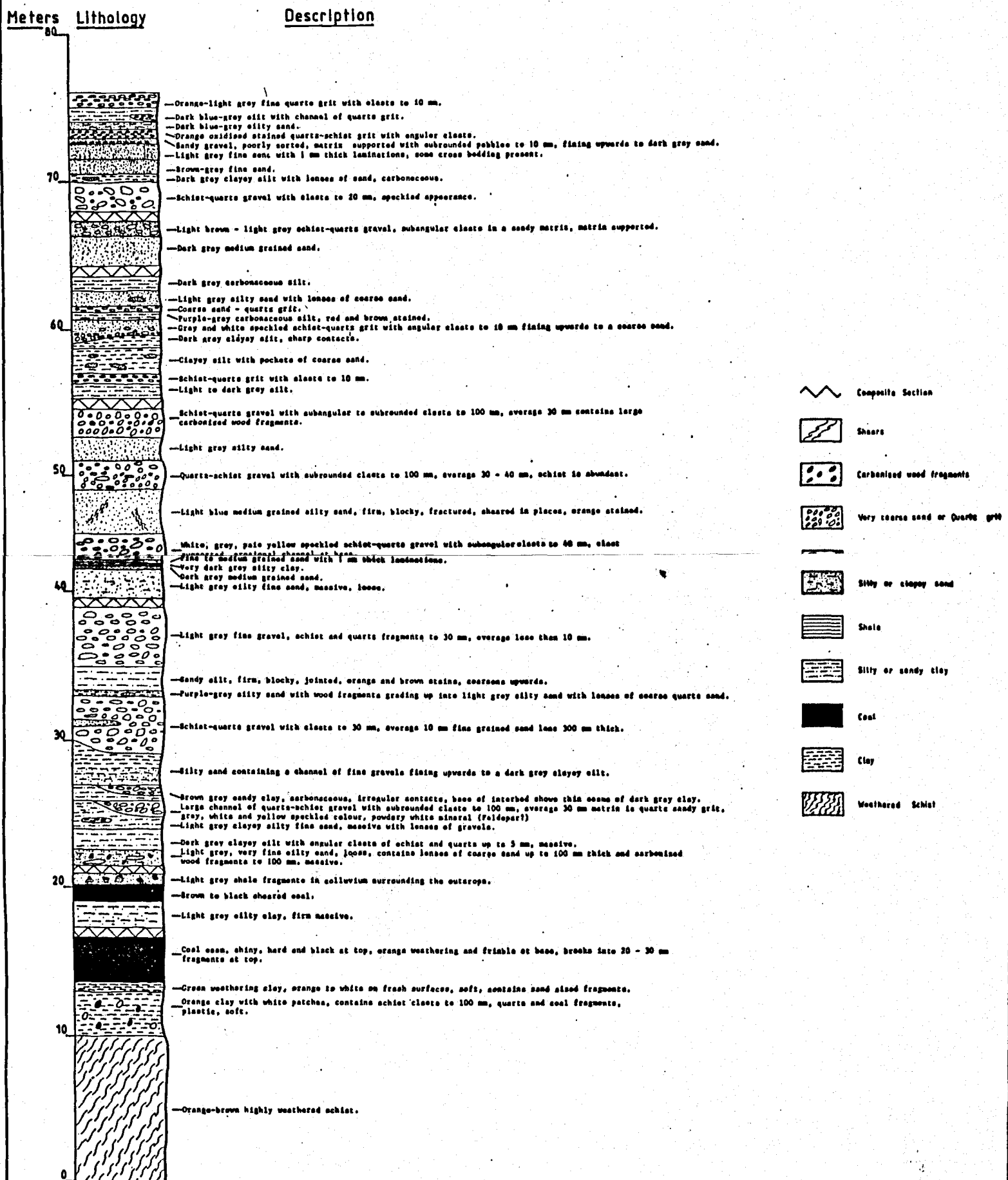


FIGURE 11

The Coal Measure Member is interpreted as a sequence of fluvial sediments that were deposited in the early Miocene (Williams, 1974) on the deeply weathered schist peneplain. The sequence consists of massive gravels (often channel bedded) that fine upward into sand and/or silt (with local lenses of gravel and sand). Carbonaceous silt and clay beds are interpreted as overbank deposits. The occurrence of carbonized wood fragments in the unit indicates a local forest environment, while the presence of lignite seams indicates that there were large freshwater swamps in which organic matter accumulated.

#### 4.3.2 Oil Shale Member

In the Lower Nevis Basin, the Oil Shale Member of the Nevis Formation conformably overlies the Coal Measure Member (Williams, 1974). In the Upper Nevis Basin, oil shale is rare and only occurs as structural slivers caught up in the Nevis Fault Zone (Plate 1). It does not crop out well and is mainly seen as float. The oil shale is best exposed as a ridge (10 m wide x 20 m high) south of Whittens Creek (see photos in Figures 12 and 13, Plate 1, GR 276 800 E, 337 200 N). It is also exposed at GR 275 000 E, 333 900 N on Plate 1.

The oil shale is highly fissile, cream-colored shale at the surface and dark grey a few cm below the surface. It is partially indurated. The shaly partings are generally thin (1 mm) but locally the partings thicken to 1-2 cm. A true thickness of the oil shale cannot be determined because it is bounded by faults. In the Lower Nevis Basin, the oil shale ranges in thickness from 15 m to 166 m (Williams, 1974). Williams (1974) determined that the lower horizons of oil shale



FIGURE 12 - Oblique aerial photo looking northwest at the Nevis Fault Zone south of Whittens Creek. Note the thin slivers of oil shale and schist faulted against the Qwg1 gravels and the late Quaternary fault scarp crossing the Qf4 surface in the upper right corner of the photo. Photo by Kelvin Berryman, New Zealand Geological Survey.

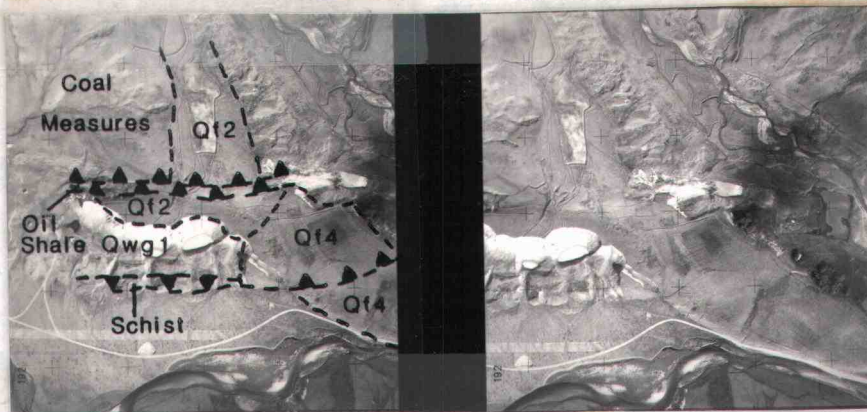


FIGURE 13 - Vertical aerial photos, in stereo, of the Nevis Fault Zone south of Whittens Creek. Note the thin slivers of oil shale and schist faulted against the Qwg1 gravels and the late Quaternary fault scarp crossing the Qf4 fan surface. Photos by D.L. Homer, New Zealand Geological Survey (GS 571-7,8) taken on November 8, 1983 at 0925 AM from an altitude of 5500 ft.



contain an average of 13.3 gallons of oil per ton.

The oil shale may have been deposited in a deep lake basin. Its relationship to the coal measures in the Upper Nevis Basin is uncertain as all observed contacts are faulted.

#### 4.4 Quaternary Deposits

In the Upper Nevis Basin, Quaternary deposits unconformably overlies schist and Tertiary sediments. These deposits include fluvial river gravels, alluvial fan gravels, reworked alluvium, loess, and flood-plain deposits.

##### 4.4.1 Early Quaternary Weathered Gravels (Qwg1 and Qwg2)

The oldest Quaternary deposit is highly weathered fluvial gravel. On the geologic map (Plate 1), the gravel is divided into two units, Qwg1 and Qwg2. Both units are similar in appearance, but due to slight differences in grain size, angularity, and in their mode of occurrence, they are mapped separately. They may be part of the same deposit. The weathered gravel which crops out north of Drummond Creek is designated Qwg1. The weathered gravel south of Drummond Creek is Qwg2.

Qwg1 has been extensively sluiced for gold and forms vertical cliffs where the gold miners have exposed it (Figure 14). It is dark orange-brown subrounded to subangular sandy schist gravel. It is coarsely bedded on a scale of several meters. Interbeds of sand and fine gravel form irregular and discontinuous horizons up to 0.5 m thick. The unit as a whole is firm and clast supported. It is com-

posed of poorly sorted schist and quartz clasts averaging 8 cm in size with a maximum of 20 cm. The matrix is composed of coarse sand with minor silt. The whole deposit is moderately to highly weathered such that the clasts are pervasively oxidized and discolored but are still hard. Exposures of Qwg1 gravels show a variety of attitudes ranging from horizontal to steeply dipping (Plate 2 and Figure 14).

Qwg2 is similar to Qwg1. The main differences are that Qwg2 is typically finer grained with an average clast size of 3 cm and a maximum of 10 cm and it tends to be more angular than Qwg1. Both Qwg1 and Qwg2 are interpreted to be fluvial gravels that were probably deposited by an ancestral Nevis River. The clasts, which consist wholly of schist and quartz indicate a local source in the schist mountains surrounding the basin. Qwg1 and Qwg2 unconformably overlies Tertiary sediments and/or schist and unconformably underlie younger late Quaternary alluvial fan and loess deposits. Since Qwg1 and Qwg2 are significantly more weathered than any of the younger Quaternary deposits, an early Quaternary age (probably early to middle Pleistocene; 2 - 0.5 my) is inferred for them.

#### 4.4.2 Late Quaternary Deposits

##### 4.4.2.1 Alluvial Fan Surfaces (Qf1 to Qf5)

In the Upper Nevis Basin, there are five sub-planar geomorphic surfaces that are labelled Qf1 to Qf5 on the geologic map (Plate 1). The surfaces are differentiated by their relative elevations and by differences in their degree of dissection.



FIGURE 14 - View to the south of northwest dipping Qwg1 gravels within the Nevis Fault Zone (Plate 1, G.R. 276 000 E, 336 500 N). Photo by Sarah Beanland, New Zealand Geological Survey.

Qf1 to Qf4 are the surfaces of several older alluvial fans that were deposited at the base of the Hector Mountains and are now found as isolated terrace remnants within the Linear Block (Plate 1, Figures 8, 9) and at the northwest end of the basin. These fans are presently cut off from their original source of alluvial material. The surface with the highest topographic position is Qf1. It forms an undulating, dissected surface at 880-945 m (2900-3100 ft) in altitude, which is 60-90 m (200-300 ft) above the Nevis River. Qf1 is only recognized south of Kingston Creek. The next highest surface, Qf2, is located at 820-850 m (2700-2800 ft) in altitude, which is 30-60 m (100-200 ft) above the Nevis River. Qf2 is less dissected and more planar than Qf1 and is only recognized north of Kingston Creek. Qf3 and Qf4 are quite planar, non-dissected surfaces that are only preserved locally and are limited in extent. They are of intermediate elevation between Qf1, Qf2 and the lowest surface Qf5. Qf3 and Qf4 are distinguished by their average elevation of 10-20 m and 6 m respectively above the extensive Qf5 surface.

Qf5 is the surface of an alluvial piedmont which dominates the floor of the basin south of Drummond Creek. The piedmont consists of several coalescing alluvial fans deposited by streams flowing out of the Hector Mountains. Qf5 is also the surface of a single alluvial fan associated with deposition from Roaring Lion Creek at the base of the Garvie Mountains. The Qf5 surface is generally 2-3 m above the Nevis River where the distal edges of the alluvial fans intersect the Nevis River floodplain. Although the Qf5 surface is incised from 0.5-7.5 m by the floodplains (labelled Holocene on the geologic map, Plate 1) of streams flowing out of the Hector and Garvie Mountains, the apices of the fans are still connected to their source areas.

Throughout this report, the terms Qf1 to Qf5 will refer to both the surface of the alluvial fan as well as the fan deposit itself (discussed in Section 4.4.2.2).

#### 4.4.2.2 Alluvial Fan Deposits (Qf1 to Qf5)

The fanglomerate deposits underlying the Qf1 to Qf5 surfaces are similar and will be discussed collectively. These deposits consist of dark brownish-grey massive sandy gravel that is unconsolidated, very poorly sorted, and poorly stratified. The gravel is clast supported with an average grain size of 5-10 cm and maximum clast size of 40 cm. The cobbles and boulders are subrounded and are composed of schist and minor quartz. The fine- to coarse-grained sandy matrix also contains variable amounts of silt and clay. Uncommon horizons of fine or coarse gravel with little or no matrix are present. The gravels tend to be imbricated with long axes plunging northwest indicating stream flow direction to the southeast. The gravels have undergone very little weathering and are quite fresh in appearance. In natural outcrop, the gravels are whitish grey due to a thin coating of dusty clay; but where the miners have sluiced the gravels out of the outcrop with water, they are dark grey and very fresh.

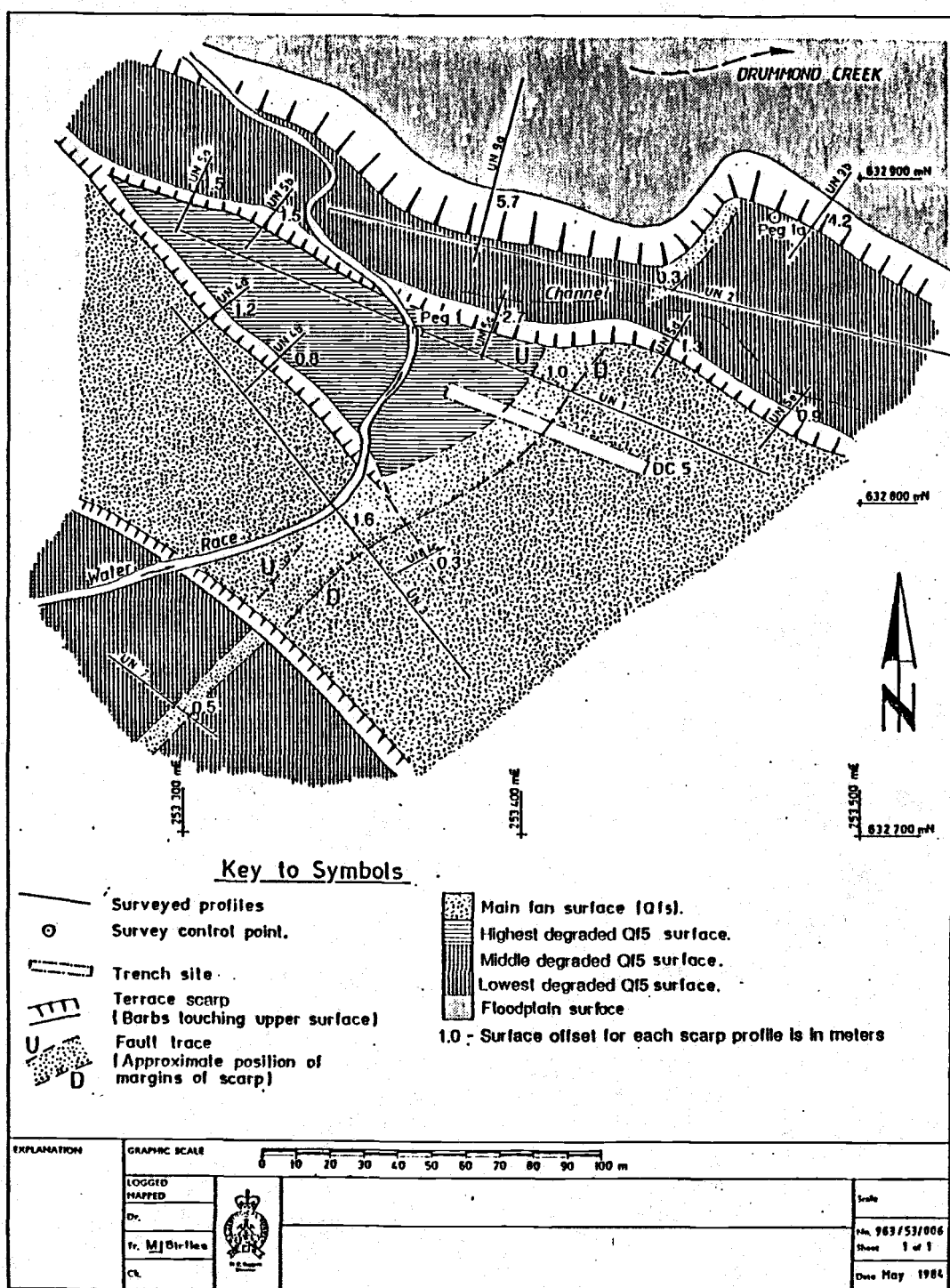
In the trenches (located on Plate 1 and described in detail in Appendix A) the upper 0.5 m below the ground surface consists of gravels that are commonly stained an orange to light brown color. This is probably a result of soil development. Thin (5 cm), discontinuous horizons of manganese oxide concentrations stain the gravels black. These manganese horizons normally occur from 2-5 m in the deposits.

The gravel deposits underlying the Qf1 to Qf5 surfaces represent episodes of alluvial fan aggradation that can tentatively be correlated with other major aggradational events that have occurred during maximum glacial advances throughout Central Otago. The estimated ages of these fans are discussed in Section 4.5.

#### 4.4.2.3 Degraded Qf5 Surfaces

Throughout the Upper Nevis Basin, the Qf5 surface has locally been incised 1-3 m and a series of degradational terraces have been preserved. They have been mapped on Plate 1 collectively as Degraded Qf5 surfaces. On the south bank of Drummond Creek, at the DC-5 trench site, several degradational terraces are well preserved. Figure 15 is a large-scale, geologic map of the DC-5 area where these terraces have been mapped separately as Highest, Middle and Lowest Degraded Qf5 surfaces according to their relative position below the Qf5 surface. The Highest Degraded Qf5 surface is 1 m below the Qf5 surface and is limited in extent. The Lowest Degraded Qf5 surface is 2.5 m below the Qf5 surface and 1.5 m below the Highest Degraded Qf5 Surface. The lowest surface is approximately 20-50 m wide and is located on the south bank of Drummond Creek, 4-5 m above the floodplain, almost continuously to the base of the Hector Mountains. The Middle Degraded Qf5 surface is presumed to be intermediate in elevation between the Highest and Lowest Degraded Qf5 surfaces (the distance was not measured).

The degradational surfaces are underlain by a veneer of reworked fanglomerate (up to 1 m thick). The age of formation of the degradational surfaces postdates the deposition of the Qf5 fan. The age is



discussed in more detail in Section 4.5 and in Appendix B.

#### 4.4.2.4 Loess Deposits

A fine silt to sandy silt, that varies in thickness from 15 cm to 1.0 m, drapes many surfaces in the basin. This deposit was not mapped. It is interpreted to be loess that was deposited during or immediately after the most recent glacial advance of Hawea age, 23-16,000 years (Officers of the New Zealand Geological Survey 1983,1984).

#### 4.4.2.5 Floodplain Deposits (H)

The floodplains of tributary streams are undulating, swampy surfaces. The surfaces are being actively eroded by meandering streams that are commonly incised 1.0 m below the floodplain level. The Nevis River floodplain is a broad, low-relief surface that loses 60 m in altitude from the south to the north end of the basin. This represents a gradient of approximately 5 m per km.

The floodplain sediments include sand and gravel deposited by tributary streams and the Nevis River. Freshwater swamps and bogs located in the floodplains are in the process of forming peat where the ground surface is saturated with standing water, and organic residues (ie. from sphagnum mosses) are able to accumulate. At the north end of the basin, on the north bank of Whittens Creek, a 45 cm thick peat is buried 2.35 m beneath gravels re-deposited from an overlying terrace (Plate 1, GR 276 700 E, 337 700 N). The buried peat is located 80 cm above the present floodplain of Whittens Creek. The peat has a radio-



carbon age of  $9670 \pm 130$  years (Sample # NZ 6543A) which suggests that there has been very little downcutting (less than 1 m) by Whittens Creek through the Holocene. The age of the modern floodplain surfaces are younger than the age of the buried peat and hence are less than  $9670 \pm 130$  years.

#### 4.5 Age of Late Quaternary Deposits and Landforms

##### 4.5.1 Relative Ages

Determining the absolute ages of the late Quaternary deposits is difficult because of a scarcity of datable material (ie. fossils, charcoal, tephra, etc.). A radiocarbon date of  $9670 \pm 130$  years was determined for the buried peat described in section 4.4.2.5. This is the only absolute age control in the whole Upper Nevis Basin. Several relative dating techniques were undertaken. First, the relative ages of the Qf1 to Qf5 fans were determined by their relative elevations with Qf1 being the highest and oldest deposit and Qf5 being the lowest and youngest. The degree of dissection of the surfaces is also a key to their relative age. The Qf1 surface is highly dissected and undulating whereas the Qf5 surface is only slightly dissected (ie. the degradational terraces, Section 4.4.2.3) and still retains all the characteristics of a recent alluvial piedmont. Qf2 to Qf4 are surfaces that are progressively younger than the Qf1 surface.

##### 4.5.2 Soil Development

Soil profiles were measured on all of the fan surfaces (Qf1 to Qf5) and Degraded Qf5 surfaces to develop a soil chronosequence for relative dating of the surfaces. The details of this study are presented in Appendix C, and only the results are discussed here. The soils on all the surfaces were found to be weakly developed and are probably Hawea to younger than Hawea in age (23,000 years or less), based on correlation with soils from the Upper Clutha Valley (Leamy and Saunders 1967). According to L. Basher (1984, pers. comm.), the soils may be less than 10,000 years old. The youthfulness of the soils on all the surfaces can be attributed to modification of the soil forming process by wind erosion and/or loess deposition during the last glacial period.

#### 4.5.3 Morphologic Modification of River-Cut Terrace Scarps with Time

Scarp morphology techniques that have been used to assess the age of fault scarps and wave-cut shoreline scarps in the western United States were applied to river-cut terrace scarps and fault scarps (see section 5.7.2.4) in the Upper Nevis Basin. The morphologic techniques are based on the theory that the geomorphic character of a scarp changes in a predictable way as the scarp is degraded with time, and that the degree of degradation can be quantified to determine the age of the scarp. A river-cut terrace scarp forms when a downcutting river carves its banks to a very steep angle (greater than the angle of repose of the material it is eroding) and when the river ultimately abandons its channel, it leaves a terrace scarp above the surface of its abandoned floodplain. The terrace scarp immediately begins to degrade by parallel retreat with basal accumulation and the shape of its profile will be

modified through time. The age that is assessed for the terrace scarp, based on its degree of degradation, yields the age of the surface at the base of the scarp. The details of a scarp morphology study carried out in the Upper Nevis Basin are presented in Appendix B and only the results are discussed here.

The age assessed for the Qf5 surface is based on the degree of degradation of terrace scarps that separate the Qf3 and Qf4 surfaces from the Qf5 surface. Two techniques were applied to the data. The graphical technique ( $\theta$  versus  $\log H$ ) yields an age of late Pleistocene and the analytical technique (diffusion equation) yields an age of 23,900-29,600 years. The late Pleistocene age agrees with geologic constraints (Section 4.5.4), and the age based on the diffusion equation is slightly older but agrees fairly well with ages assessed in Section 4.5.4.

The age assessed for the floodplain surface is based on the degree of degradation of terrace scarps that separate the Qf3, Qf4, Qf5 and Degraded Qf5 surfaces from the floodplain surfaces. The  $\theta$  versus  $\log H$  method yields an age of Holocene, and the diffusion equation method yields an age of 3100-3900 years. These ages agree well with the constraint that the ages be less than  $9670 \pm 130$  years based on the radio-carbon date obtained from a buried peat located above the floodplain of Whittens Creek (see Section 4.4.2.5).

The ages assessed for the Degraded Qf5 surfaces are based on the degree of degradation of terrace scarps that separate the Qf5 surface from the Degraded Qf5 surfaces. The  $\theta$  versus  $\log H$  method yields an age of Holocene for the Highest and Lowest degraded Qf5 surfaces. The diffusion equation technique yields an age of 2000-2100 years for the Highest Degraded Qf5 Surface and 3000-3600 years for the Lowest Degrad-

ed Qf5 surface. The Holocene age agrees well with geologic constraints (see Section 4.5.4), but the ages assessed using the diffusion equation method are younger than the ages assessed for the floodplain and are unrealistic.

The ages for the Qf5 and floodplain surfaces are accepted with reservation as they are derived by comparison with scarps formed in more arid climates in the western United States. However, the values assessed for the Qf5 and floodplain surfaces are consistent with geologic constraints on their ages (Section 4.4.2.5 and 4.5.4).

#### 4.5.4 Geologic Constraints

Alluvial fan aggradation in a basin can result from 1) tectonic uplift of adjacent ranges and/or 2) deposition of glacial outwash from alpine glaciers. In the Central Otago region, a combination of these two factors has resulted in alluvial fan buildout.

In the Clutha Valley (Figure 2) a series of alluvial fans and outwash terraces has been correlated with terminal moraines, and a glacial chronology has been established (Officers of the New Zealand Geological Survey, 1984). The maximum aggradation of outwash gravels and alluvial fans coincides with maximum ice advance when harsher conditions and reduced vegetation allow increased erosion, and higher precipitation provides water for transportation of the erosional debris. After the ice begins to retreat, and lakes form behind the terminal moraine loops, outwash surfaces are abandoned and incised. Alluvial fans may continue to aggrade for some time after maximum ice advance but will ultimately begin to degrade when the climate becomes less harsh, vegetation is

restored, precipitation decreases and there is less debris for the stream to transport.

The ages of the late Quaternary glacial events of the Clutha Valley have been estimated (Officers of the New Zealand Geological Survey,

1984) as follows:	Northburn	c. 500,000 years
	Lowburn	c. 250,000 years
	Lindis	c. 140,000 years
	Luggate	c. 70,000 years
	Albert Town	c. 50-35,000 years
	Mt. Iron	c. 23-18,000 years
	Hawea	c. 18-16,000 years

The outwash surfaces related to the Mt. Iron and Hawea advances merge 10 km downstream of their terminal moraines so that at greater distances and in subsidiary catchments, the Mt. Iron and Hawea advances may be represented by one composite deposit and surface (Mt Iron/Hawea c. 23,000-16,000 yrs). A recent radiocarbon date obtained for a buried soil located above a Hawea outwash surface in the Kawarau River area is dated at 20,500 years (S. Beanland 1984, pers. comm.). This would date the Hawea surface as somewhat older than the age proposed above, probably 22-23,000 years. An age of 23,000 years is adopted for the age of the Hawea glacial advance in this paper.

Although there are no glacial cirques, moraines, or other direct evidence of extensive glaciation in the Hector Mountains on the northwest side of the Upper Nevis Basin, there are glacial cirques below the highest peaks of the Garvie Mountains (on their east side, trending away from the Upper Nevis Basin) and in the Remarkable Mountains to the northwest. The Upper Nevis Basin probably experienced a harsh, periglacial climate during glacial advances. There is evidence of periglacial activity in the Upper Nevis Basin in the form of nivation cirques which do not form under ice but form under year-round snow pack condi-

tions (Bloom, 1978). Suggate (1978, Vol.2, p. 621) discussed how aggradation of alluvial fans in non-glaciated valleys with a periglacial climate is similar to and can be correlated with aggradation in glaciated valleys. He states...

"Periglaciation at higher altitudes provide(s) an abundance of waste that cause(s) rivers to aggrade in non-glaciated areas. Fans of solifluction debris, crudely bedded during short transport by water characterise the margins of broad valleys and commonly fill the narrower ones where successive periods of aggradation and erosion have resulted in sequences of terraces".

In the Upper Nevis Basin, five alluvial fans (Qf1 to Qf5) have been described (sections 4.4.2.1 and 4.4.2.2) and mapped on Plate 1. These fans cannot be traced to terminal moraines but the episodes of aggradation represented by each fan are tentatively correlated to the glacial chronology of the Clutha Valley. The youngest and most widespread fan surface is Qf5. Earlier phases of erosion have almost completely destroyed the pre-existing fan surfaces, leaving only remnants at higher elevations (Qf1 to Qf4). The Qf5 fan alluvium is a single unit (approximately 5 m thick) which overlies deformed Tertiary sediments and schist (as observed in the trenches, Appendix A). The Qf5 alluvium was apparently deposited over a planed-off erosional surface and since then, the Qf5 fan surface itself has been incised from 0.5-7.5 m. The freshness of the Qf5 gravels, and the youthfulness of the Qf5 alluvial piedmont suggests that Qf5 was deposited during a late stage of the most recent glacial advance (Hawea). The subsequent downcutting has left stranded, degradational terraces (Degraded Qf5 surfaces) and has deeply incised the surface which is typical of interglacial periods. The older fan remnants (Qf1 to Qf4) may represent successively older glacial events but it is likely that the record is largely incomplete.

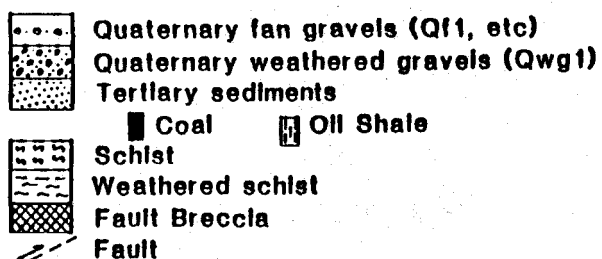
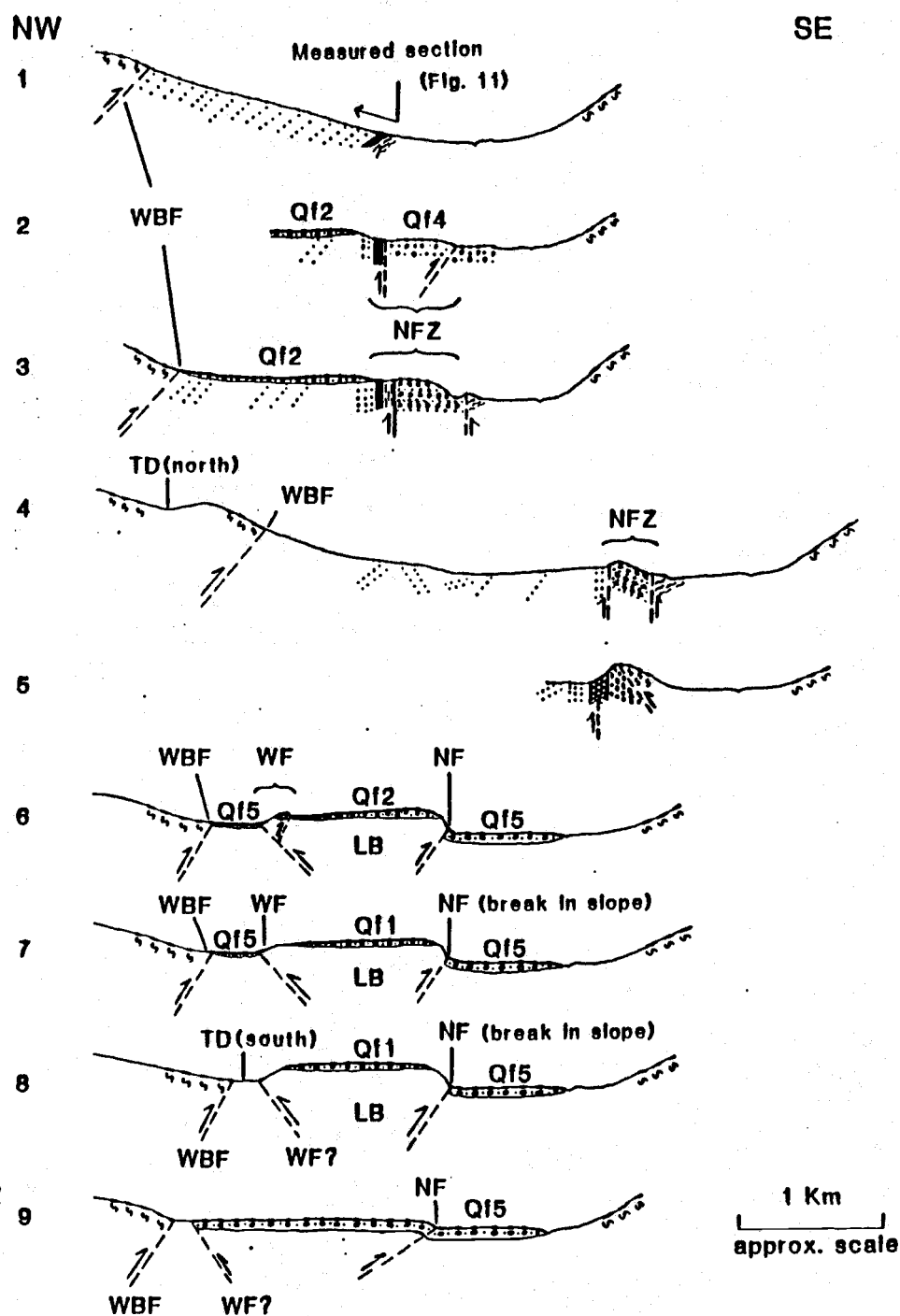
## 5.0 STRUCTURAL GEOLOGY AND NEOTECTONICS

### 5.1 Introduction

The structural geology of the Upper Nevis Basin is presented on the geologic map (Plate 1), the structural features map (Plate 2) and in the geologic cross sections in Figure 16. The cross sections are located on Plate 2. The structural geology of the Upper Nevis Basin comprises three northeast trending faults (Western Boundary Fault, Nevis Fault, Wrights Fault) and a mid-valley horst (the Linear Block). One kilometer to the west of the Western Boundary Fault at the north end of the basin is a distinct topographic depression (labelled Topographic Depression (north) which may be the trace of another fault. A feature which is of structural significance in the Upper Nevis Basin is the down-warped peneplain surface, located in the Garvie Mountains on the east side of the basin.

### 5.2 Western Boundary Fault

The Western Boundary Fault is located along the western margin of the basin. It is a northwest dipping reverse fault which thrusts the schist of the Hector Mountains over Tertiary sediments (Plates 1,2; Figures 10, 16 [all cross sections]). The photo in Figure 10 shows that the Western Boundary Fault is expressed geomorphologically by resistant schist above a slumped terrain that is underlain by Tertiary sediments. The fault trace is slightly lobate (convex towards the southeast) suggesting a fairly low angle westerly dip. The schist of



WBF - Western Boundary Fault  
 NFZ - Nevis Fault Zone  
 NF - Nevis Fault  
 WF - Wrights Fault  
 LB - Linear Block  
 TD - Topographic Depression  
 Cross sections located on Plate 2.

FIGURE 16 - Structural cross sections, Upper Nevis Basin.



the Hector Range has been deeply dissected by streams which have deposited a sequence of alluvial fans on the basin floor. The location of the fault trace is concealed by these fan deposits between Drummond Creek and the southern end of the basin and its precise location is difficult to ascertain. The Western Boundary Fault is the master fault in the Upper Nevis Basin and it extends to the south and north as the major fracture in the Nevis Fault segment of the Nevis-Cardrona Fault system.

### 5.3 Topographic Depression (north)

One kilometer northwest of the Western Boundary Fault at the north end of the basin is a linear topographic depression (labelled Topographic Depression (north) on Plates 1, 2; Figures 10, 16 [cross section 4]). This linear feature may be a fault trace as it is northeast trending and subparallel to the other faults in the Upper Nevis Basin. The exposure is very poor in this region, and no evidence for a fault is available. If the topographic depression represents erosion along a fault trace, the fault may be a northwest dipping reverse fault subparallel to the Western Boundary Fault or an antithetic reverse fault dipping southeast (see Section 5.8).

### 5.4 Peneplain Surface

In the Garvie Mountains on the east side of the basin, the exhumed Cretaceous peneplain surface (discussed in Section 2.2.2 and 2.2.4) is downwarped into the Upper Nevis Basin. Figure 7 shows this sub-planar

feature which is horizontal in the uplands of the Garvie Mountains and becomes moderately west dipping into the Upper Nevis Basin.

## 5.5 Linear Block

The Linear Block is a northeast trending mid-valley horst (Plates 1, 2; Figures 8, 9, 16, [cross sections 6, 7, 8]). It is bound on the southeast by the northwest dipping Nevis Fault and on the northwest by the southeast dipping Wrights Fault. The Linear Block is a late Quaternary feature that has been tilted towards the northwest by uplift along the Nevis Fault (Figure 9). The Linear Block is well defined between Drummond Creek and Wrights Creek. South of Wrights Creek, the southeast boundary is distinct, but the northwest boundary is obscure. The northwest boundary is marked by a topographic depression (labelled Topographic Depression (south) on Plates 1, 2 and Figure 16) between the hills of the Linear Block and the base of the Hector Mountains. It is not certain whether Wrights Fault extends along the entire length of the Linear Block. The Linear Block does not extend north of Drummond Creek.

## 5.6 Wrights Fault

### 5.6.1 Fault Trace Location and Style of Deformation

Wrights Fault defines the northwest boundary of the Linear Block (Plates 1, 2; Figures 8, 9, 16 [cross sections 6-9]). It is well defined between Drummond Creek and Wrights Creek where it truncates rem-

nants of Qf1, Qf2, Qf3, and Qf4 fans (Plate 1, Figure 9). South of Wrights Creek, there is a distinct topographic depression (labelled Topographic Depression [south]) between the schist of the Hector Mountains and the Linear Block (Figure 8). It is uncertain how far Wrights Fault extends to the south of Wrights Creek. It may extend to the southern end of the basin coincidental with or closely adjacent to the Western Boundary Fault.

A fault breccia consisting of highly sheared schist is present where Wrights Fault intersects Kingston Creek. Although trenches could not be excavated across Wrights Fault because of swampy ground conditions, Wrights Fault is presumed to be a southeast dipping reverse fault because the topography suggests that the sense of motion is up on the southeast side.

#### 5.6.2 Late Quaternary Tectonic Deformation

The truncation of late Quaternary fan deposits (Qf1 to Qf4) by Wrights Fault provides evidence for late Quaternary tectonic deformation. There is a linear break in slope crossing Qf2 and Qf3 surfaces between Drummond Creek and Kingston Creek (Figures 9, 16 [cross section 6]) that may be a late Quaternary fault scarp. This possible fault uplifts the west side of the Qf2 surface relative to the east side. Therefore, this possible fault may be an antithetic splay off of Wrights Fault forming a small uplifted horst between the splay fault and Wrights Fault. Wrights Fault does not appear to have moved since the Qf5 fans were deposited as there are no fault scarps observed crossing the Qf5 surface. Wrights Fault has probably been less active than

the Nevis Fault in the late Quaternary since total uplift is less and the Qf5 surface is not offset.

## 5.7 Nevis Fault

The Nevis Fault extends for 13 km along the axis of the basin (Plates 1,2; Figure 16 [Cross Sections 2-9]). It is divided for convenience into two segments. The northern segment extends from Whittens Creek to Drummond Creek. The southern segment extends from Drummond Creek to the southern end of the basin.

### 5.7.1 Northern Segment

#### 5.7.1.1 Fault Trace Location and Style of Deformation

The northern segment of the Nevis Fault is a complex fault zone. There are two sub-parallel reverse faults in the Nevis Fault zone. A graben containing deformed Qwg1 gravels is bounded by one fault on the northwest side of the zone and one on the southeast side (Plates 1,2; Figures 10, 12, 13, 16 [Cross Sections 2, 3, 4, 5], 17). The Qwg1 gravels within the fault zone exhibit highly variable attitudes along strike, suggesting that there may be minor faults cutting across and deforming the gravels.

The fault on the northwest side of the Nevis Fault zone is vertical to steeply northwest dipping and displaces Tertiary sediments over Qf4 fan gravels and Qwg1 gravels in a reverse sense. Cross section 2 (Figure 16) and the photos in Figures 13, 17, and 18 show that the



FIGURE 17 - Oblique aerial photo looking southeast at the Nevis Fault Zone south of Whittens Creek. Tertiary sediments, overlain by Qf2 fan gravels, are faulted over Qf4 gravels on the north side of the fault zone and Qwg1 gravels on the south side of the fault zone along a vertical to steeply northwest dipping fault. A late Quaternary fault scarp crosses the Qf4 fan surface on the left side of the photo. Photo by Kelvin Berryman, New Zealand Geological Survey.



FIGURE 18 - View looking south at Tertiary coal measures faulted over Qf4 fan gravels along a nearly vertical to steeply northwest-dipping reverse fault (northwestern fault in the Nevis Fault Zone).





FIGURE 19 - Schist faulted over Qwg1 gravels along a high angle south-east dipping reverse fault (southeastern fault in the Nevis Fault Zone). Fault is shown in cross section 5, Figure 16.

Tertiary sediments are faulted over Qf4 fan gravels. Cross section 3 (Figure 16) and the photos in Figures 12 and 13 show that a seam of lignite from the Coal Measure Member and a thin sliver of the Oil Shale Member are juxtaposed along a vertical contact. This suggests either internal faulting within the Tertiary sediments or steep drag folding associated with the thrusting of Tertiary sediments over Quaternary gravels. In several localities along the northwestern fault of the Nevis Fault zone, there are large pods of sheared schist (up to 4m across) and fault breccia. Figure 10 and Cross Section 5 (Figure 16) show the location of coarse fault breccia containing large (up to 1m), angular blocks of unweathered schist in a crushed schist matrix. This indicates that the northwestern fault of the Nevis Fault zone disrupts the schist basement as well as the Tertiary sediments.

The fault on the southeast side of the Nevis Fault zone is well exposed in the locality where Cross Section 5 is drawn. Figure 19 shows this high angle east-dipping fault which displaces schist over Qwg1 gravels in a reverse sense. North of the cross section 6 locality, the schist crops out sporadically. The dip of the fault is less certain but is presumed to be nearly vertical. The attitude of the schist is variable along strike.

#### 5.7.1.2 Late Quaternary Tectonic Deformation

From 0-1 km south of Whittens Creek, a Qf4 fan obscures the Qwg1 gravels and schist (Plate 1). The Qf4 fan is cut by a late Quaternary fault scarp (Figures 16 [Cross Section 2], 17). Movement on the fault was up on the northwest side of a northwest-dipping reverse fault.

Although this fault trace is coincidental with the trace of the southeastern fault of the Nevis Fault zone, they cannot be the same fault because the faults dip in opposite directions. The west-dipping late Quaternary fault across the Qf4 surface is possibly a right en-echelon step of the northwest-dipping fault that defines the northwest side of the Nevis Fault zone.

North of Whittens Creek, there is no evidence for the Nevis Fault. Cross section 1 (location of measured section Fig. 11) which is located north of Whittens Creek shows Tertiary sediments deposited directly on the weathered schist basement. The Nevis Fault either dies out or merges with the through-going Western Boundary Fault north of Whittens Creek.

### 5.7.2 Southern Segment

#### 5.7.2.1 Fault Trace Location and Style of Deformation

The southern segment of the Nevis Fault defines the southeastern boundary of the Linear Block (Plates 1,2; Figures 8, 9, 16). The fault trace truncates Qf1 and Qf2 fans and occurs as a discontinuous late Quaternary fault scarp crossing Qf3, Qf4, Qf5 surfaces, degraded Qf5 surfaces, and the floodplain of Wrights Creek. The fault trace becomes obscure where it crosses the southeast spurs of the higher hills in the Linear Block. Breaks in slope and other irregularities in the landscape of these hills suggest that the deformation is continuous across them.

Trenching investigations along this segment of the Nevis Fault



(trench sites are located on Plate 1) reveal a low angle ( $25^{\circ}$ - $35^{\circ}$ ) northwest-dipping reverse fault where Tertiary sediments and/or weathered schist are displaced over late Quaternary fan gravels. Details of the trenching investigations, including trench logs and photos, are presented in Appendix A.

The Nevis Fault trace is slightly lobate in plan view and is convex towards the southeast (Plates 1,2; Figure 20). In places, the fault trace sidesteps up to 100m across intervening floodplains and the southeast spurs of the hills in the Linear Block. On the average, the fault trends  $035^{\circ}$ . Five hundred meters southwest of the DC-8 trench site and southeast of the main Nevis Fault, a 200 m long fault splay displaces a Qf3 fan (Plates 1,2; Figure 21). The splay strikes  $065^{\circ}$  whereas the main Nevis Fault trend is  $025^{\circ}$ . One kilometer north of DC-8 is a graben-like feature (Plates 1,2; Figure 22) formed between the main trace of the Nevis Fault (an east-facing scarp separating Qwg2 and Qf4 gravels) and a west-facing scarp (located within the Qf4 gravels) that is located 50 m to the southeast of the main trace of the Nevis Fault. The origin of the west-facing scarp is unknown but may be a fault which bounds a graben between Qwg2 and Qf4. This possible graben has been enhanced by erosion.

#### 5.7.2.2 Late Quaternary Tectonic Deformation

Fault scarps formed during late Quaternary activity on the Nevis Fault are distinct to subtle, southeast-facing scarps along which the northwest side has been raised. Figures 23 and 24 show scarps that are broad, rounded features. They range in height from 0.3 m to 15.6 m.

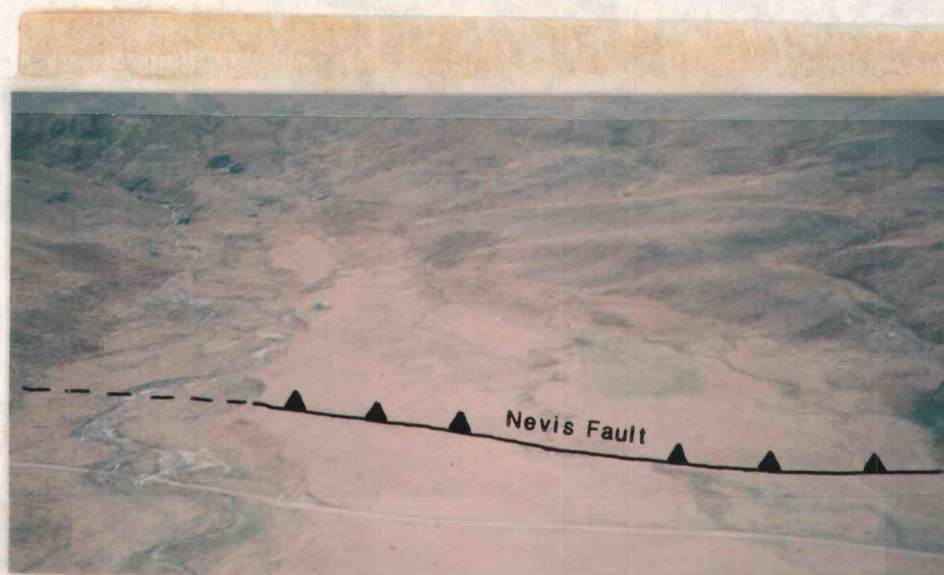


FIGURE 20 - Oblique aerial photo looking west at the Nevis Fault crossing the Qf5 fan surface as a late Quaternary fault scarp in the DC-9 locality. The fault scarp is a lightly shaded break in slope in the center of the picture (approximately 1 cm above the road in photo). The fault trace is slightly lobate (convex towards the basin). Note the meandering intrafan streams crossing the fault scarp.

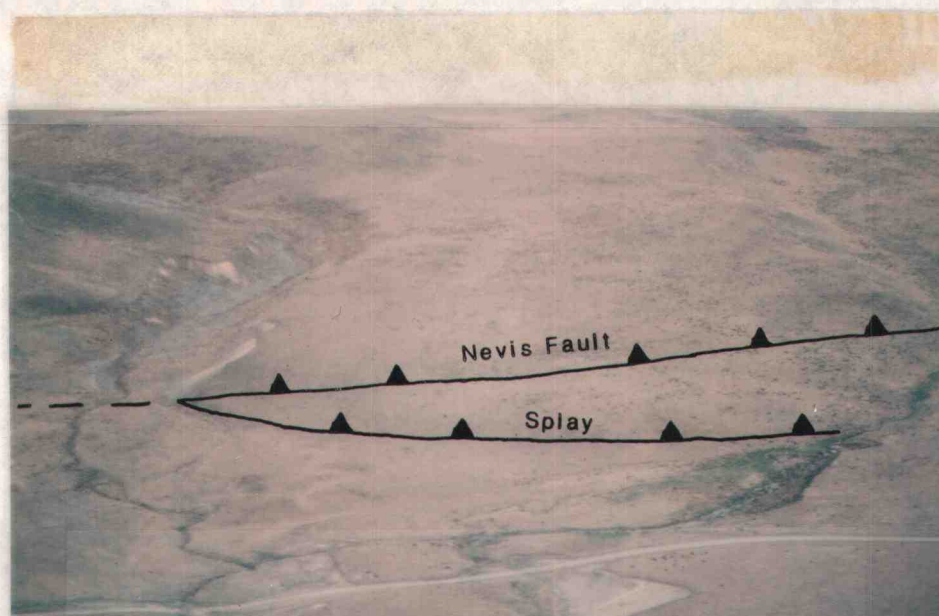


FIGURE 21 - View looking west at the Nevis Fault splaying across a Qf3 fan remnant, south of the DC-8 trench site.



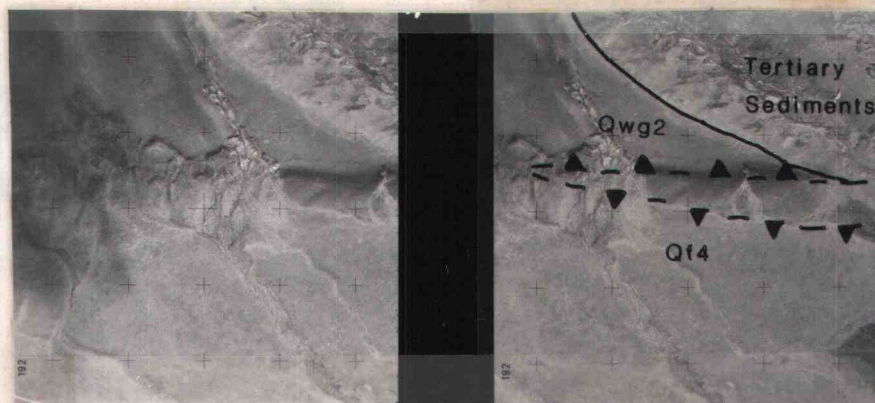


FIGURE 22 - Vertical aerial photos, in stereo, of graben-like feature (located 1 km north of DC-8) formed along the Nevis Fault between Qwg2 gravels and Qf4 fan gravels. Photos by D.L. Homer, New Zealand Geological Survey (GS 559-10,11) taken on November 7, 1983 at 1710 PM, from an altitude of 7000 ft.

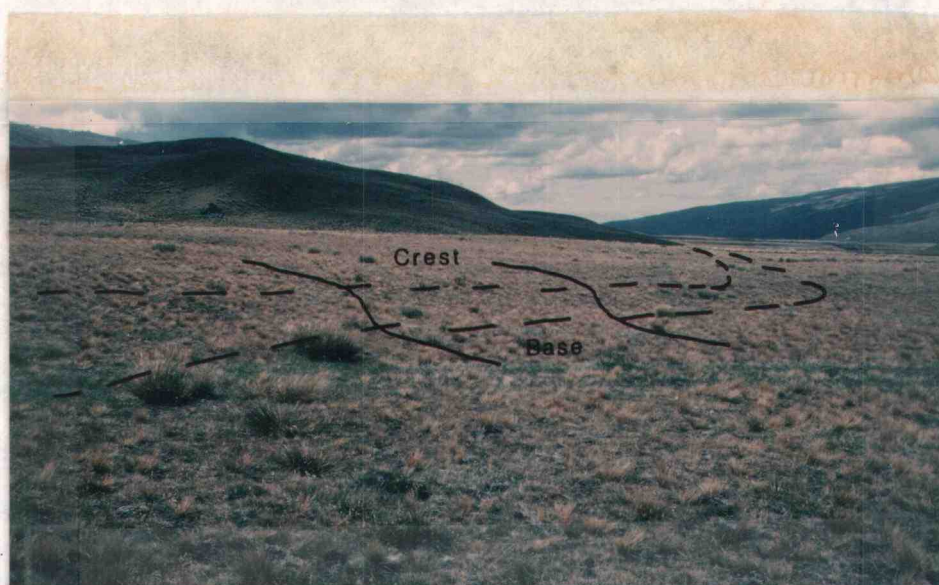


FIGURE 23 - View looking north at the Nevis Fault offsetting the Qf5 surface in the DC-9 locality. Note the broad, rounded, subtle nature of the fault scarp.



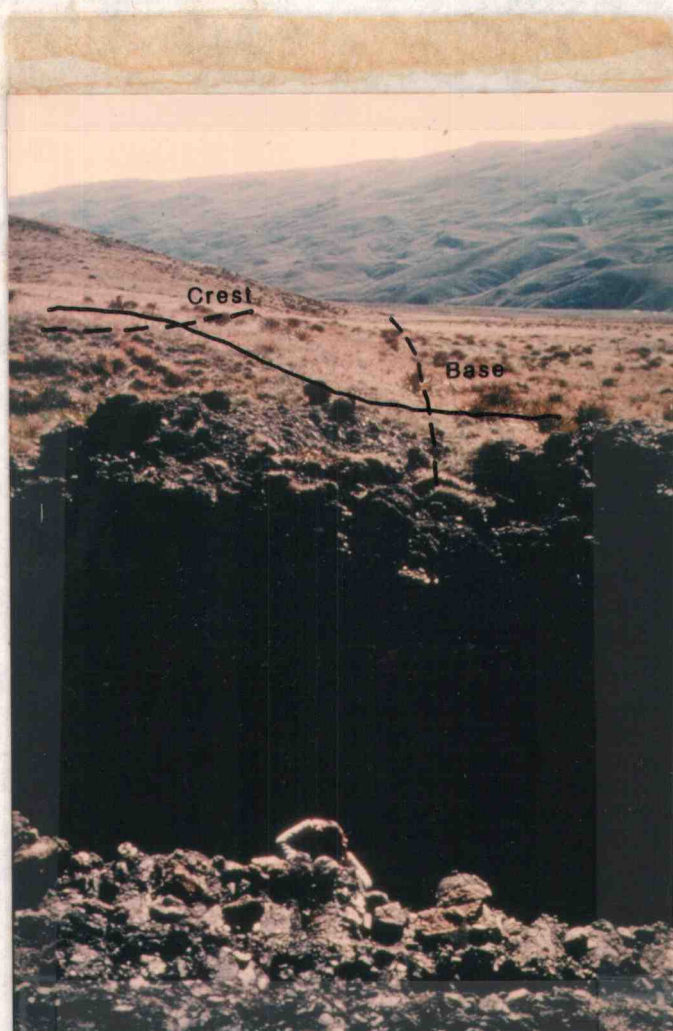


FIGURE 24 - View looking north at the Nevis Fault offsetting the Qf5 surface on the north side of the DC-7 trench. Photo by Sarah Beauland, New Zealand Geological Survey.

The scarps are degraded and are commonly dissected by small intrafan streams (Figure 20). A detailed study of the morphology of these fault scarps is presented in Appendix B. Figure 53 contains representative topographic profiles which show the morphology of these degraded fault scarps. The scarps are rounded at the crest and toe with a steep segment in the middle of the scarp which may represent the most recent faulting event (see Appendix B).

#### 5.7.2.3 Fault Interaction with Geologic Units

As discussed above and shown on Plate 1, the Nevis Fault truncates Qf1 and Qf2 fans. It offsets Qf3, Qf4, and Qf5 fan surfaces, degraded Qf5 surfaces (at the DC-5 locality) and the floodplain of Wrights Creek. Table 1 presents the estimated age of the surfaces displaced by the Nevis Fault, the vertical offset measured across the fault scarp, and the vertical offset measured in the subsurface. The total vertical offset across Qf1 and Qf2 surfaces cannot be determined because the downthrown equivalents of these surfaces are either buried by younger sediments or are not preserved. The Qf3 surface is offset by 12.9m at the DC-8 locality where the downthrown side is preserved. The Qf4 surface is offset by 6.0 m at the DC-7 locality where the downthrown side is preserved. The vertical offset of the Qf5 surface varies along strike from 0.9 m to 2.2 m with an average of 1.5 m. The highest degraded Qf5 surface at the DC-5 locality is offset by 1.0 m, the middle degraded surface by 0.5 m and the lowest degraded surface by 0.3 m.

The floodplain on the north side of Wrights Creek, 20 m south of the DC-7 trench site (see Figure 25), is offset by 0.6 m. On the south

TABLE 1 - ESTIMATED AGES OF FAULTED SURFACES AND THEIR  
SURFACE AND SUBSURFACE VERTICAL OFFSETS.

SURFACE	LOCALITY	ESTIMATED AGE (yrs)	SURFACE OFFSET (m)	SUBSURFACE OFFSET (m)
Floodplain		0 - 9,000		
Floodplain	DC-7 area	<23,000	0.6-1.3	1.7
Lowest Dg	DC-5 area	<23,000	0.3	2.5 *
Middle Dg	DC-5 area	<23,000	0.5	2.5 *
Highest Dg	DC-5 area	<23,000	1.0	2.5
Qf5		23,000	0.9-2.2	1.7-3.5
Qf4		35-50,000	6.0	unknown
Qf3		70,000	12.9	unknown

Dg - Degraded Qf5 Surface

\* - Inferred from nearby trench exposures

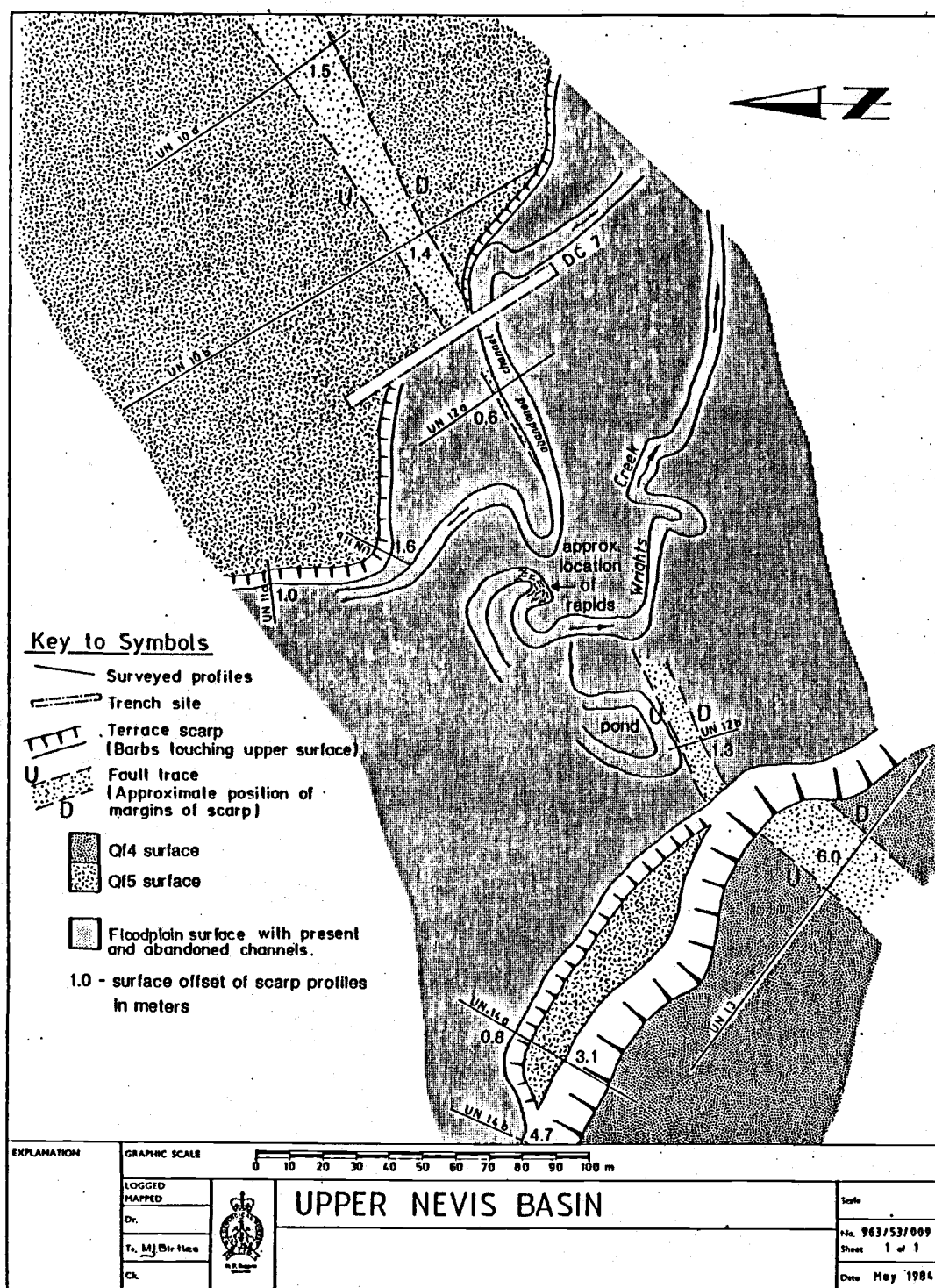


FIGURE 25 - Geologic Map, DC-7 Area

side of Wrights Creek the floodplain surface is offset by 1.3 m. Here, the fault acts as a dam to the flow of groundwater and this water is ponded on the upthrown side. The fault scarps are only preserved on the sides of the floodplain. The area between the preserved scarps is highly degraded by meandering channels of Wrights Creek. The only indication of possible fault disruption in the channel is a 1.0 m drop in stream gradient that forms a set of rapids. These rapids may represent a knickpoint where the stream has eroded across the fault scarp. The amount of possible knickpoint retreat was not determined.

The Nevis Fault only deforms the floodplain of Wrights Creek and does not deform any of the other floodplains of tributary streams in the basin. Wrights Creek floodplain is considered to be an older surface than the other tributary floodplains because it is only cut down from 1.0 to 1.6 m below the Qf5 surface, whereas the other floodplains are cut from 4.1 to 7.4 m below the Qf5 surface. The floodplain of Wrights Creek may have been cut down to its present level below the Qf5 surface, then abandoned for a long period of time before it was rejuvenated by a modern stream. This would explain why the fault scarps are preserved across the Wrights Creek floodplain and not across the other floodplains. The floodplain surface of Wrights Creek is tentatively correlated with the highest degraded Qf5 surface (at the DC-5 locality) because the highest degraded Qf5 surface is incised about the same amount below the Qf5 surface as the floodplain of Wrights Creek.

#### 5.7.2.4 Scarp Modification with Time

Scarp morphology techniques which have been used to assess the



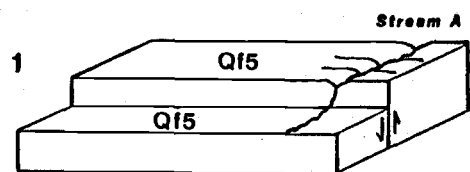
age of fault scarps and wave-cut shoreline scarps in the western United States were applied to the Nevis Fault scarps. The morphologic techniques are based on the theory that the geomorphic character of a scarp changes in a predictable way as the scarp is degraded through time and that the rate of degradation can be quantified to determine the age of the scarp. The details of this study are presented in Appendix B and only the results are presented here.

The age assessed for the most recent event occurring on the Nevis Fault using the  $\theta$  vs  $\log H$  technique is Holocene; and, using the diffusion equation technique, the age is 4,500 years. These ages are accepted, with reservation, as they are derived by comparison with scarps formed in more arid climates of the western United States. However, these values are consistent with each other and with constraints on the age of the most recent faulting event discussed in the next section.

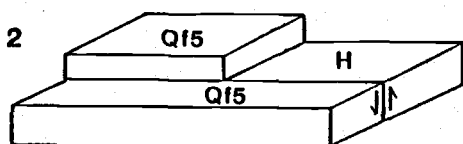
#### 5.7.2.5 Displacement History

##### 5.7.2.5.1 Evidence for Recurrent Movement

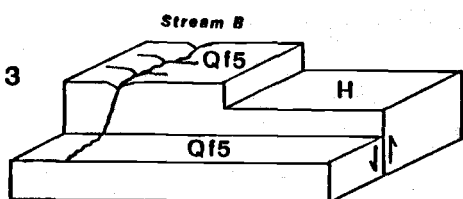
There are two lines of evidence that suggest there has been recurrent movement on the Nevis Fault. The data are presented in Table 1. First, the Nevis Fault offsets older surfaces (Qf3, Qf4) by greater amounts than younger surfaces (Qf5, degraded Qf5, and floodplain). Second, the base of the Qf5 fan alluvium is offset by a greater amount than the surface of the Qf5 fan, suggesting that one or more faulting events occurred while the Qf5 fan was being deposited and one or more events occurred after the fan was deposited.



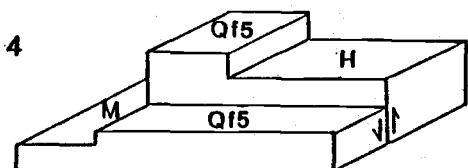
Faulting event 1



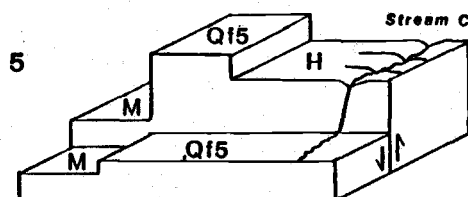
Formation of highest degradational surface



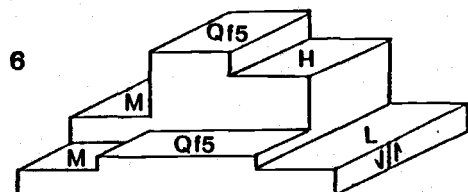
Faulting event 2



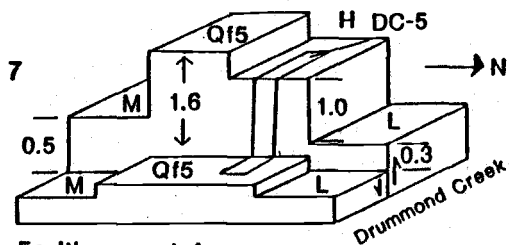
Formation of middle degradational surface



Faulting event 3



Formation of lowest degradational surface



Faulting event 4

H - Highest Degraded Qf5 Surface  
M - Middle Degraded Qf5 Surface  
L - Lowest Degraded Qf5 Surface

FIGURE 26 - A sequence of faulting and degradational events on the Nevis Fault producing the geometry of landforms observed at the DC-5 locality.

Evidence of progressive deformation is best preserved at the DC-5 locality where it is possible to assess the number of events that have occurred on the Nevis Fault since about 23,000 years ago. In the DC-5 area, at least five faulting events are recognized on the Nevis Fault; one or more event(s) occurred during the period when the Qf5 fan was being deposited and four events occurred after the fan was deposited. In this area, the total offset of the Qf5 fan surface (the top of the Qf5 fan deposit) is 1.6 m (Table 5, Appendix B, UN-3). In the DC-5 trench, the total offset of the base of the Qf5 fan deposit is 2.5 m (Figure 31). The difference in offset, 0.9 m, between the top of the fan deposit and the bottom of the fan deposit may represent one (or more) faulting event(s) which occurred during the period of time when the fan was being deposited. Any surface rupture at the time of the faulting event(s) has been obscured by Qf5 fan alluvium that was deposited at a later time.

Figure 15 is a large-scale geologic map of the DC-5 area showing four surfaces of different ages that are displaced by different amounts. Figure 26 depicts a sequence of four faulting events, each followed by stream erosion which may have formed the series of faulted surfaces observed at the DC-5 locality. Diagram 1 shows the first faulting event which occurred after the Qf5 fan was completely deposited. The fault raised the northwest side of the Qf5 surface causing Stream A (an intrafan stream) to cut down while seeking grade with the new fan slope. Diagram 2 shows that Stream A cut downward until the upthrown side was at the same level as the downthrown side and a degradational terrace was formed; this terrace has been designated as the Highest Degraded Qf5 surface. A second faulting event (Diagram 3)

raised the Qf5 surface and the Highest Degraded Qf5 surface. Diagram 4 shows that a period of downcutting (Stream B) followed the second faulting event and formed the Middle Degraded Qf5 surface, at a level below the Qf5 and Highest Degraded Qf5 surfaces. Diagram 5 shows a third faulting event which uplifted all of the surfaces. Another period of downcutting (Stream C in Diagram 6) followed the third faulting event, formed the Lowest Degraded Qf5 surface, and left only a remnant of the Highest Degraded Qf5 surface on the upthrown side. A fourth faulting event (Diagram 7) lifted up the Lowest Degraded Qf5 surface. Subsequently, Drummond Creek has cut downward 4-5 m below the Lowest Degraded Qf5 surface.

In conclusion, five events which occurred since about 23,000 years (the estimated age of the Qf5 fan, see Section 4.5.4) are identified at the DC-5 locality. Each event had an average of 0.3 to 0.5 m of vertical offset. The minimum value of 0.3 m is based on the offset of the Lowest Degraded Qf5 surface, which represents the offset during the most recent event. The maximum value of 0.5 m is based on five events measured at the DC-5 locality which produced a total of 2.5 m offset of the base of the Qf5 fan deposit (assuming one event occurred during the deposition of the Qf5 fan and four events occurred after the fan was deposited). A value of 2.6 m (Table 4, Appendix B, UN-20) was measured for a single faulting event using the scarp morphology technique, however, this value is considered to be a maximum and not an average value of surface offset.

#### 5.7.2.5.2 Recurrence Interval

A minimum of five faulting events of 0.5 m or less has occurred since the Qf5 fans were deposited. If the age of the Qf5 fans are Ha-wea (see Geologic Constraints on Age Section), then at least five events have occurred in about the last 23,000 years. The average recurrence interval depends on the timing of the earliest and the most recent events and assumes an equal amount of time between events. Two possible recurrence intervals are presented in Figure 27. The average recurrence interval calculated is from 4,000 to 5,000 years.

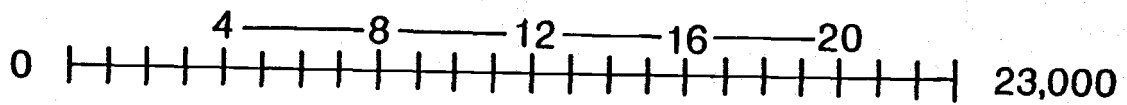
#### 5.7.2.5.3 Fault Activity

A long term rate of slip of 0.20-0.25 mm/yr is calculated for the Nevis Fault assuming a fault dip of 30°, dip-slip displacement of 1.0 m and a recurrence interval of 4,000 to 5,000 years. According to the classification of fault activity set forth by Matsuda (1975) and adopted by the American Nuclear Society (1980), the Nevis Fault has moderate fault activity.

#### 5.7.2.6 Maximum Credible Earthquake

A maximum credible earthquake (MCE) is an estimation of the maximum magnitude that is expected during an earthquake on a known fault. MCE values can be obtained by several different methods which have been developed from data on historical earthquakes throughout the world. Bonilla and Buchanan (1970) and Slemmons (1977) have shown that linear

Recurrence Interval: 4000 years



Recurrence Interval: 5000 years

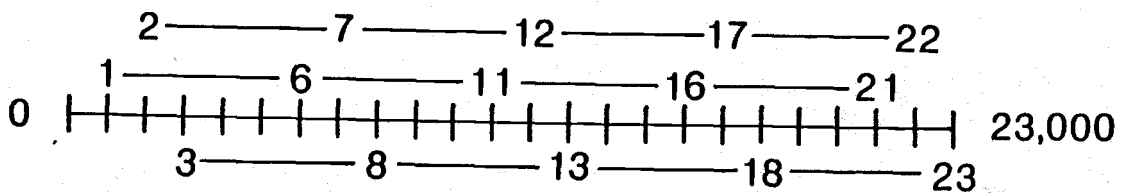


FIGURE 27 - Possible recurrence intervals for the Nevis Fault assuming five movements in about 23,000 years.

relationships exist between earthquake magnitude and 1) fault displacement (D), 2) fault rupture length (L), 3) the product of displacement and length (DL), and 4) the product of displacement squared and length ( $D^2L$ ). The parameters which statistically show the best correlation to earthquake magnitude (Slemmons, 1977) are 1) fault displacement and 2) fault rupture length.

From data presented in Section 5.7.2.5 a value of 0.5m was assessed for the average vertical offset occurring during a single fault rupture on the Nevis Fault. Using a value of  $30^\circ$  for the average dip of the fault, dip-slip displacement is 1.0 m. The length of the active trace of the Nevis Fault is substantiated for 7 km south of Drummond Creek. North of Drummond Creek, there is a late Quaternary fault trace crossing the Qf4 surface south of Whittens Creek. This suggests that the fault activity is continuous for 13 km throughout the basin. Both values are considered below in an evaluation of the maximum credible earthquake.

The formula for MCE using fault displacement (Slemmons, 1982) is:

$$MS = 6.793 + 1.306 \log D$$

MS = calculated magnitude of "causative" earthquake

D = Dip-slip measurement in meters

For D = 1.0 m

$$MS = 6.8$$

The formula for MCE using length of surface rupture (Slemmons, 1982) is:

$$MS = 2.021 + 1.142 \log L$$

L = length of surface rupture

For L = 7 km

$$MS = 6.4$$

For  $L = 13 \text{ km}$

$$MS = 6.7$$

The three values calculated above are similar and the maximum MS value of 6.8 is assumed for a possible surface rupture on the Nevis Fault.



## 5.8 Structural Evolution of the Basin

This section presents four structural models to explain the structural features that are present in the Upper Nevis Basin. The four models are:

Model 1: Parallel, northwest-dipping reverse faults.

Model 2: Bending moment faults formed by compression in a synform adjacent to a faulted antiform (Yeats, in press).

Model 3: Migration of a thrust-front from a master boundary fault to a frontal active fault.

Model 4: Strike-slip faulting.

### 5.81 Model 1 - Parallel, Northwest-Dipping Reverse Faults

The first structural model is shown in Diagram 1, Figure 28. The Upper Nevis Basin was formed by downwarping of the Cretaceous peneplain surface and overlying Tertiary sedimentary cover into a synform by drag folding on the downthrown side of the Western Boundary Fault. The Tertiary sediments were ultimately eroded off the highlands, and a wedge of unfaulted sediments was preserved beneath the Western Boundary Fault (see Figure 16, Cross Sections 1, 3, 4). In this model, the Western Boundary Fault, Nevis Fault and the north topographic depression are parallel, northwest-dipping reverse faults. The Linear Block is a structural block located between the Nevis and Western Boundary Faults that was uplifted and strongly back-tilted by movement on the Nevis Fault. The Western Boundary Fault comprises a wide zone along which erosion has produced a topographic depression between the schist at the base of the Hector Mountains and the sediments in the Linear Block (for

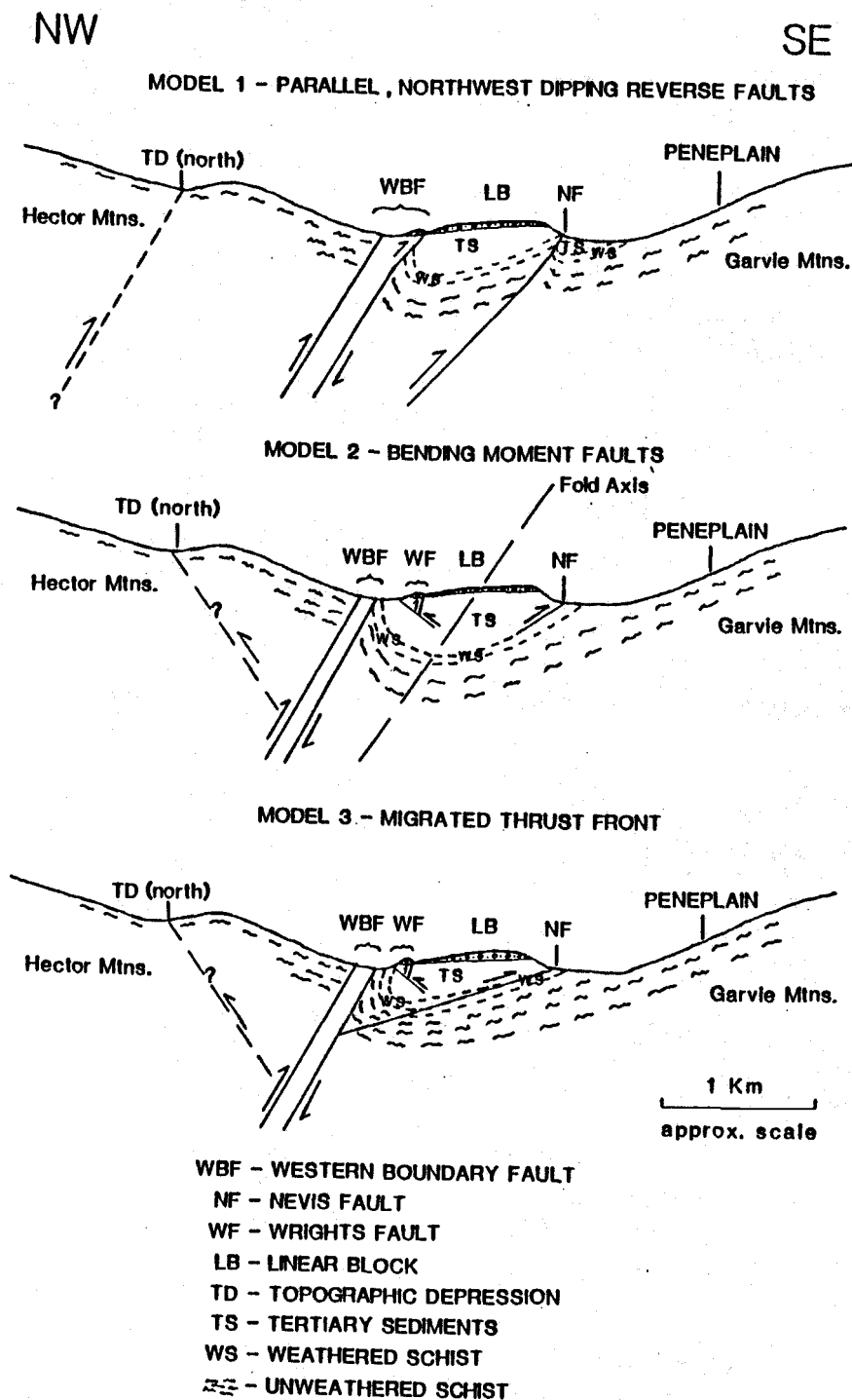


**FIGURE 28 - Structural Models  
Upper Nevis Basin**

example, note the southern topographic depression on Plates 1 and 2 and in Cross Sections 6-8, Figure 16). In model 1, Wrights Fault is not a southeast-dipping reverse fault but is the surface trace of the northwest-dipping Western Boundary Fault. The small fault scarps crossing the Qf<sub>2</sub> and Qf<sub>3</sub> surfaces south of Drummond Creek (see Figure 9 and Cross Section 6, Figure 16) represent late Quaternary movement on the Western Boundary Fault. To explain the uplift and backtilting of the Linear Block, the Western Boundary Fault must have been relatively inactive in the Quaternary compared to the Nevis Fault.

Model 1 does not adequately explain why the focus of activity would migrate from the Western Boundary Fault to the Nevis Fault. One explanation is that the two faults were pre-existing zones of weakness in the basement, which is common in the Central Otago region (Turnbull, 1975). When the master fault (Western Boundary Fault) became inactive in the early Quaternary, the focus of activity shifted to a pre-existing zone of weakness and produced a new fault (Nevis Fault), along which most of the late Quaternary tectonic deformation has taken place in the Upper Nevis.

#### 5.8.2 Model 2 - Bending Moment Faults

The second structural model is shown in Diagram 2 in Figure 28. In this model, the Western Boundary Fault separates an antiform/synform pair. The Cretaceous peneplain surface and overlying Tertiary sedimentary cover was downwarped by drag folding into a synform, which formed the Upper Nevis Basin, on the downthrown side of the Western Boundary Fault. The Tertiary sediments were eroded off the Hector and Garvie

Mountains, and a wedge of infaulted Tertiary sediments was preserved in the basin. As compressional deformation continued, bending moment faults (Nevis and Wrights Faults) developed in the region of minimum curvature along the concave axis of the syncline (Yeats, in press). These northwest- and southeast-dipping reverse faults uplifted a northeast-trending horst block (the Linear Block) in the middle of the basin. Since bending moment faults occur symmetrically about the axis of a syncline, this model requires an asymmetric tightly folded syncline at depth in the Upper Nevis Basin to allow for the near coincidence of Wrights Fault and the Western Boundary Fault.

One problem with the bending moment model is that the Nevis Fault is younger than Wrights Fault (the Nevis Fault offsets floodplain and Qf5 surfaces whereas Wrights Fault does not). Another problem is that the Nevis Fault has experienced a greater amount of uplift than Wrights Fault (the Linear Block is backtilted towards the northwest). Ideally, bending moment faults would release strain equally about their axis, with similar amounts and rates of deformation on both sides of the axis. Therefore, the bending moment model may not adequately explain the origin of the Linear Block. The bending moment model does not explain the complex nature of the northern segment of the Nevis Fault (discussed in Section 5.7.1) because Wrights Fault does not extend north of Drummond Creek. The bending moment model also does not explain why the Western Boundary Fault has become inactive in the late Quaternary.

### 5.8.3 Model - Thrust-Front Migration

The third and preferred model is presented in Diagram 3, Figure 28. In this model (proposed by Ikeda, 1983), reverse faulting is transferred from a master boundary fault (the Western Boundary Fault) to a low-angle frontal active fault (the Nevis Fault) whose leading edge may be buried at some depth below the surface. Uplift along a fault whose leading edge is buried creates a backtilted, tectonic bulge (the Linear Block) at the surface behind the frontal active fault. The tectonic bulge may be bounded by a secondary antithetic fault (Wrights Fault). The north topographic depression may be an antithetic reverse fault associated with the Western Boundary Fault.

In Ikeda's model, as movement on the master boundary fault causes the range to be uplifted, basin-fill sediments accumulate on its down-thrown side, resulting in the formation of a thick sedimentary wedge. Because the sedimentary wedge is softer than the basement rocks, fault slip in the basement produces shear-stress concentration in the wedge along the wedge-basement interface. The wedge material may be mechanically anisotropic due to its stratified nature, so the fault is likely to propagate along the wedge-basement interface as a bedding slip or detachment thrust. Consequently, the master boundary fault becomes inactive while the focus of activity shifts to the detachment thrust and the location of surface faulting advances basinward. When the leading edge of the detachment thrust is buried, the area between the master boundary fault and the frontal active fault is uplifted to form a tectonic bulge, strongly backtilted, and secondary antithetic faults form on the mountainward flank of the tectonic bulge.

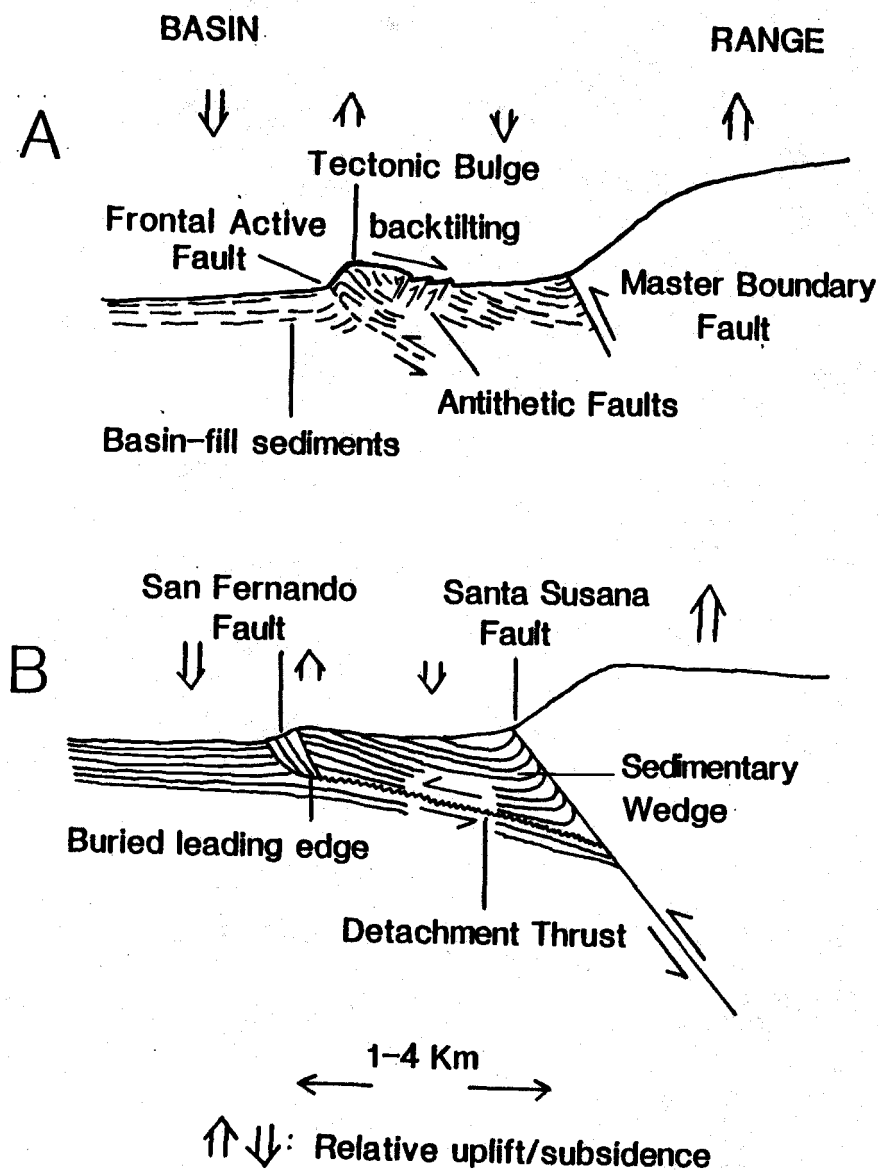


FIGURE 29 - A. Schematic cross section showing migration of fault activity from the inactive Master Boundary Fault to the Frontal Active Fault and development of a Tectonic Bulge (modified from Ikeda, 1983, Fig. 1) B. Schematic cross section of the San Fernando/Santa Susana Faults, CA showing the detachment thrust along interface between sedimentary wedge and basement rocks, and complex faulting above a buried leading edge (modified from Ikeda, 1983, Fig. 16).

Figure 29A is a schematic cross section showing Ikeda's model of thrust-front migration reproduced from his 1983 paper. Its features are very similar to the structural features of the Upper Nevis Basin shown in Diagram 3, Figure 28. The Upper Nevis Basin differs from Ikeda's model in that a sedimentary wedge (derived by erosion from an uplifted range) never really accumulated in the Upper Nevis Basin to the extent that he describes in his examples from Japan and San Fernando, California (Ikeda, 1983). However, the Tertiary sediments that are preserved in the Upper Nevis Basin may have acted like Ikeda's "sedimentary wedge" in that they are thicker where they are trapped beneath the Western Boundary Fault and gradually are truncated by erosion toward the east and are absent in the Garvie Mountains. The detachment thrust origin of the Nevis Fault (Ikeda's frontal active fault) is substantiated by the occurrence of deformed Tertiary sediments and weathered schist in the trenches (see Appendix A) which suggests that the fault has propagated along the interface between the weathered schist basement and the Tertiary sediments. The complex deformation observed along the northern segment of the Nevis Fault may be due to strong deformation expressed at the surface overlying the buried leading edge of a detachment thrust, as in the San Fernando Fault (Figure 29B). The northern segment of the Nevis Fault is located in the narrowest part of the Upper Nevis Basin. The observed complexities may also be related to the fact that the frontal active fault (Nevis Fault) cannot advance any further basinward because in this area (north of Drummond Creek) it is less than 0.5 km from the opposite side of the basin.

The thrust-front migration model is the best model to explain the variation in age of the faults in the Upper Nevis Basin. The faults

are older from northwest to southeast; the Western Boundary Fault is older than Wrights Fault which is older than the Nevis Fault. The thrust-front migration model explains why thrusting has migrated from a master boundary fault (Western Boundary Fault) to a frontal active fault (Nevis Fault). Wrights Fault is a secondary feature related to deformation within the tectonic bulge (Linear Block) which explains why its total offset and activity is less than the Nevis Fault.

#### 5.8.4 Model 4 - Strike-slip Faulting

A fourth model which may be partly responsible for the structural deformation observed in the Upper Nevis Basin invokes a component of strike-slip motion that is masked by a dominant component of vertical motion. A component of strike-slip motion may have been involved in originally forming the basin by pull-apart (Aydin and Nur, 1982). Subsequent large vertical motion has masked the evidence for strike-slip motion. Strike-slip faulting may account for the "slivers" of material (oil shale, schist, Qwgl gravels) that are faulted against each other in the northern segment of the Nevis Fault (see Section 5.7.1). Strike-slip faulting (probably oblique convergence) may also account for the pinch and swell effect of the Upper and Lower Nevis Basins located along the Nevis segment of the Nevis-Cardrona Fault System (Figure 3). Strike-slip faulting is predicted to be right-lateral on the basis of regional tectonics (Section 2.1.3 and Officers of the New Zealand Geological Survey, 1984; Section 2.2.3.2).



## 6.0 CENTRAL OTAGO MASTER FAULTS

### 6.1 Nevis-Cardrona Fault System

#### 6.1.1 Style of Deformation

The style of deformation along the Nevis-Cardrona Fault system varies from south to north. Figure 30 presents schematic cross sections through each of the basins which occur along the Nevis-Cardrona Fault system. In the south, the Upper Nevis Basin (Diagram 1, Figure 30) is bounded on the northwest by a major reverse fault (Western Boundary Fault) and to the southeast by the downwarped peneplain surface. Tertiary sediments are infaulted on the downthrown side of the Western Boundary Fault, and an uplifted horst block in the middle of the basin (Linear Block) is bounded by inward-dipping late Quaternary reverse faults (Wrights and Nevis Faults).

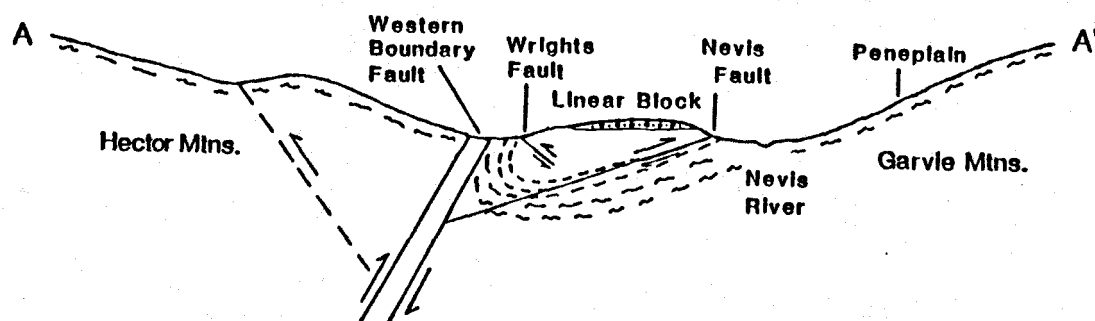
The Lower Nevis Basin (Diagram 2, Figure 30) is bounded on the northwest by the Schoolhouse Fault. The Nevis Fault, which is the major crustal fracture in the Lower Nevis Basin, trends north-northeast along the axis of the basin. The east side of the basin is bounded by several southeast-dipping reverse faults (Dell Fault, Hogans Fault and two unnamed faults along the southeast margin, see Figure 2 of Beanland et al., 1984). Several late Quaternary fault traces disrupt the basin floor that are associated with the Nevis Fault (Curving trace, X trace, and Ben Nevis trace). Another late Quaternary trace disrupts the floor of the basin on the east side (Coal Creek trace).

Where the Nevis-Cardrona Fault system bifurcates across the Kawa-

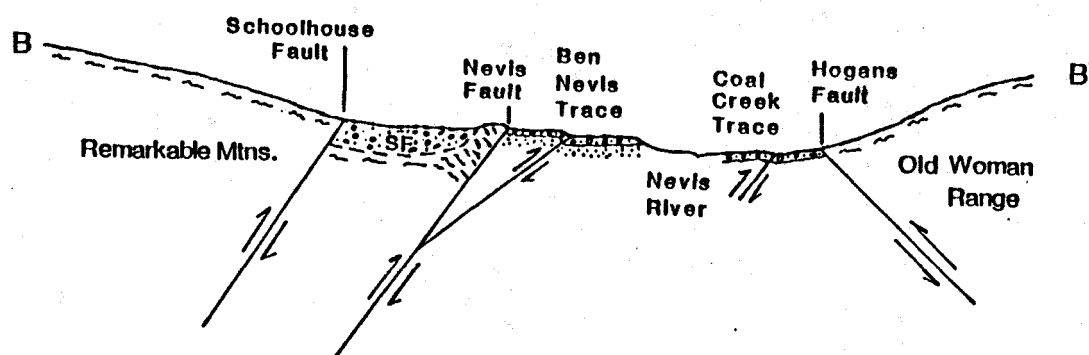
NW

## 1 UPPER NEVIS BASIN

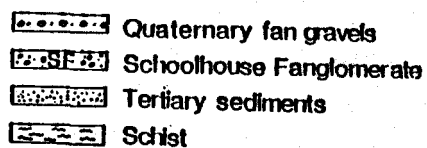
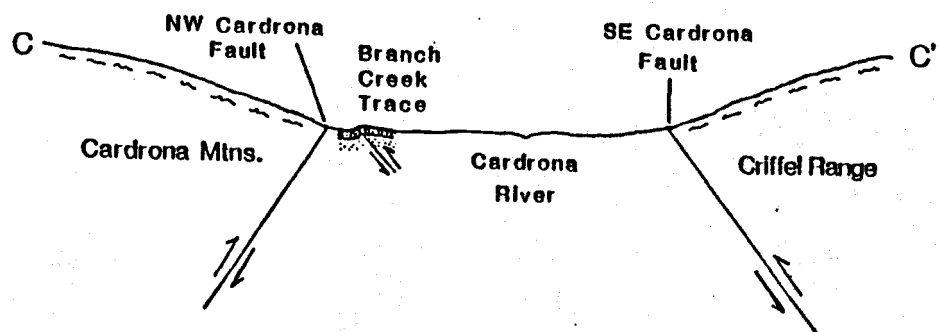
SE



## 2 LOWER NEVIS BASIN



## 3 CARDRONA BASIN



0 1 2 Km  
approx. scale

FIGURE 30 - Schematic cross sections through basins along the Nevis-Cardrona Fault System. Cross sections are located on Figure 3.

rau River (see Figure 3), the region is complexly faulted and folded. A late Quaternary northwest-dipping reverse fault is documented where the Crown Segment intersects the Kwarau River (Kwarau Trace, Beanland, 1984) and a possible late Quaternary fold is located where the Roaring Meg Segment intersects the Kwarau River (Victoria Warp, Beanland, 1984).

The Cardrona Basin (Diagram 3, Figure 30) is bounded on the northwest by a northwest-dipping reverse fault (Northwest Cardrona Fault) and on the southeast by a southeast-dipping reverse fault (Southeast Cardrona Fault). There are several late Quaternary fault traces on the northwest side of the basin associated with movement on the Northwest Cardrona Fault. One trace, Blackman's Creek Trace, shows evidence for 10 m of right-lateral strike-slip movement (Beanland, 1984). This is the only place where strike-slip deformation has been documented on the Nevis-Cardrona Fault System.

#### 6.1.2 Fault Activity

Trenching investigations were carried out on the Nevis-Cardrona Fault system along the Nevis segment (Beanland and Barrow, 1984c; Beanland, et al., 1984), the Crown Segment (Beanland and Fellows, 1984) and the Cardrona segment (Beanland, 1984). The results of the fault activity for each segment are presented in Table 2. The age of displaced surface and recurrence intervals have been modified from the data published in the above papers because of a recent radiocarbon date that dates the age of the Hawea glacial advance as older than the 16,000 years previously reported. The radiocarbon date of 20,500 years

TABLE 2 - QUATERNARY FAULT ACTIVITY IN CENTRAL OTAGO

FAULT	FAULT SEGMENT	LOCALITY	FAULT TRACE	AGE OF FAULTED SURFACE (years)	NUMBER OF FAULTING EVENTS	SURFACE OFFSET PER DISPLACEMENT (meters)	LENGTH OF POSSIBLE SURFACE RUPTURE FOR ENTIRE FAULT SEGMENT (km)	AVERAGE RECURRENCE INTERVAL (years)	COMMENTS
NEVIS-CARDRONA FAULT SYSTEM	Nevis	Upper Nevis Basin	Nevis	c. 23,000	5	c. 0.5	c. 13	4-5,000	
		Lower Nevis Basin (Beanland et al., 1984)	Coal Creek	c. 23,000	2	c. 1.0		8-22,000	
			X-Fault	c. 23,000	1	c. 1.0		?	
	Crown	Kawarau River (Beanland and Fellows, 1984)	Kawarau	c. 23,000	3-6	c. 1.0-2.0	c. 30	4-11,000	
	Cardrona	Cardrona Basin (NW Cardrona Fault) (Beanland, 1984)	Blackmans Ck.	c. 23,000	7	c. 1.0	c. 30	3,000	10 m dextral offset
			Branch Creek	c. 23,000	3	c. 1.3	c. 30	6-11,000	
			Maori Gully	< 10,000	1	c. 1.2	c. 30	?	
DUNSTAN		Manuherikia Basin (ONZGS, 1983)	Waikeri & Devonshire	c. 23,000	?	c. 2.0	c. 20-60	8,000	
PISA/GRAND-VIEW		Cromwell-Tarras Basin (ONZGS, 1984)		c. 35,000-70,000	?	?	c. 30	?	

(S.Beanland, 1984, pers. comm.) was determined from a soil located approximately 1 m above the Hawea outwash surface. This radiocarbon date supports an age of c. 23,000 years for the Hawea glacial outwash surface. The table shows that late Quaternary faulting has taken place on discrete segments of the entire Nevis-Cardrona Fault system. Most of the activity occurs along fault traces associated with major faults on the northwest side of the basins or along the basinal axis. Only two traces are documented on the east side of a basin (Coal Creek trace, Lower Nevis Basin and Southeast Cardrona Fault trace, Cardrona Basin). It is uncertain whether each event on the discrete fault segments occurred at the same time or whether the focus of activity has shifted through time. In any event, the Nevis-Cardrona Fault system has experienced repeated deformation in the late Quaternary that appears to be most intense in the Upper Nevis Basin, the Kawarau River area and in the Cardrona Basin.

## 6.2 Dunstan Fault

### 6.2.1 Style of Deformation

The overall style of tectonic deformation in the Central Otago region was discussed in Section 2.1.3 and is shown in Figures 2 and 6. This section addresses the late Quaternary deformational features on the Dunstan and Pisa Faults.

The Dunstan Fault trends northeast and consists of a master fault at the foot of the Dunstan Mountains and five discrete segments in the Manuherikia Basin along which late Quaternary deformation is recognized

(Officers of the New Zealand Geological Survey, 1983; I. Madin, 1985, pers. comm.). From southwest to northeast, the segments are known as Waikerikeri, Brassknocker, Devonshire, Drybread and Cambrians respectively. Each segment consists of two or three subparallel fault traces. The traces that are located farthest from the master range front fault (from 0.1 to 3 km out in the basin) are manifested by basin-facing scarps, have their northwest side uplifted and are considered synthetic to the master fault. The traces that are closest to the master range front fault are range-facing, have their southeast side uplifted and are considered antithetic to the master fault. The two sets of faults bound a horst structure that varies in width from 100 m to 1 km.

#### 6.2.2 Fault Activity

Evidence for repeated deformation in the late Quaternary has been documented on the Waikerikeri and Devonshire segments. A preferred recurrence interval of 8,000 years within the range of 7,500-50,000 years for the Waikerikeri segment and 3,700-14,500 years for the Devonshire segment has been determined for the Dunstan Fault (the reference for 8000 years is from a letter written to the Commissioner of Works, from the Director of the New Zealand Geological Survey (Ref. 963/12 -14), dated 15 December, 1983, re-assessing the recurrence interval value of 12,500 years originally published in Officers of the New Zealand Geological Survey, 1983). Vertical displacement for a single event is estimated as 2 m. The length of possible surface rupture for a single fault movement ranges from 20 km (Devonshire segment) to a total of 60 km. Twenty kilometers is considered most likely.

## 6.3 Pisa Fault

### 6.3.1 Style of Deformation

The Pisa Fault and the Grandview Fault are a part of the same master fault system (Figure 2). The Pisa fault is north-northeast trending and is located at the southeast boundary of the Carrick, Pisa, and Lindis Peak ranges. The Grandview Fault diverges to the northwest at Queensberry and extends to Lake Hawea. Both synthetic and antithetic late Quaternary fault traces occur to the southeast of the Pisa range-front master fault between the Kawarau River and Queensberry. These late Quaternary faults bound raised horst blocks (100-200 m wide) along the northwest margin of the Cromwell-Tarras Basin. A late Quaternary, subsurface fold extends along the north half of this segment of the Pisa Fault and along the Grandview Fault.

### 6.3.2 Fault Activity

The surface deformation described above is the result of repeated fault movement between 250,000-170,000 years ago and 70,000-35,000 (Officers of the New Zealand Geological Survey, 1984). The deformation may have extended for 30 km. There is no evidence of tectonic activity on either the Pisa or Grandview Faults in the last 35,000 years.

#### 6.4 Comparison with the Upper Nevis Basin

The late Quaternary deformational features on the Pisa and Dunstan Faults are quite similar to those of the Upper Nevis Basin. Narrow (less than 2 km wide) horst blocks are faulted up along the northwest margin of the basins where antithetic faults occur very close to (less than 1 km) and sometimes nearly coincidental with the master range front fault. Fault activity is quite variable between the Pisa, Dunstan, and Nevis-Cardrona Fault systems. Both the Dunstan Fault and the Nevis-Cardrona Fault system have experienced repeated deformation in the last c. 23,000 years whereas the Pisa Fault has not experienced activity in the last 35,000 years. The focus of fault activity apparently shifts through time.

The most important result of this regional comparison of late Quaternary fault activity in the Central Otago region is that although the historic and instrumental records show that there has been very little earthquake activity since 1956 in Central Otago, there is potential for future earthquake activity along the many late Quaternary faults throughout the region.



## 7.0 SUMMARY AND CONCLUSIONS

The Upper Nevis Basin is an elongate, structurally-controlled intermontane basin located in the southern part of the Nevis segment of the Nevis-Cardrona Fault system. Basement rock in the Upper Nevis Basin is Haast Schist. The upper 50 m of the schist is deeply weathered and is overlain by non-marine fluvio-lacustrine sediments that are correlated with Tertiary sediments of the Nevis Formation (Williams, 1974) in the Lower Nevis Basin. Quaternary deposits overlie the Tertiary sediments with angular unconformity. Early Quaternary deposits consist of highly weathered fluvial gravels. Late Quaternary deposits consist of (1) a series of five alluvial fans, (2) reworked fan gravels, (3) loess and (4) floodplain deposits.

The only absolute age control of the Quaternary deposits in the Upper Nevis Basin is a radiocarbon date of  $9670 \pm 130$  (Sample # NZ 6543A) years recovered from a buried peat. The peat represents a former stand of the floodplain of Whittens Creek; the age of the modern floodplain is inferred to be younger than this date.

The five alluvial fans are relatively dated by means of their relative elevation and degree of dissection. Qf1, the highest and most strongly dissected fan surface, is the oldest and Qf5, the lowest and least dissected (most planar) fan surface, is the youngest.

Soil development on the fan surfaces proved to be a poor relative dating tool because the soils on all of the fan surfaces are weakly developed and are probably less than 10,000 years old. The youthfulness of the soils is attributed to modification of the soil-forming process by wind erosion and/or loess deposition.

Morphologic modification of river-cut terrace scarps is found to be a fairly good relative dating tool to assess the age of the surfaces lying at the base of the scarps. Two scarp morphology techniques are employed to date the scarps, hence the surfaces lying at the base. The graphical method ( $\theta$  versus  $\log H$ ) dates the Qf5 surface as late Pleistocene, the degraded Qf5 surfaces as Holocene and the floodplain surface as Holocene. The analytical method (diffusion equation) dates the Qf5 surface as 23,900-29,600 years and the floodplain surface as 3,000-3,900 years. The latter method is unsuccessful for realistically dating the degraded Qf5 surfaces. The results of the scarp morphology study are found to be consistent with ages based on geologic constraints, however, the techniques are based on a comparison with data collected in more arid climates in the western United States. The effect of increased precipitation on scarp degradation rates is uncertain but is assumed to be negligible in this study.

The age of the fan deposits are tentatively correlated with individual glacial advances occurring in the nearby Clutha Valley based on the theory that during maximum glacial advance there is an increase in alluvial fan aggradation occurring in areas which have harsh periglacial climates. The youngest fan deposit Qf5, is considered to be Hawea age (about 23,000 years) and each higher fan remnant is considered to represent subsequently older glacial events.

Structures in the Upper Nevis Basin are northeast-trending. The Western Boundary Fault is a northwest-dipping reverse fault which displaces schist of the Hector Mountains over Tertiary sediments in the basin. The Linear Block is a mid-valley uplifted horst block that is bounded on the southeast by a northwest-dipping late Quaternary reverse

fault (Nevis Fault) and on the northwest by a southeast-dipping late Quaternary reverse fault (Wrights Fault). The age of the faults decreases from northwest to southeast; the Western Boundary Fault is older than Wrights Fault which is older than the Nevis Fault. A topographic depression northwest of the Western Boundary Fault may be the trace of another reverse fault. The Cretaceous peneplain surface, located in the Garvie Mountains, is downwarped toward the northwest into the Upper Nevis Basin.

The Nevis Fault defines a complex fault zone north of Drummond Creek and is observed as a late Quaternary fault scarp crossing the fan surfaces south of Drummond Creek. Five trenches were excavated across the Nevis Fault, exposing a northwest-dipping reverse fault where schist and/or Tertiary sediments are displaced over Quaternary fan gravels. Scarp morphology techniques were applied to the Nevis Fault scarps. The age of most recent movement is assessed to be Holocene according to the  $\theta$  vs  $\log H$  method and 4,400-4,500 years according to the diffusion equation technique. These ages agree well with geologic constraints on the age of most recent movement. Five faulting events are recognized on the Nevis Fault since about 23,000 years ago based on progressive deformation of a sequence of terraces in the DC-5 area. A recurrence interval of 4,000 to 5,000 years, a long-term rate of slip of 0.20-0.25 mm/year and a maximum credible earthquake of M 6.8 are calculated for the Nevis Fault.

Four structural models are presented to explain the structural evolution of the Upper Nevis Basin. The structural models are (1) parallel, northwest-dipping reverse faults, (2) bending moment faults occurring in the concave axis of a synform, formed by drag on the down-

thrown side of a master reverse fault, (3) migration of faulting from a master boundary fault to a frontal active fault along a detachment thrust and (4) strike slip faulting. Model 3 is the preferred model because it best explains all of the observed deformational features and it also explains why the faults decrease in age from northwest to southeast.

The Nevis-Cardrona Fault system contains three basins along its length which vary in their structural style. The Dunstan and Nevis-Cardrona Fault systems have been active in the late Quaternary (since about 23,000 years). The Pisa Fault has not been active in the last 35,000 years. This indicates that the focus of activity is variable and may shift through time. The most important result of this study is the documentation of late Quaternary tectonic deformation on the Nevis Fault. Although there is a lack of historical seismicity in the Central Otago Region, there are several large faults (Nevis-Cardrona, Pisa, and Dunstan Faults) that have ruptured repeatedly in late Quaternary time and are still capable of rupturing.

## 8.0 REFERENCES CITED

- Adams, C.J.D., 1979, Age and origin of the Southern Alps, in Walcott, R.I. and Cresswell, M.M. (eds), The origin of the Southern Alps: Royal Society of New Zealand, Bull. 18: 73-78, Wellington, New Zealand.
- and Ware, 1977, Subcrustal earthquakes beneath New Zealand, location determined with a laterally inhomogenous model: New Zealand Journ. of Geol. and Geoph., v. 20: 59-83.
- Allen, C.R., 1975, Geological criteria for evaluating seismicity: Geol. Soc. America Bull., v. 86: 1041-1057.
- American Nuclear Society, 1980, Criteria and guidelines for assessing capability for surface faulting at nuclear power plant sites: ANSI N-180/ANS 2.7, 25 p. (draft).
- Aydin, A. and Nur, A., 1982, Evolution of pull-apart basins and their scale independence: Tectonics, v. 1: 91-105.
- Beanland, S., 1984, Late Quaternary faulting in the Cardrona Valley, Central Otago, New Zealand: New Zealand Geol. Survey EDS Immediate Report 84/017 Lower Hutt, New Zealand, 14 p.
- and Barrow, S.A., 1984a, Geology of the Upper Nevis Basin in relation to active tectonics, Central Otago: New Zealand Geol. Survey EDS Immediate Report 84/005, Lower Hutt, New Zealand, 14 p.
- and Barrow, S.A., 1984b, Quaternary geology and late Quaternary tectonic deformation of the Upper Nevis Basin, Central Otago: New Zealand Geol. Survey EDS Immediate Report 84/006, Lower Hutt, New Zealand, 21 p.
- and Barrow, S.A., 1984c, Trenching investigations of active faulting in the Upper Nevis Basin, Central Otago: New Zealand Geol. Survey EDS Immediate Report 84/004, Lower Hutt, New Zealand, 21 p.
- and Fellows, D.L., 1984, Late Quaternary tectonic deformation in the Kawarau River Area, Central Otago: New Zealand Geol. Survey EDS Immediate Report 84/019, Lower Hutt, New Zealand, 16 p.
- Fellows, D.L. and Barrow, S.A., 1984, Late Quaternary faulting in the Lower Nevis Basin, Central Otago: New Zealand Geol. Survey EDS Immediate Report 84/018, Lower Hutt, New Zealand, 17 p.
- Berryman, K.R., Hull, A.G. and Wood, P.R., 1984, Late Quaternary deformation at the Dunstan Fault, Central Otago, New Zealand: in press.

Berberian, M., 1979, Earthquake faulting and bedding thrust associated with the Tabas-e-Golshan (Iran) earthquake of September 16, 1978: Bull. of the Seism. Soc. of America, v. 69, no. 6: 1861-1889.

Bishop, D.G., 1972, Progressive metamorphism from prehnite-pumpellyite to greenschist facies in the Dansey Pass area, Otago, New Zealand: Geol. Soc. America Bull., v. 83: 3177-3198.

Bloom, A.L., 1978, Geomorphology: a systematic analysis of late Cenozoic landforms: Prentice-Hall, Inc., Englewood Cliffs, New Jersey, 07632, 510 p.

Bonilla, M.G., 1973, Trench exposures across surface fault ruptures associated with the San Fernando earthquake, in "San Fernando, California, earthquake of February 9, 1971": National Oceanic and Atmospheric Administration, U.S. Dept. of Commerce, Rockville, Maryland, v. 3: 173-182.

----- 1979, Historic surface faulting - map patterns, relation to sub-surface faulting, and relation to pre-existing faults: U.S. Geol. Survey Open-File Report 79-1239: 36-65.

----- and Buchanan, J.M., 1970, Interim report on worldwide historic surface faulting: U.S. Geol. Survey Open-File Report, December 1970, Washington, D.C.

Bucknam, R.C. and Anderson, R.E., 1979, Estimation of fault-scarp ages from a scarp-height-slope-angle relationship: Geology, v.7: 11-14.

Clark, M.M., Grantz, A. and Rubin, M., 1972, Holocene activity of the Coyote Creek Fault as recorded in the sediments of Lake Cahuilla: U.S. Geol. Survey Prof. Paper 787: 112-130.

Colman, S.M. and Watson, K., 1983, Ages estimated from a diffusion equation model for scarp degradation: Science, v. 221: 263-265.

Culling, W.E.H., 1963, Soil creep and the development of hillside slopes: Journ. Geol., v. 71: 127-161.

-----1965, Theory of erosion on soil-covered slopes: Journ. Geol., v. 73: 230-254.

Halliday, G., 1982, Engineering geological investigations at the KW23 damsite: Ministry of Works and Development CVD Investigations Report 300, Cromwell, New Zealand.

Hanks, T.C., Bucknam, R.C., Lajoie, K.R. and Wallace, R.E., 1983, Modification of wave-cut and faulting controlled landforms: in press, U.S. Geol. Survey, 345 Middlefield Rd. Menlo Park, California, 94025.

Henderson, J., 1923, Notes on the geology of the Nevis Valley, Otago: New Zealand Journ. of Science and Technology, v. 6: 123-138.

- Hirano, M., 1968, A mathematical model of slope development - an approach to the analytical theory of erosional topography: Journ. of Geosciences, Osaka City University, Japan, v. 11: 13-52.
- 1972, Quantitative morphometry of fault scarp with reference to the Hira Mountains, central Japan: Japanese Journ. Geol. and Geography, v. 42: 85-100.
- 1975, Simulation of development process of interfluvial slopes with reference to graded form: Journ. Geol., v.83: 113-123.
- Hurley, P.M., Hughes, H., Pinson, W.H., Jr. and Fairbairn, H.W., 1962, Radiogenic argon and strontium diffusion parameters in biotite at low temperatures obtained from Alpine Fault uplift in New Zealand: Geochimica et Cosmochimica Acta, v. 26: 67-80.
- Ikeda, Y., 1983, Thrust front migration and its mechanisms - evolution of intraplate thrust fault systems: Bull. Dept. of Geography, University of Tokyo, v. 15: 125-159
- Leamy, M.L. and Saunders, W.M.H., 1967, Soils and land use in the Upper Clutha Valley, Otago: Soil Bureau Bull. 28, New Zealand Dept. of Scientific and Industrial Research, Govt. Printer, Wellington, New Zealand, 110 p.
- Macfarlane, D.F., et. al., 1982, Kawarau River power investigations. Reconnaissance geology of alternative proposals: New Zealand Geol. Survey EG Immediate Report 82/035.
- Machette, M.N., 1982, Quaternary and Pliocene faults in the La Jencia and southern part of the Albuquerque-Belen Basins, New Mexico: Evidence of fault history from fault-scarp morphology and Quaternary geology: New Mexico Geol. Society Guidebook, 33rd Field Conference, Albuquerque Country II.
- Matsuda, T., 1975, Magnitude and recurrence interval of earthquakes from a fault: Zisin, ser. 2, v. 28: 269-283. (In Japanese)
- McCalpin, J.P., 1982, Quaternary geology and neotectonics of the west flank of the northern Sangre de Cristo Mountains, South-Central Colorado: Colorado School of Mines Quarterly, v. 77, no. 3, 97 p.
- McKay, A., 1897, Report on the older auriferous drifts of Central Otago: Government Printer, Wellington, New Zealand.
- Molnar, P., Atwater, T., Mammerickx, J. and Smith, S.M., 1975, Magnetic anomalies, bathymetry and the tectonic evolution of the South Pacific since the Late Cretaceous: Geoph. Journ. of the Royal Astron. Society, v. 40: 383-420.
- Mutch, A.R., 1963, Geological Map of New Zealand, 1:250,000, Sheet 23 - Oamaru: Department of Scientific and Industrial Research, New Zealand Geological Survey, Wellington, New Zealand.

Nash, D.B., 1980, Morphologic dating of degraded normal fault scarps: Journ. Geol., v. 88: 353-360.

----- 1984, Morphologic dating of fluvial terrace scarps and fault scarps near West Yellowstone, Montana: Geol. Soc. America Bull., v. 95: 1413-1424.

Norris, R.J. and Carter, R.M., 1982, Fault bounded blocks and their role in localising sedimentation and deformation adjacent to the Alpine Fault, southern New Zealand: Tectonophysics, v. 87: 11-23.

----- Carter, R.M. and Turnbull, I.M., 1978, Cainozoic sedimentation in basins adjacent to a major continental transform boundary in southern New Zealand: Journ. Geol. Soc. London, v.135: 191-205.

Officers of the New Zealand Geological Survey, 1983, Seismotectonic hazard evaluation of the Clyde dam site: Department of Scientific and Industrial Research, New Zealand Geol. Survey Engineering Geology Report EG375, 2 vol., Lower Hutt, New Zealand.

----- 1984, Seismotectonic hazard evaluation for Upper Clutha power development: Department of Scientific and Industrial Research, New Zealand Geol. Survey Engineering Geology Report EG377, Lower Hutt, New Zealand.

Sieh, K., 1978, Pre-historic large earthquakes produced by slip on the San Andreas Fault at Pallet Creek, California: Journ. of Geoph. Research, v. 83: 3907-3939.

Slemmons, D.B., 1977, Faults and earthquake magnitude: state of the art for assessing earthquake hazards in the United States: U.S. Army Engineer Waterways Experiment Station, Vicksburg, Mississippi, Misc. Paper S-73-1 Report 6, 129 p.

----- 1982, Determination of design earthquake magnitudes for micro-zonation: Third International Microzonation Conference Proceedings: p. 119-130.

Smith, W.P., 1971, Earthquakes at shallow and intermediate depths in Fiordland, New Zealand: Journ. of Geoph. Research, v.76: 4901-4907.

Suggate, R.P., 1961. Rock stratigraphic names for the South Island schist and undifferentiated sediments of the New Zealand geosyncline: New Zealand Journ. of Geol. and Geoph., v.4, no.4: 392-399.

----- 1978, ed., The geology of New Zealand: New Zealand Geol. Survey, 2 vol., 820 p.

Thomson, R., 1983, Nevis Valley faulting - a progress note: Unpublished note in New Zealand Geol. Survey files 963/52,53.

Turnbull, I.M., 1981, Contortions in the schists of the Cromwell district, Central Otago, New Zealand: New Zealand Journ. of Geol. and Geoph., v. 24: 65-86.



- Barry, J.M., Carter, R.M. and Norris, R.J., 1975, The Bobs Cove beds and their relationship to the Moonlight Fault Zone: Journ. of the Royal Soc. of New Zealand, v. 5, no. 4: 355-394.
- Walcott, R.I., 1978, Present tectonic and late Cenozoic evolution of New Zealand: Geoph. Journ. of the Royal Astron. Soc., v. 52: 137-164.
- 1984, Structural evolution of New Zealand during the Neogene: in press.
- Wallace, R.E., 1977, Profiles and ages of young fault scarps, north-central Nevada: Geol. Soc. America Bull., v. 88: 1267-1281.
- Weissel, J.K., Hayes, D.E. and Herron, E.M., 1977, Plate tectonic synthesis: the relative motions between the Australian, New Zealand and Antarctic continental fragments since the late Cretaceous: Marine Geology, v. 25: 231-277.
- Willett, R.W., 1943, The Nevis oil-shale deposit, Nevis Survey District Otago Central: New Zealand Journ. of Science and Technology, v. B24, no. 6: 239-254.
- Williams, G.J., 1974, Cenozoic geology of the Lower Nevis Basin, New Zealand with special reference to oil shale deposits: New Zealand Department of Scientific and Industrial Research, Bull. 212, Wellington, New Zealand, 36 p.
- Wood, B.L., 1962, Geological map of New Zealand, 1:250,000, Sheet 22 - Wakatipu: Department of Scientific and Industrial Research, New Zealand Geological Survey, Wellington, New Zealand.
- 1978, The Otago schist megaculmination: its possible origins and tectonic significance in the Rangitata Orogen of New Zealand: Tectonophysics, v. 47: 339-368.
- Yeats, R.S., in press, Faults related to folding, including examples from New Zealand, in Reilly, W.I. (ed.), Proceedings of the symposium on recent crustal movements of the Pacific region, Wellington, New Zealand, 9-14 February, 1984: Royal Society of New Zealand.

## APPENDICES

## Appendix A - TRENCHING INVESTIGATIONS

### A-1.0 Introduction

To better understand the style and history of movement along an active fault, trenches may be excavated across the fault scarp to create subsurface exposure (Clark, et. al., 1972; Bonilla, 1973; Sieh, 1978; Officers of the New Zealand Geological Survey, 1983, 1984). From detailed mapping of the trench walls, it may be possible to determine 1) the type of fault(s) present, 2) the number of displacements that have occurred (if recurrent movement is evident), 3) the amount of each displacement and 4) the age of each displacement (if datable material is present).

In the Upper Nevis Basin, five trenches were excavated across the active trace of the Nevis Fault. Their locations are shown on Plates 1 and 2 and trench details are summarized in Table 3. From north to south, they are labeled DC-5 to DC-9. Trench sites were located to give as much information as possible on evidence of recurrent movement and youthfulness of surface rupture. Therefore sites were located on the youngest surfaces across which scarps exist as well as on surfaces that seemed to show progressive deformation. The floodplains of streams crossing the fault trace would have been good surfaces to trench because they are the youngest surfaces, but they were too saturated with ground water to be safely trenched.

A D-8 bulldozer was used to excavate the trenches. The first step in the process was to remove the topsoil from the trench site and push it several meters off to one side. Then the trench was dug approxi-

TABLE 3 - SUMMARY OF TRENCH DETAILS

TRENCH	DC-5	DC-6	DC-7	DC-8	DC-9
LOCATION (west end)					
MAP: NZMS 1 (S142)	748337	739329	732318	714291	705277
NZMS 260	F42/866332	F42/858324	F42/851314	F43/835289	F43/827276
R.L. west/east end (m above sea level)	821.0/818.4	833.6/829.5	835.8/831.9	861.0/856.1	873.6/871.1
TRENCH BEARING	125°	135°	150°	130°	140°
SURFACE VERTICAL OFFSET (m)	1.0	1.5	1.4 (NE side) 0.6 (SW side)	2.2	1.5
SCARP HEIGHT (m)	1.3	1.8	1.5 (NE side) ? (SW side)	3.0	1.9
FAULT ATTITUDE	025°/34 NW	045°/25 NW	065°/35 NW	045°/25 NW	050°/33 NW
SUBSURFACE VERTICAL OFFSET	2.5	3.5	1.7	?	?

mately 5 m deep, 5 m wide, and 50 m long with the fault scarp located above the center. When the fault zone was uncovered, the trench was deepened to expose both the upthrown and downthrown sides.

When the excavation was completed, an air compressor was used to blow air on the walls of the trench to clean them of loose debris. Rock hammers, picks, shovels, and brushes were handy tools to use for cleaning the trench walls. It was common for ground water to seep into the trench and accumulate at the bottom. The ponding created a hazard to the bulldozer and prevented deepening of the trench. The compressor was used to pump water out of the bottom of the trench.

The trench wall that was shaded for most of the day was chosen for detailed mapping. A 2-m x 2-m grid of string was hung across the wall for scale. The wall was then mapped and logged at a scale of 1:40 and photographs were taken.

When logging was completed, as much water as possible was removed from the trench. The trench was filled in and the original topsoil spread out over the surface. The area was reseeded and after a few months, very little trace of a trench site remained.

## A-2.0 Detailed Trench Descriptions

### A-2.1.0 Trench Descriptions: DC-5

#### A-2.1.1 Introduction

The northernmost trench in the Upper Nevis Basin, DC-5, was excavated across the fault trace on the south bank of Drummond Creek (see

Plate 1). In this locality, the Qf5 surface has been downcut and three lower degradational surfaces are preserved above the floodplain of Drummond Creek. Figure 15 is a large-scale geologic map of the DC-5 area showing the location of the Nevis Fault and the trench site, relative to the different surfaces. DC-5 was excavated in this area because the age of the surfaces are relatively young and there is evidence for progressive deformation of these surfaces (Figure 26 and Section 5.7.2.5.1). DC-5 was excavated partly on the highest degradation surface (Figure 15 and 26). This surface exists only on the upthrown side of the fault trace. Its downthrown equivalent is coincident with the downthrown side of the Qf5 surface. A detailed description of the formation of these surfaces with respect to recurrent movement on the Nevis Fault is presented in Section 5.7.2.5.1.

It was originally intended to trench the fault scarp on all four surfaces, however the presence of a water race on the Qf5 surface and high water levels in DC-5 discouraged this. The water table is only about 2 m below the ground surface, and the rate of inflow into the trench prevented excavation deeper than 4.5 m. A trench log is shown in Figure 31 and the photos in Figures 32, 33, and 34 show subsurface exposures in DC-5. A northwest-dipping reverse fault was identified in the trench but is not clear in the photographs.

#### A-2.1.2 Stratigraphy

In DC-5, 2.5-4.0 meters of fresh schist fan alluvium unconformably overlies deformed and sheared Tertiary sediments and weathered schist

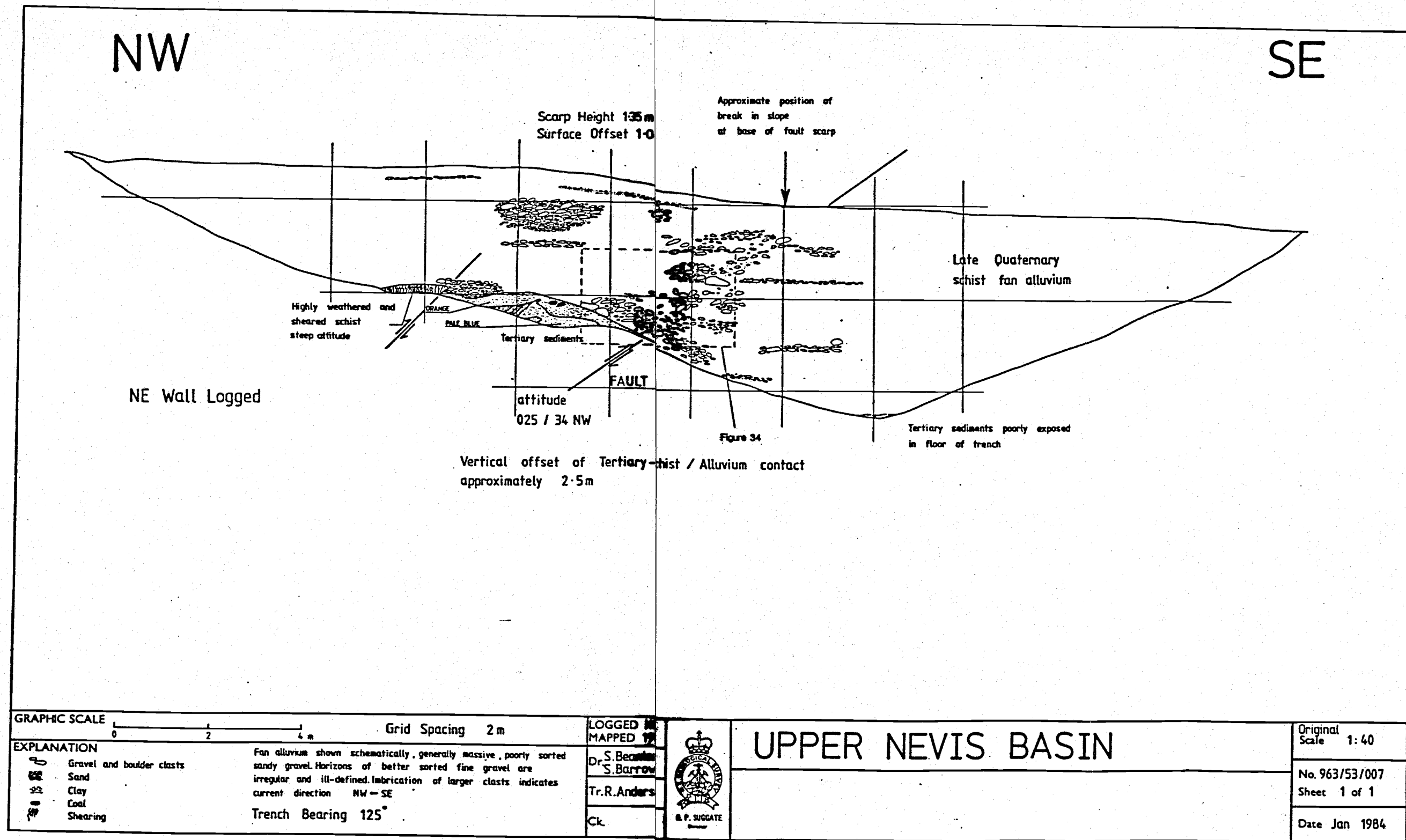


FIGURE 31 - Trench log, DC-5





FIGURE 32 - Quaternary fan gravels (Qf5) overlying deformed, weathered schist and Tertiary sediments (containing pods of coal) in the north-east wall of DC-5.

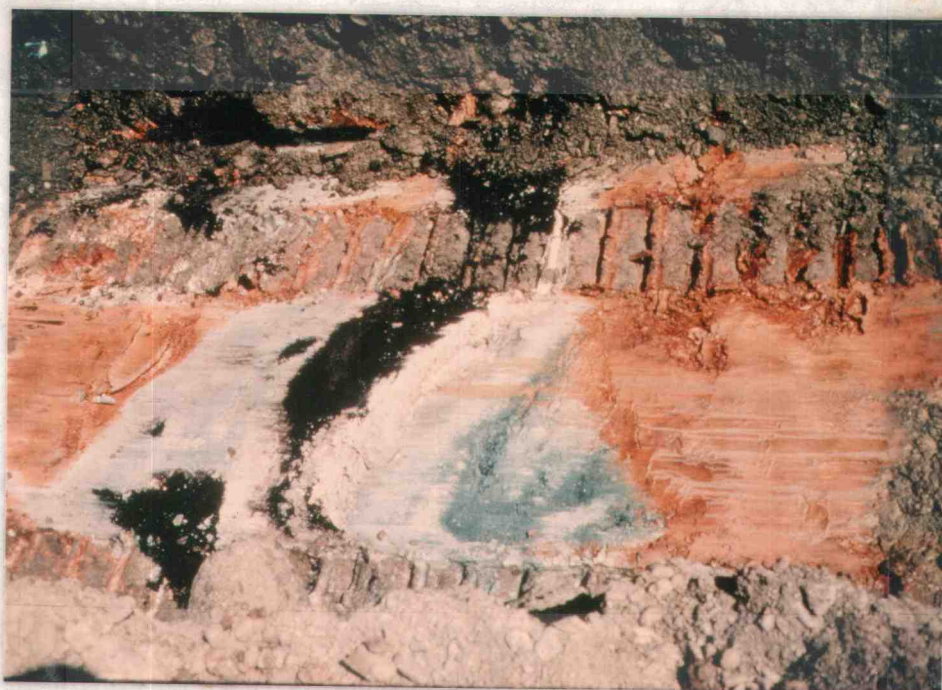


FIGURE 33 - Large black pod of coal and orange and blue weathered schist and Tertiary sediments in floor of DC-5 trench. Photo by Sarah Beanland, New Zealand Geological Survey.



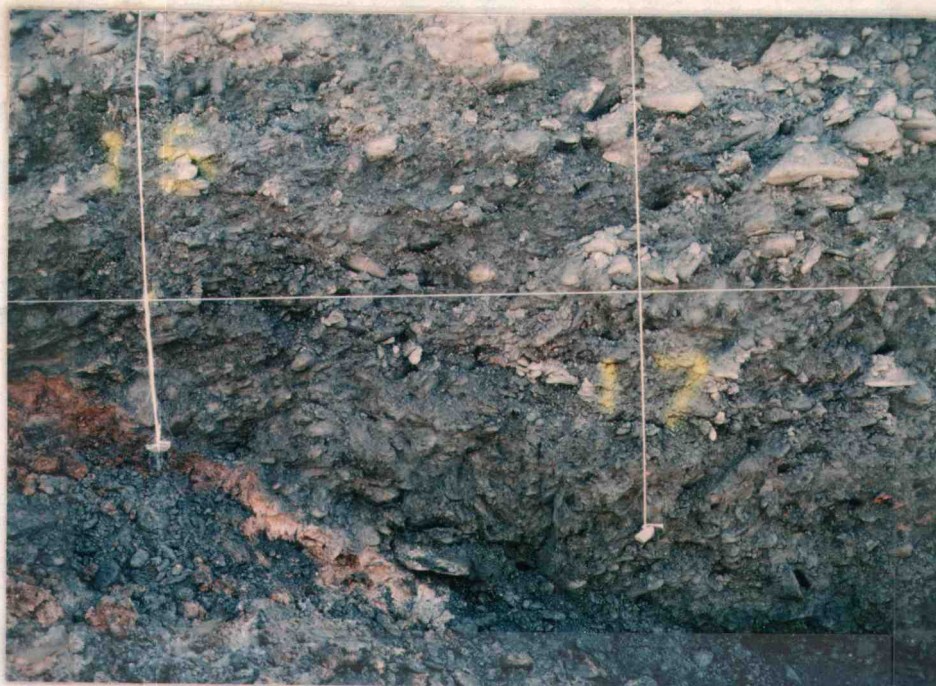


FIGURE 34 - Subtle fault zone in fan gravels (fault passes through the number 17), note subtle warping of gravels and alignment of gravels parallel to fault zone, northeast wall of DC-5.

(see Figure 31). The base of the fan alluvium is inferred to be approximately parallel to the ground surface and cuts across the underlying rocks with a strong angular unconformity.

Late Quaternary fan alluvium: This comprises a dark brownish grey, massive unweathered sandy gravel with cobbles and boulders to 40 cm. The gravel is loose, very poorly sorted and very poorly stratified. Occasional subhorizontal strata of fine or coarse gravel with no matrix are present. Subrounded clasts are of schist, and occasionally quartz, average diameter 5 to 10 cm, and the fine-to-coarse sandy matrix contains variable proportions of silt and clay. The unit is clast supported. Clasts are imbricated with their long axes plunging northwest, indicating deposition from a northwest direction, probably a paleo-Drummond Creek. Near-surface, the clasts are stained, and the matrix changes color to light brown. Soil development reaches a depth of 50 cm. Occasional horizons of manganese staining are present, especially near the base of the deposit.

Tertiary sediments and weathered schist: The sediments comprise mainly a bluish white, massive, micaceous silty clay deposit (see Figure 32) which contains lenses of angular quartz fragments, an unidentified white powdery (crushed?) mineral and pods of coal and carbonaceous silty clay. The unit is firm and poorly- to well-sorted, and in places has fine interbeds of blue, white and grey colored silt and sand. The clay portions are moderately plastic. The upper 0.25 m is oxidized to an orange color above a sharp but highly irregular contact. On the southwest wall there is a large pod of hard, black, shiny coal which is highly sheared and friable in places (see Figure 33).

Schist is present as a completely weathered, soft, dark creamy-

orange sticky clay with relict foliation and quartz laminae. This rock is intensely sheared and is plastic when damp. In places a dark green discoloration is associated with proximity to pods of coal. Rare areas of coherent schistose rock, only partly altered to clay, are noted.

### A-2.1.3 Structural Description

The contact between the fan alluvium and underlying schist and Tertiary sediments is warped down towards a fault (see Figure 31). The fault is a 0.5-m-wide zone of disturbance within the alluvium but the actual fault contact between the deformed schist/Tertiary sediments and alluvium was not excavated. The trench floor just reached the base of the alluvium on the downthrown side and a total vertical displacement of approximately 2.5 m was measured across the fault assuming the base of the alluvium to be horizontal. Within the fan alluvium the fault expression is extremely subtle (see photo in Figure 34). Several indistinct gravel horizons end abruptly against a 0.5-m-wide zone of chaotic and relatively loose gravel which often collapsed from the trench wall. Occasional orientation of clasts parallel to the fault zone and a slightly higher matrix content enabled recognition of the fault.

The schist and Tertiary sediments are intensely sheared throughout, and original bedding relationships are almost entirely destroyed. The fault identified in DC-5 has reverse movement on a northwest-dipping plane. The Tertiary sediments and schist are deformed throughout the exposure, suggesting that the fault occurred within a wider, pre-existing zone of deformation. Vertical displacement of 2.5 m measured in the trench is greater than the vertical surface offset of 1.0 m.

Since the surface on the upthrown side is degradational (Highest Degraded Qf5 surface), this discrepancy in offset represents progressive deformation. Figure 26 summarizes the sequence of faulting events that has occurred at the DC5 locality. Four faulting events are recognized (diagrams 1, 3, 5, and 7) which have occurred after the Qf5 fan was deposited. These four faulting events have resulted in a total of 1.6 m of vertical offset of the original Qf5 fan surface. One or more faulting events must have occurred while the fan was being deposited to account for the difference between the 1.6 m of surface offset and 2.5 m of subsurface vertical offset. The surface across which DC-5 is excavated has undergone three faulting events (diagrams 3, 5, and 7) since its formation.

No evidence for horizontal displacement is recognized although this does not preclude the existence of a strike-slip component of faulting.

#### A-2.2.0 Trench Description: DC-6

##### A-2.2.1 Introduction

DC-6 is located across a very distinct fault scarp where the fault trace crosses the Qf5 surface on the north side of Kingston Creek (see Plate 1).

Problems were experienced with the high level of the water table during both trench excavation and logging, as the water level rose in the trench to a depth of 2 m.

A trench log is shown in Figure 35 and the photos in Figures 36,

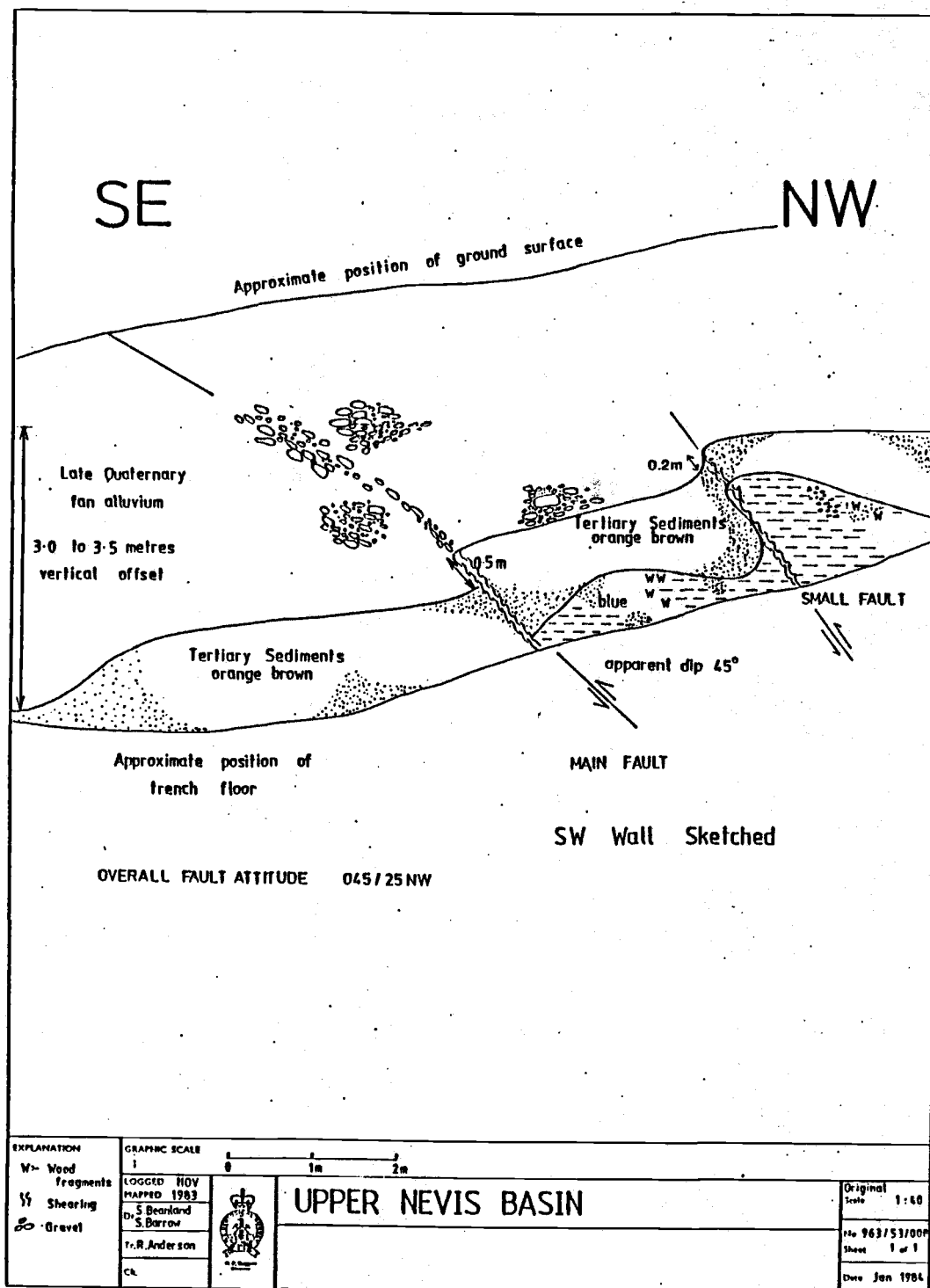


FIGURE 35 - Trench Log, DC-6





FIGURE 36 - Quaternary fan gravels (Qf5) overlying folded and faulted Tertiary sediments in the southwest wall of DC-6.



FIGURE 37 - Sand layer interbedded with Qf5 fan gravels drag folded on the upthrown side of a subtle fault zone in the northeast wall of DC-6.





FIGURE 38 - Close up view of southwest wall of DC-6 showing highly deformed Tertiary sediments, note tectonically incorporated Quaternary fan gravels.

37, and 38 show subsurface exposures in DC-6. The trench exposed a northwest-dipping reverse fault, readily identifiable in the gravels and Tertiary sediments.

#### A-2.2.2 Stratigraphy

Several meters of fresh schist fan alluvium overlie Tertiary sediments in DC-6 (see Figures 35, 36).

Late Quaternary fan alluvium: This deposit is very similar to that described for DC-5. A horizon of bluish grey sand approximately 0.5 m thick and 1 m long is present on the northwest wall, on the up-thrown side of the fault (see Figure 37). This is bent strongly down to the southeast where it ends within the fault zone. No equivalent horizon is recognized on the downthrown side of the fault.

Tertiary sediments: These are dominately blue, massive micaceous clayey silts with pods and lenses of purplish-brown carbonaceous silty clay, purplish-grey sand and fine gravel containing wood fragments and pale orange-brown loose sand (see photo in Figure 38). Approximately one meter of orange-brown sand overlies blue sand at the top of the Tertiary sediments (see Figure 38). The blue-orange color contrast is sharp and approximately parallel to the overlying Tertiary sediment/alluvium contact. However, the textural change across the contact is transitional. The color change is probably due solely to oxidation. The orange-brown sand shows fine color laminations in places, also probably a weathering phenomena. Occasional clasts of subangular to sub-rounded schist up to 15 cm occur within the upper orange brown sediments and are probably tectonically incorporated from overlying gravel.



### A-2.2.3 Structural Description

The main fault exposed in DC-6 displaces the top of the Tertiary sediments by approximately 0.5 m along the fault plane and consists of a narrow, intense zone of shearing in the Tertiary sediments. The sediments are also sheared at a smaller fault to the northwest (see Figure 35) where the zone of deformation is wider and the dip-slip displacement is less (0.2 m). Oxidation has occurred along the sheared zones.

Only the main fault is evident in the fan alluvium, where it consists of a 0.5-m-wide zone of oriented clasts (long axes parallel to the fault plane) which are more loosely packed than the surrounding alluvium. Figure 37 shows the looseness and darker coloration of the fault zone gravels.

Total vertical displacement across both faults is 3 to 3.5 m; the Tertiary sediment-alluvium contact indicates that this is due to both folding and faulting.

The trench reveals a wide zone of deformation associated with a distinct fault scarp at the surface. Uplift is accommodated by tilting and shearing along minor faults in a zone several meters wide. The fault plane meets the ground surface near the middle of the scarp rather than at the base. The latter is more common for reverse faults (compare Officers of the Geological Survey, 1983).

Total vertical displacement of the Tertiary sediment/alluvium contact is greater than the surface offset (3 to 3.5 m compared with 1.5 m) which suggests progressive deformation. It is uncertain how many fault movements are represented.

### A-2.3.0 Trench Description: DC-7

#### A-2.3.1 Introduction

DC-7 is located on the north bank of Wrights Creek (see plate 1). Figure 25 is a geologic map of the DC-7 area. The Qf5 surface is degraded in this area and the present day floodplain is only 1-1.6 meters lower in elevation than the Qf5 surface. DC-7 crosses the fault trace immediately south of the Qf5 fan such that the northeast wall exposes the faulted Qf5 fan and the southwest wall exposes floodplain deposits. At the trench site the floodplain is offset by approximately 0.6 m. The fault scarp crossing the floodplain is modified by an abandoned meander channel.

Problems were encountered with groundwater flowing rapidly into the trench which limited the depth of excavation and caused logging of the trench to be done quickly.

DC-7 exposed a northwest dipping reverse fault; a log is presented in Figure 39 and details are shown in Figures 40 to 43.

#### A-2.3.2 Stratigraphy

DC-7 exposes several meters of fan alluvium which unconformably overlies highly weathered, sheared schist (see Figure 39).

Late Quaternary fan alluvium: The fan alluvium is similar to that exposed in DC-5 and DC-6 and is not described in detail here. However, there is a slight difference in the color of the gravels across the fault zone; the gravels on the northwest, upthrown side are brownish-

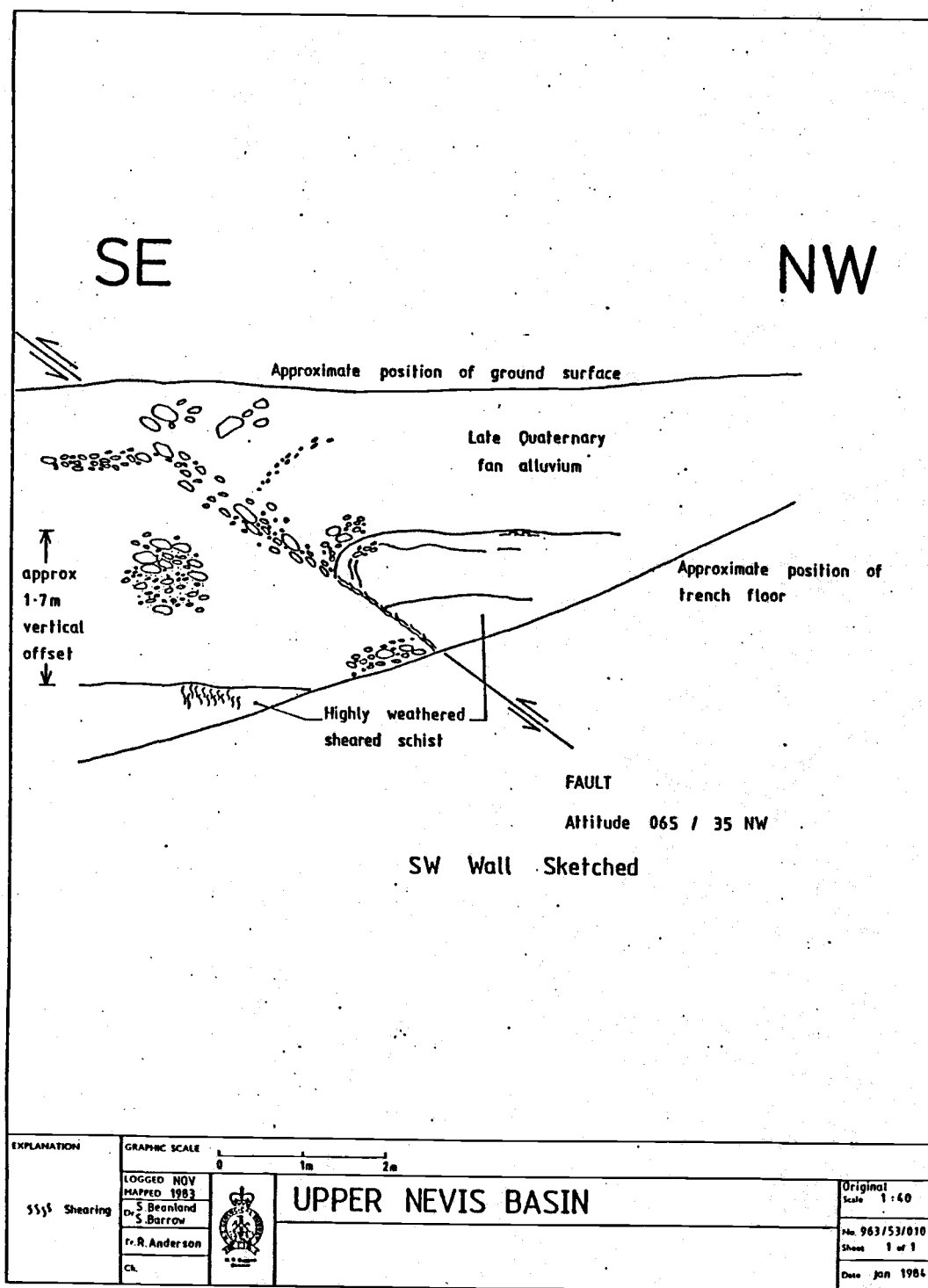


FIGURE 39 - Trench Log, DC-7

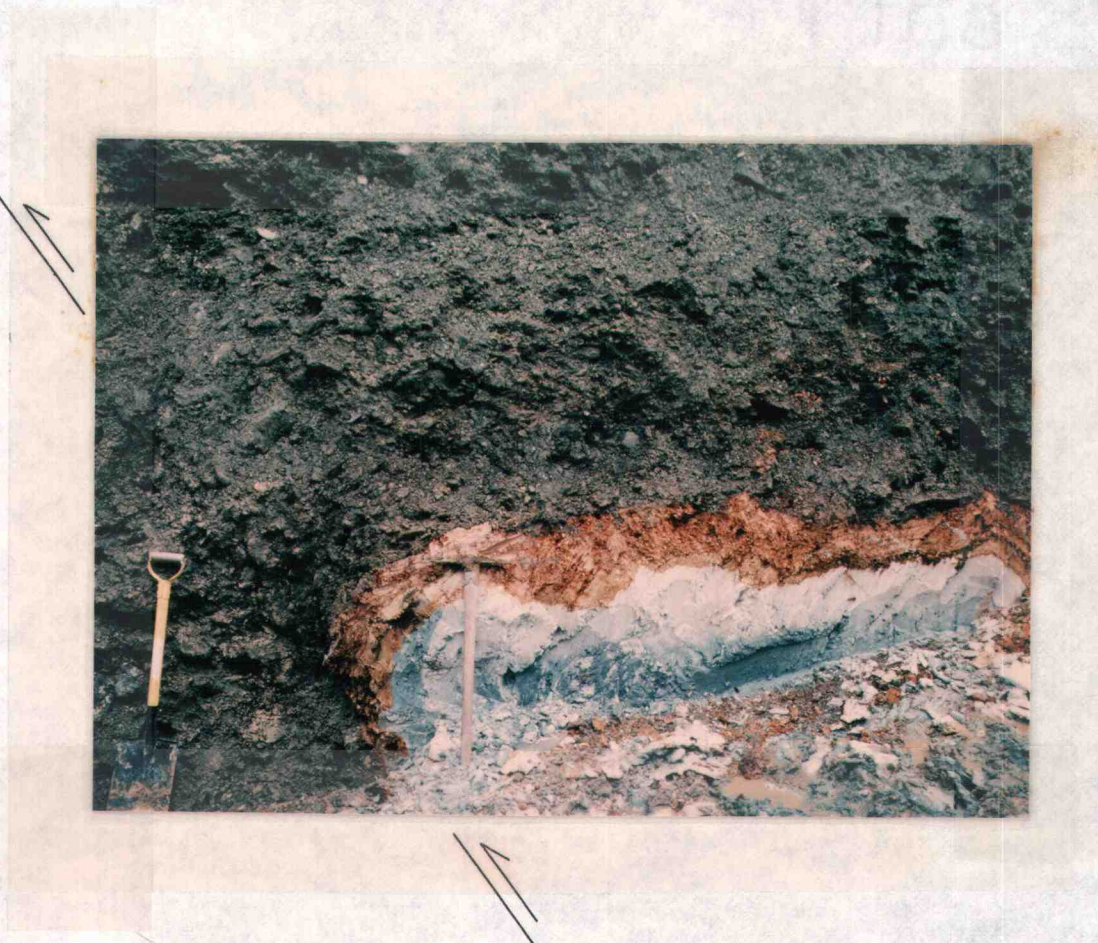


FIGURE 40 - Southwest wall of DC-7 showing deformed orange, white, and blue weathered schist thrust over Qf5 gravels, fault zone in gravels is subtle.





FIGURE 41 - Close up view of southwest wall of DC-7 showing highly deformed weathered schist and subtle fault zone in gravels.





FIGURE 42 - Northeast wall of DC-7 showing fault zone coated with manganese staining. Photo by Sarah Beanland, New Zealand Geological Survey.



FIGURE 43 - Northeast wall of DC-7 showing weathered schist thrust over Qf5 gravels.

grey whereas the gravels on the downthrown side are dark brown. In the southwest wall, the gravels near the floodplain surface are more poorly sorted and stratified than the gravels elsewhere in the trench. This may be the result of reworking during the degradation which has reduced the Qf5 surface to the modern floodplain. A sandy silt lens, 1 m long and 0.5 m thick, occurs at the base of a meander channel which cuts across the trench at the base of the surface fault scarp.

Schist: Highly weathered, sheared schist underlies the fan alluvium (see Figures 40 and 41). On the upthrown side of the fault, in contact with the fan alluvium, a 0.25-m zone of orange and dark red weathered, very finely laminated (0.1 - 1 mm thick) micaceous clay which contains relict schist foliation in places is present. This overlies 0.3 m of pale green sheared schist with relict foliation, and pods of powdery, white material (alteration product of feldspar?). Below this is an orange, light green and turquoise blue mottled highly weathered sheared schist which also contains pods of the powdery white material. On the downthrown side of the fault, orange, highly weathered sheared schist is in contact with the fan alluvium. This also is clay rich with pods of white material and relict foliation.

### A-2.3.3 Structural Description

The schist/alluvium contact is very gently sloping to the southeast on both sides of the fault but shows drag folding of the upthrown side down towards the fault within a meter of the fault (northwest side). The fault is distinctly expressed in the fan alluvium and by the overhang of schist over alluvium on the southwest wall (see Figures

40 and 41). The fault contact between the schist and fan alluvium is only a few centimeters wide and is very sharp. Shearing and oxidation occur along it.

The fault in the fan alluvium is a 0.5 to 1-m-wide zone that is looser, wetter and a darker brown color than the surrounding gravel (see Figures 40 to 43). It is locally stained black by manganese (Figure 42). On the upthrown side clasts are oriented with long axes dipping towards the fault plane due to drag folding, and clasts within the fault zone are oriented with long axes parallel to the fault.

The fault is exposed in both walls of the trench despite degradation of the fan alluvium on the southwest side. (The floodplain surface is underlain by reworked Qf5 fan alluvium.) It cannot be determined from the trench exposure whether the fault has moved in post-degradational times because the gravels underlying the floodplain have been reworked during the degradation and their lack of structure causes difficulty in tracing the fault towards the surface. The fault crossing the floodplain surface, however, suggests that faulting has occurred since Wrights Creek incised to the present level. Vertical displacement in the trench is approximately 1.7 m which is slightly greater than the 1.4 m surface offset measured on the Qf5 surface northeast of the trench.

Since the floodplain is faulted at the trench site, progressive deformation is indicated by the difference in subsurface displacement (1.7 m) and surface offset (0.6 m). The floodplain is also faulted 150 m to the southwest (surface offset 1.3 m, see Figure 25).



#### A-2.4.0 Trench Description: DC-8

##### A-2.2.4.1 Introduction

DC-8 is located on the south side of an unnamed creek which flows from the Hector Range and meets the Nevis River opposite the mouth of Roaring Lion Creek (see Plate 1). The trench was excavated on the Qf5 surface across a distinct fault scarp.

A northwest-dipping reverse fault was recognized in DC-8 and is sketched in Figure 44. The photos in Figures 45 and 46 indicate the subtlety of the deformation exposed in the trench.

No groundwater was encountered, possibly because there were no impermeable Tertiary sediments exposed in the trench and the trench was located close to the terrace scarp next to the floodplain.

##### A-2.4.2 Stratigraphy

Late Quaternary fan alluvium: The fan alluvium is the same as described in DC-5. No other lithologies are present.

##### A-2.4.3 Structural Description

The fault identified in DC-8 is subtly expressed and consists of a 0.5 m to 1 m-wide zone of poorly structured gravel. Clast orientation parallel to the fault is present, and poorly developed horizons within the alluvium on either side of the fault end abruptly against it. No horizons are traceable across the zone. No drag folding is evident

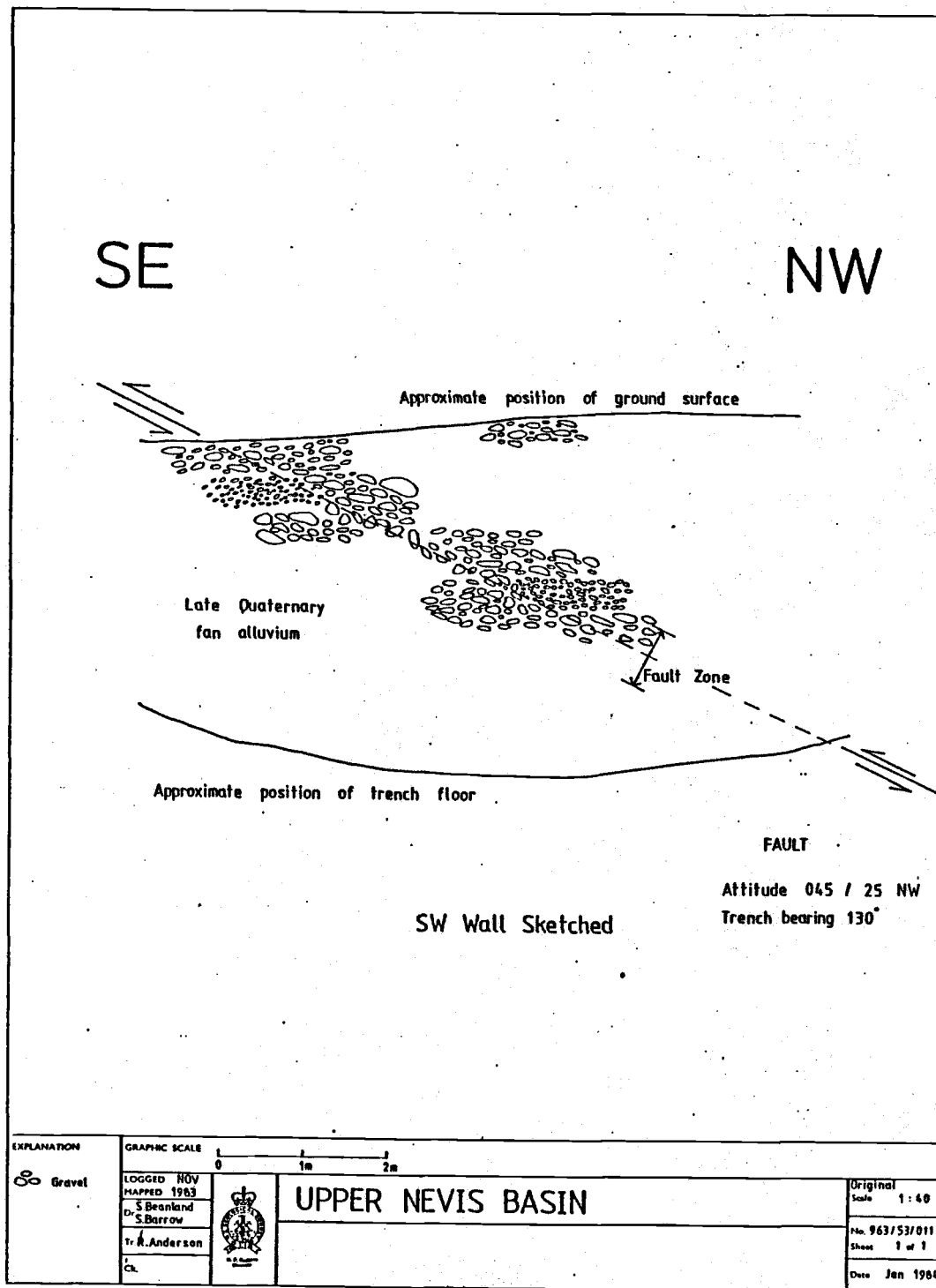


FIGURE 44 - Trench Log, DC-8



FIGURE 45 - Northeast wall of DC-8 showing subtle fault zone, pick is oriented with handle in fault plane.



FIGURE 46 - Southwest wall of DC-8 showing subtle fault zone, pick is oriented with handle in fault plane.

within the gravels.

The fault intersects the ground surface near the foot of the scarp. DC-8 did not provide any further data on magnitude of deformation or number of displacements. The poorly sorted, massive nature of the alluvium prevented clear definition of the fault zone, and it is probable that in similar natural exposures, where surface information was not available, recognition of such a fault would be extremely difficult. The photos in Figures 45 and 46 show the subtlety of the fault in the fan gravels.

#### A-2.5.0 Trench Description: DC-9

##### A-2.5.1 Introduction

DC-9 is located on the north bank of the southernmost tributary stream flowing into the Upper Nevis Basin (see Plate 1). An old miner's hut is located 300 m to the west of the trench site. The trench crosses an indistinct scarp with a surface offset of 1.5 m. Groundwater was not encountered in DC-9.

Figure 47 presents a trench log of DC-9 and the trench exposure is shown in the photos in Figures 48 and 49. A northwest dipping reverse fault is readily identified.

##### A-2.5.2 Stratigraphy

Late Quaternary fan alluvium: The fan alluvium is similar to that in DC-5. There is, however, a slight difference found between the gra-

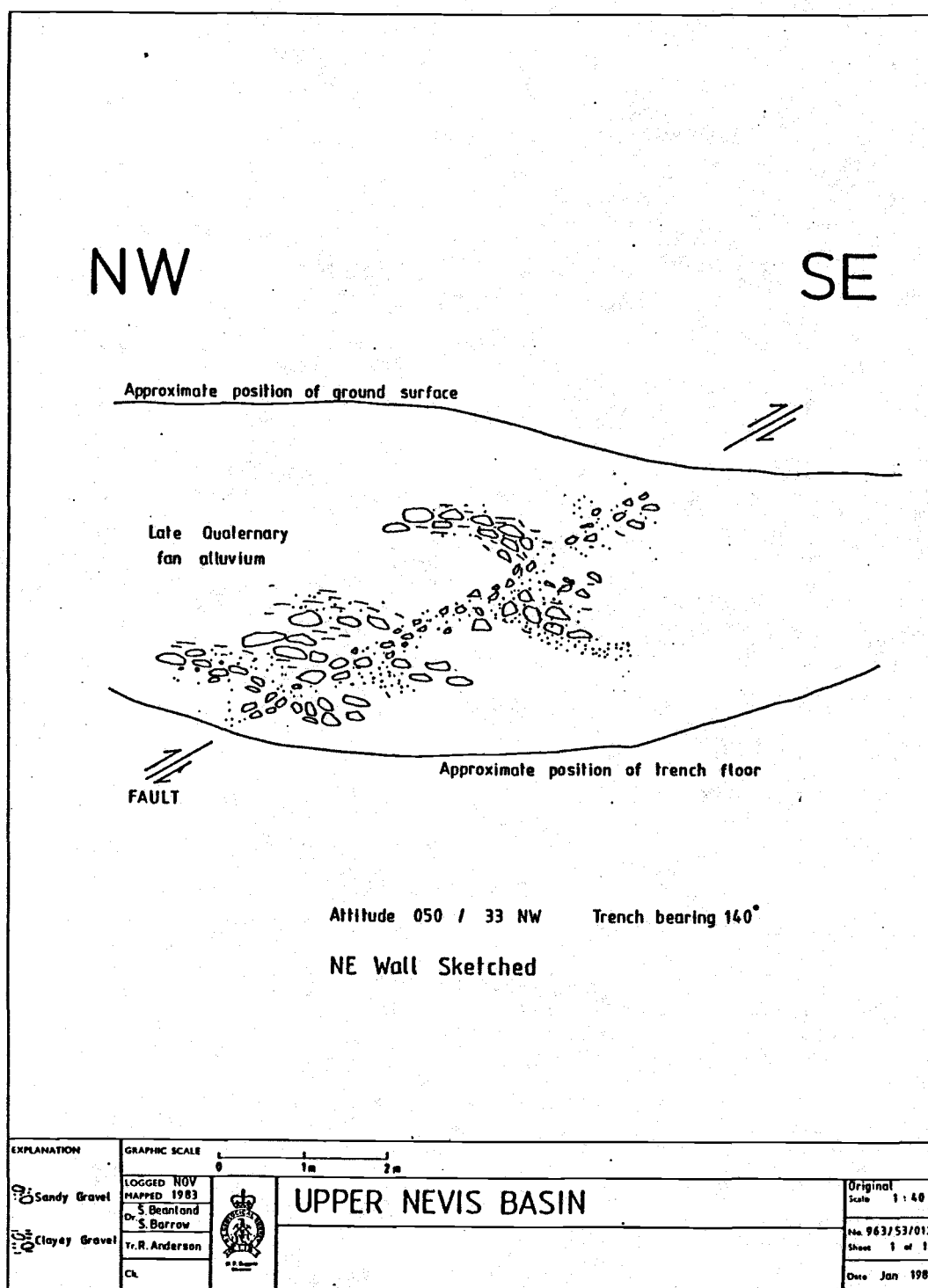


FIGURE 47 - Trench Log, DC-9





FIGURE 48 - Northeast wall of DC-9 showing subtle fault zone in gravels, top of pick touches fault plane.



FIGURE 49 - Southwest wall of DC-9 showing subtle fault zone in gravels, handle of shovel touches the fault plane.

vels across the fault zone. The gravels are coarser on the upthrown side (average clast size 10 cm) than on the downthrown side (average clast size 3 cm). The upthrown side is firm with a clay rich sandy matrix while the downthrown side is looser with a coarse, sandy matrix.

#### A-2.5.3 Structural Description

The fault is a subtle, 0.5-m-wide northwest-dipping feature and consists of very loose, chaotic subangular gravels with very little matrix. Some crudely horizontal beds are truncated at the fault. The fault zone can be seen on both sides of the trench and intersects the ground surface at the base of the scarp. Some clasts on the upthrown side of the fault show tilting towards the fault, possibly due to drag along the fault.

No data for magnitude or number of fault displacements were obtained from DC-9.

#### A-3.0 Conclusions from Trenching

All five trenches excavated in the Upper Nevis Basin exposed a northwest-dipping reverse fault associated with surface offset crossing the Qf5 fan surface, and verified that surface scarps represent deformation on late Quaternary faults. The faults were generally difficult to identify within the Qf5 fan alluvium but were easily recognizable where Tertiary sediments and/or weathered schist were in fault contact with the fan alluvium. Tertiary sediments and weathered schist were intensely sheared and deformed wherever exposed, suggesting the pre-

existence of a zone of deformation wider and presumably older than the currently active fault rupture. Progressive deformation of the Nevis Fault is recognized by the difference in offset between the surface and the subsurface at the DC-5, DC-6 and DC-7 trench sites and by the increase in offset of progressively older surfaces at the DC-5 locality. In the DC-5 area, five events are recognized; one event occurred during the time when the Qf5 fan was being deposited and four events occurred after the Qf5 fan was completely deposited (see Section 5.7.2.5.1 for details).



## APPENDIX B - SCARP MORPHOLOGY

### B-1.0 Introduction

Recent studies of the geomorphology of Late Quaternary fault scarps and wave-cut shoreline scarps in the western United States have led to the development of several techniques from which the age of these scarps can be assessed (Wallace, 1977; Bucknam and Anderson, 1979; Nash, 1980; Machette, 1982; McCalpin, 1982; Hanks, et al., 1983; Colman and Watson, 1983). These techniques are based on the theory that the geomorphic character of a scarp changes in a predictable way as the scarp is degraded with time.

### B-2.0 Fundamentals of Scarp Degradation

Wallace (1977) was the first to describe the sequence of steps that occur during the degradation of a fault scarp in unconsolidated alluvium (Figure 50A-50E) illustrates the steps of scarp degradation occurring after a single faulting event. Surface rupture along a fault during an earthquake usually produces a fault scarp with a steep face (the "free face") and a sharp "crest" (labelled "c" in Figure 50). The free face has a slope between  $45^\circ$  and overhanging (Figure 50A). Because the material is unconsolidated, debris immediately begins to spall off the free face by gravity. It accumulates at the base of the scarp and forms a "debris slope" at the angle of repose of the material (between  $34-37^\circ$ ) (Figure 50B). Below the debris slope, a wedge of alluvium accumulates (the "wash slope") which overlaps the debris slope

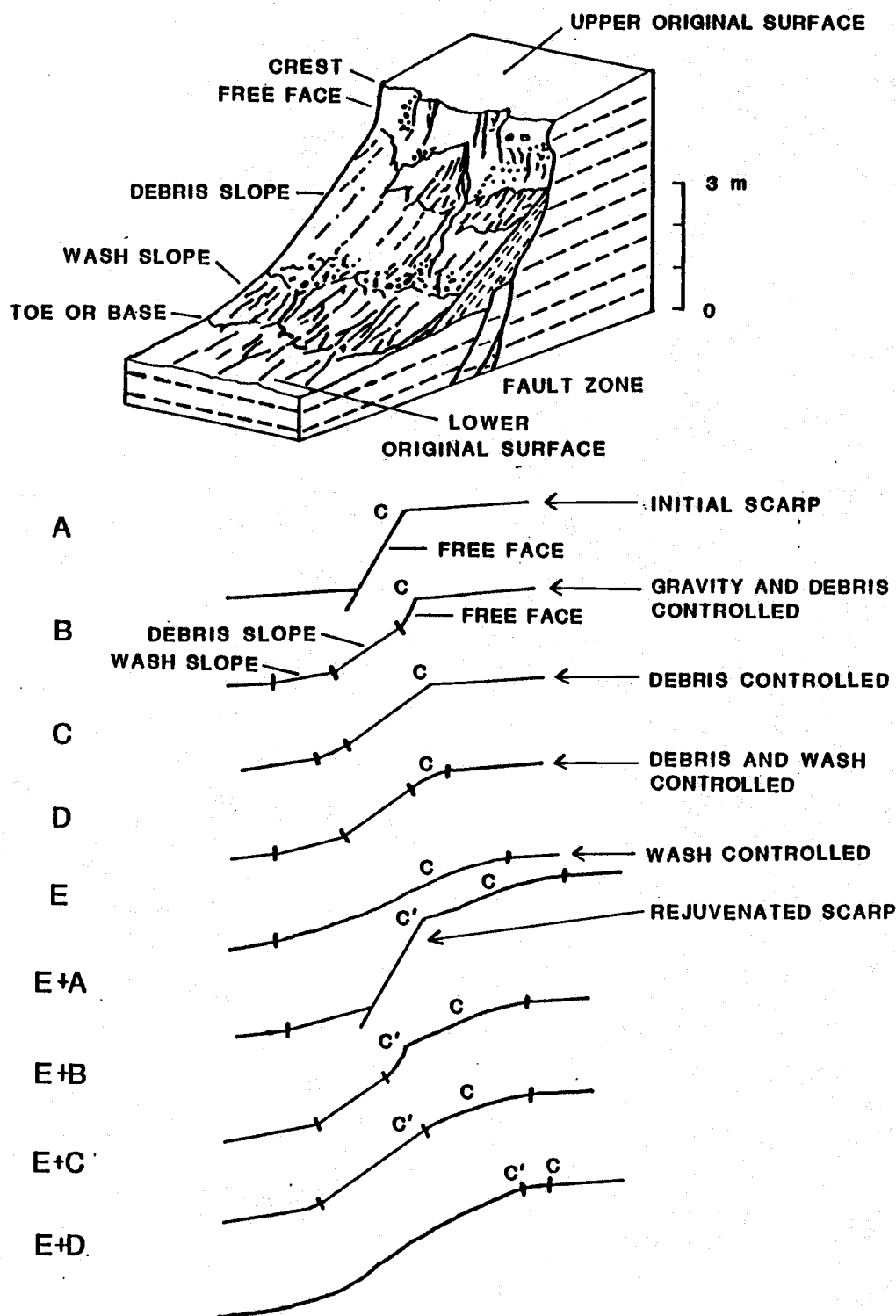


FIGURE 50 - Sequence of steps in the degradation of a single event fault or terrace scarp (A to E) and a multiple event fault scarp (E+A to E+D). "c" represents the original scarp crest, "c'" represents the crest of the rejuvenated scarp. Modified from Wallace, 1977, Fig. 2 and McCalpin, 1982, Fig. 46.

and the lower original fan surface (Figure 50B). The free face eventually buries itself (Figure 50C) and the crest becomes rounded (Figure 50D). As wash-controlled erosion and sedimentation processes become dominant, the slope of the scarp gradually decreases and the shape of the profile is modified with time (Figure 50E).

Although Wallace's work was done on scarps which formed during normal faulting events, subsequent studies have shown that the same sequence of steps applies to scarps formed by other processes as well. Processes such as undercutting by wave erosion to form a seacliff (Bucknam and Anderson, 1979; Hanks, et al., 1983) or undercutting by a river to form a terrace (Pierce, K.L., 1984; pers. comm.; Nash, 1984) can produce a scarp that will degrade in the same way as a fault scarp.

### B-3.0 Degradation of Reverse Fault Scarps and River-cut Terrace Scarps

The trenching investigation in the Upper Nevis basin (Appendix A) exposed a northwest dipping reverse fault in each of the trenches excavated across the Nevis Fault. Most of the recent scarp morphology studies have concentrated on the degradation of normal fault scarps and wave-cut shoreline scarps. It is the purpose of this study to try the same techniques on reverse fault scarps and river-cut terrace scarps in the Upper Nevis Basin.

#### B-3.1 Reverse Fault Scarps

Scarps formed during a reverse faulting event may differ in their morphology from a normal fault at the time of surface rupture. With

time however, the morphologic changes accompanying scarp degradation may be similar. Figure 51 illustrates three possible initial configurations of surface deformation accompanying a reverse faulting event. There are many combinations of these three configurations that are possible; therefore, the configurations shown in Figure 51 are considered to be "end-members". Diagram 1A shows that when surface rupture occurs the reverse fault scarp may be vertical to overhanging. Diagram 1B shows that if the scarp is vertical, the free face is formed immediately; and, if the scarp is overhanging, the free face forms as soon as the overhanging material falls off. The slumped material accumulates at the base of the scarp, forming a debris slope underlying the free face, much like the initial configuration of a normal fault scarp (see Figure 50). In this case, scarp degradation will occur in a similar way as for normal faults. In support of this style of surface rupture, Berberian (1978) showed that many of the reverse fault scarps associated with the Tabas e-Golshan, Iran, earthquake of September 16, 1978 had very steep (up to  $80^\circ$ ) near-vertical faces.

Diagram 2A (Figure 51) shows that surface rupture may be caused by a "tank tread" model of reverse faulting where unconsolidated alluvium displaced by the fault immediately spills over itself in a chaotic fashion and may be overridden by the fault. The unconsolidated material will settle out and adjust itself to a new equilibrium at the angle of repose of the material (Diagram 2B). In this case, a free face may or may not be developed. If there is no free face, the scarp will begin to degrade by wash-controlled processes rather than gravitational. Reverse fault scarps of this type may degrade to a rounder and gentler form sooner than normal fault scarps because no additional time is

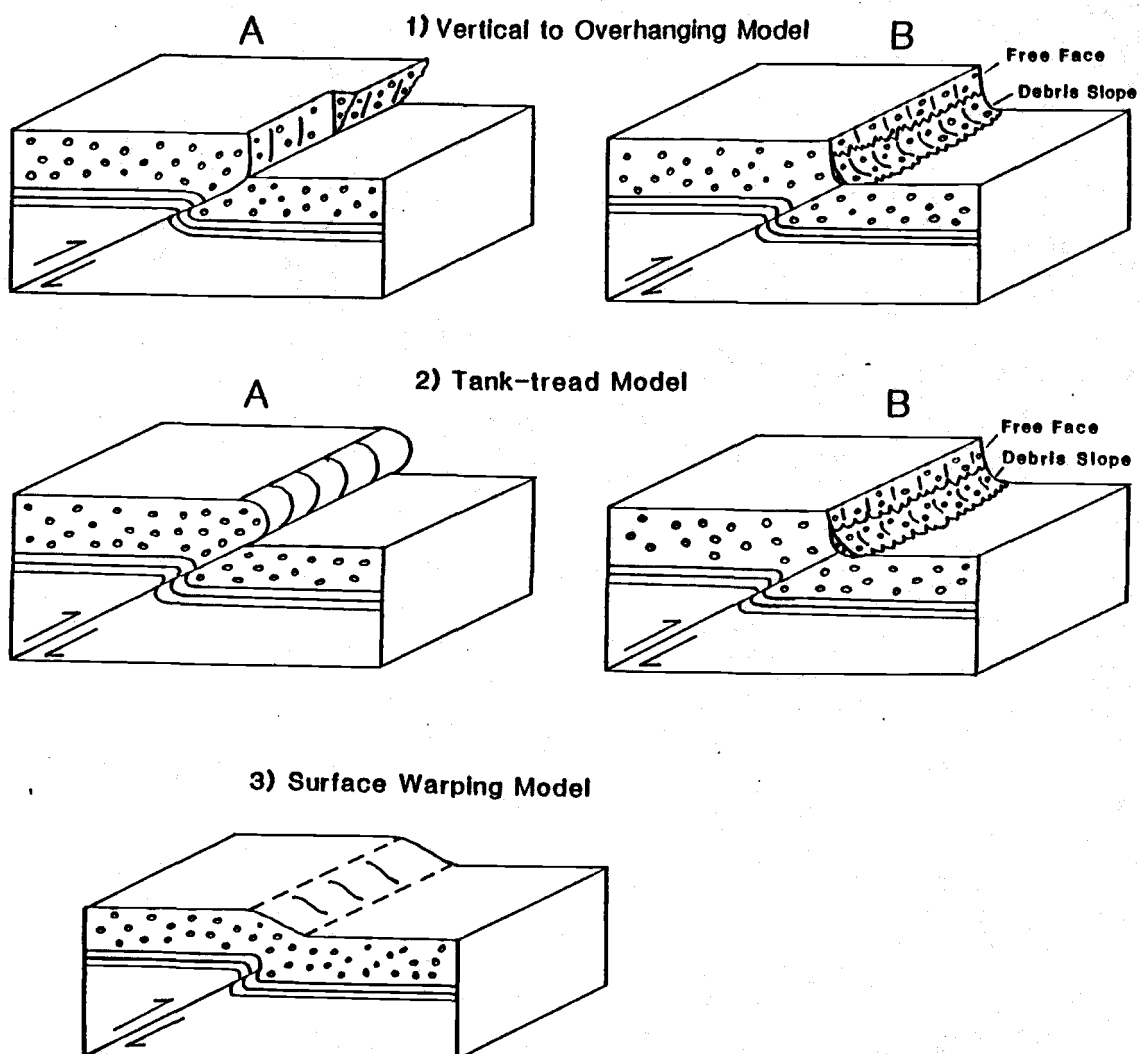


FIGURE 51 - Initial configurations of a reverse faulting event.

necessary to erode a free face. If a free face does form initially, then the scarp will degrade similarly to a normal fault scarp.

Diagram 3 (Figure 51) shows that the initial configuration may be one of surface warping with no actual surface rupture. In this case, the surface offset would be due to folding of the surface rather than fault rupture. If the initial slope angle of the warp is near or greater than the angle of repose of the material, then the scarp morphologic techniques discussed in this appendix will probably be applicable. If the slope angle of the warp is less than the angle of repose, then the techniques may not be applicable.

It is assumed that in the Upper Nevis Basin, all scarps were formed by surface rupture in the style of Diagrams 1 or 2 (Figure 51) rather than by surface warping (Diagram 3). One line of evidence supporting surface rupture as in Diagrams 1 or 2 is that in the trenches, the fault plane almost intersects the ground surface (it is shallowly buried by material degraded from the fault scarp; see trench logs and photographs in Appendix A) whereas with surface warping as in Diagram 3, the fault plane does not intersect the ground surface.

### B-3.2 River-cut Terrace Scarps

A river-cut terrace scarp forms when a downcutting river carves its banks to a slope angle greater than the angle of repose of the material it is eroding. When the river ultimately abandons its channel, it leaves a terrace scarp rising above the surface of its abandoned floodplain. The terrace scarp will degrade in the same fashion as a normal fault scarp. The age assessed for the terrace scarp, based on

its degree of degradation, yields the age of the surface at the base of the scarp because the scarp began to degrade at the same time as the surface at its base was abandoned. Terrace scarps provide a range of scarp heights that can be used to determine the age of the surface at their base. It is assumed that the time of formation of a terrace scarp is short compared to the elapsed time since its formation.

#### B-4.0 Comparison of Upper Nevis Basin with Western United States

To compare scarp morphology data from different regions, especially between the western United States and New Zealand, may or may not be legitimate. The factors that influence the rate of scarp degradation must be compared and the effects of any factors that differ must be weighed. The factors which most influence the rate of scarp degradation are 1) landscape, 2) texture and cohesion of the faulted, wave-cut, or river-cut material, 3) climate and 4) vegetational cover.

The general landscape of the Upper Nevis Basin is a basin and range topography that is very similar to the basin and range topography of western Utah, Nevada, Colorado and New Mexico where other scarp morphology studies have been done. The fault scarps, wave-cut shoreline scarps, and river-cut terrace scarps in all of these studies were cut across alluvial fan surfaces composed of unconsolidated, coarse alluvium eroded from adjacent ranges.

The climate of the Upper Nevis Basin is semi-arid with an average rainfall of slightly greater than 50 cm per year. It is wetter than the arid climates of New Mexico and Utah which have average rainfalls of 12 cm per year. It is uncertain what the effect of a wetter climate

is on scarp degradation rates. The effect of higher precipitation may be to increase degradation rates since downslope movement is mainly wash controlled and limited to processes such as soil creep, raindrop impact and slope wash (Colman and Watson, 1983) which are precipitation-dependent. However, higher precipitation would allow a heavier vegetational cover to develop which would protect the slopes from downslope movement thereby slowing down the degradational process. Bucknam and Anderson (1979) stated that in their study area in western Utah, the ground is covered 7-20% by sagebrush and shadscale. In the Upper Nevis Basin, the ground is covered approximately 75% by tussock grasses, speargrass and sphagnum mosses. Clearly, the Upper Nevis Basin has a greater vegetational cover than western Utah. Although the Upper Nevis Basin has a wetter climate, the fact that it has a greater vegetational cover may mean that the scarp degradation rate is slower than western Utah. On the other hand, the two effects may balance, allowing the degradation rates to be similar in both regions. It is assumed for this study that the degradational rates are similar between the western United States where scarp morphology has been studied and the Upper Nevis Basin despite their differences in climate and vegetational cover. This assumption is made with caution, because scarps of the Upper Nevis Basin are not age calibrated.

#### B-4.0 Scarp Morphometric Parameters

Quantitative scarp morphology data is derived from detailed topographic profiles which are measured perpendicular to the trace of the fault or terrace scarp. Scarp morphometric parameters such as scarp



height ( $H$ ), maximum scarp-slope angle ( $\theta$ ), original surface slope ( $\infty$ ), and surface offset ( $D$ ), were defined by Bucknam and Anderson (1979). Figure 52A is a diagrammatic profile of a fault scarp formed during a single faulting event which shows how the various parameters are graphically determined.

Machette (1982) expanded Bucknam and Anderson's work to include scarps formed by multiple faulting events. He recognized that a multiple event fault scarp will have the steep scarp slope angle of the most recent event and an anomalously high scarp height ( $H_m$ ) which is the cumulative result of more than one event. Scarps which are formed by multiple movements can be recognized in the field by 1) pronounced breaks in slope or bevels on scarp profiles (Figure 52B), 2) benches or terraces along channels that dissect the scarp, 3) multiple knickpoints on channels that dissect the scarp, 4) scarp heights that exceed the maximum recorded for a single event (10.7 m; Richter, 1958), 5) complex erosion-sedimentation records, and 6) displacement of older deposits by greater amounts than younger deposits (Wallace, 1977). Multiple event scarps display distinct breaks in slope above and/or below the steepest part of the scarp (Figure 52B). These bevels are the erosional remnants of fault scarp profiles formed during previous fault movements (Machette, 1982; McCalpin, 1983). Figure 50 (E+A to E+D) shows the sequence of steps in the degradation of a multiple event fault scarp where c-c' represents the bevel. Figure 52B shows the scarp morphometric parameters for a multiple event fault scarp. The steepest scarp slope angle ( $\theta$ ) is the slope of the most recent faulting event. The slope angle ( $\theta'$ ) is the angle of the beveled surface representing the previous scarp profile. The scarp height of a single event is ( $H_s$ )

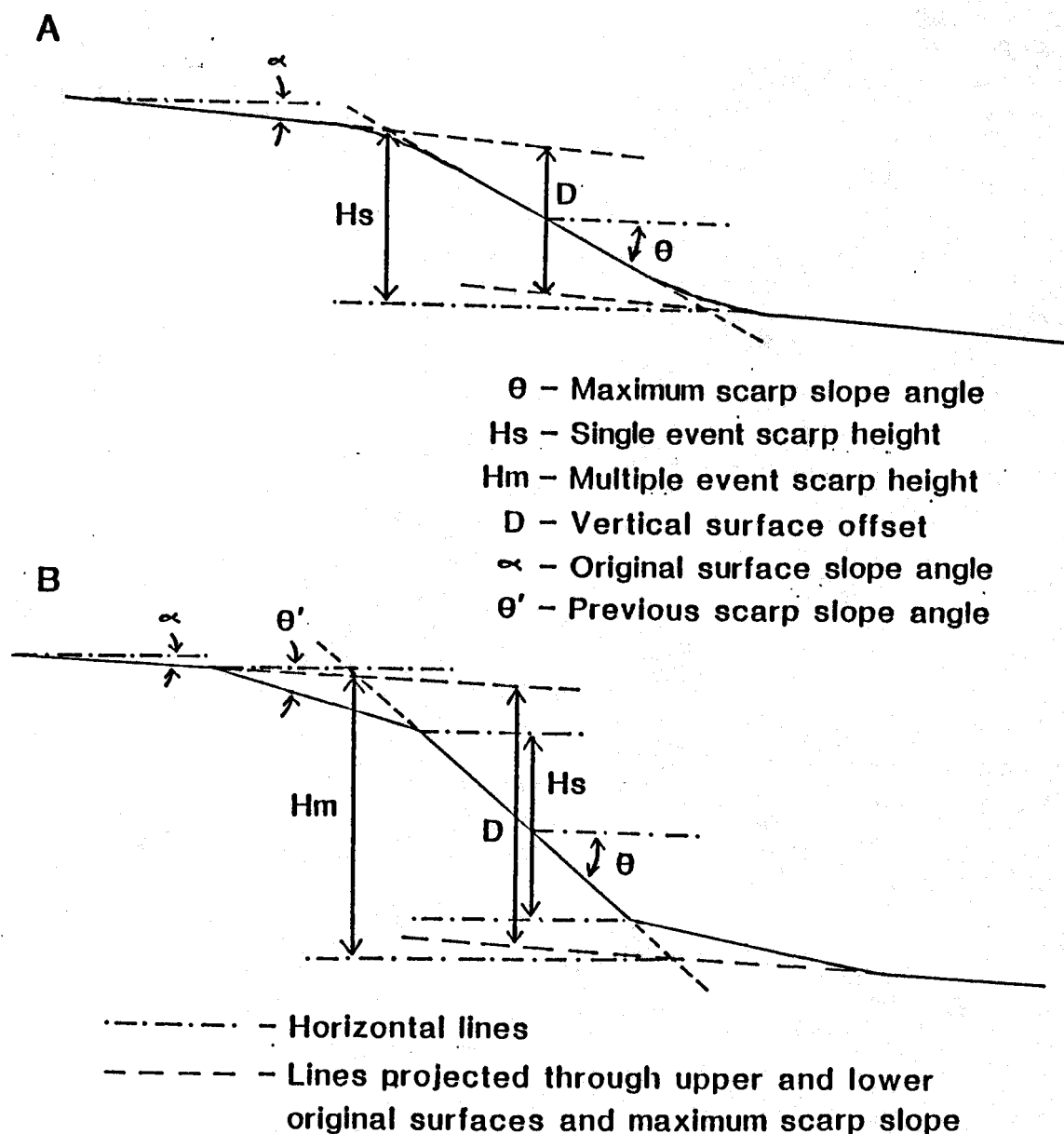


FIGURE 52 - Diagrammatic profiles of A. a single-event fault scarp (modified from Bucknam and Anderson, 1979, Fig. 1) and B. a multiple-event fault scarp (modified from Machette, 1982, Fig. 3) showing how the scarp morphometric parameters are graphically determined.

while the scarp height of the multiple event is ( $H_m$ ). Note that surface offset ( $D$ ) cannot be determined for the single event.

#### B-6.0 Method of Data Collection

In the Upper Nevis basin, scarp morphology data were derived from detailed topographic profiles measured in the field using theodolite and electronic distance measurement (EDM) equipment. Profiles were measured from an instrument station to a traveling reflecting prism pole that was carried in a direction perpendicular to the fault scarp or terrace scarp. Geographical coordinates for each point on the profile were calculated from bearing and distance measurements from the instrument station. Topographic levels were derived from vertical angles relative to the instrument station. Coordinates and levels are accurate to 5 cm. The combined Theodolite-EDM was a Sokkisha SDM3C and Sokkisha triple reflecting prism mounted on a telescopic prism pole. Scarp profiles were plotted at 1:100 and 1:250 scales. Each scarp was also plotted at five times vertical exaggeration (1:50) to highlight subtle features. Scarp morphology parameters,  $H_s$ ,  $H_m$ ,  $\theta$ ,  $\alpha$ , and  $D$  were calculated from these profiles. Representative fault scarp profiles are shown in Figure 53 and terrace scarp profiles in Figure 54. Table 4 displays data for single event fault scarps, Table 5, for multiple event fault scarps and Table 6 for river-cut terrace scarps. The data for terrace scarps in Table 6 are grouped according to the surface that lies at the base of the scarp. Each group of terrace scarps should represent a single age.

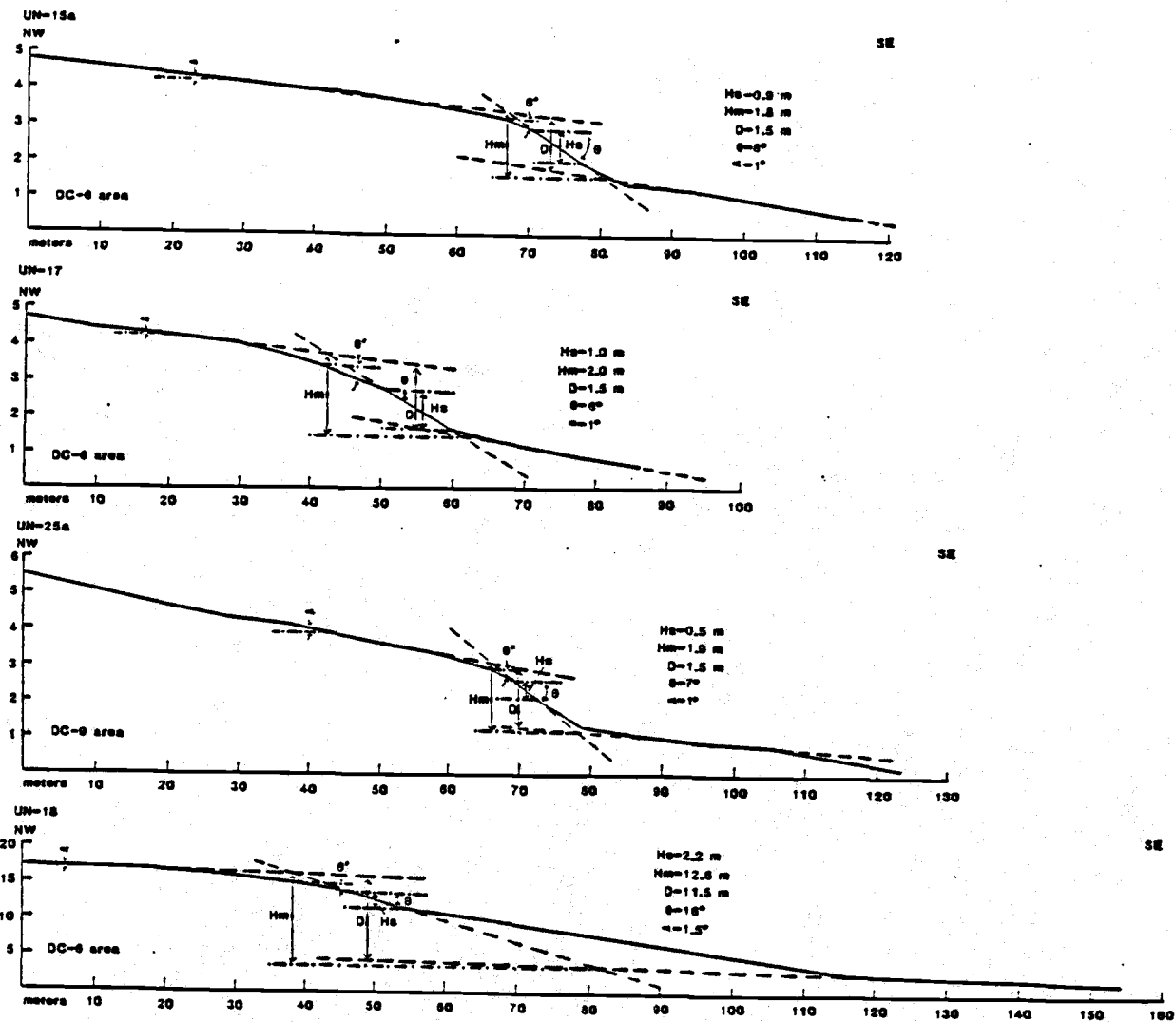


FIGURE 53 - Representative fault scarp profiles, Upper Nevis Basin. UN-15a, 17 and 25a are multiple event fault scarps crossing the Qf5 surface. UN-18 crosses a Qf3 surface.

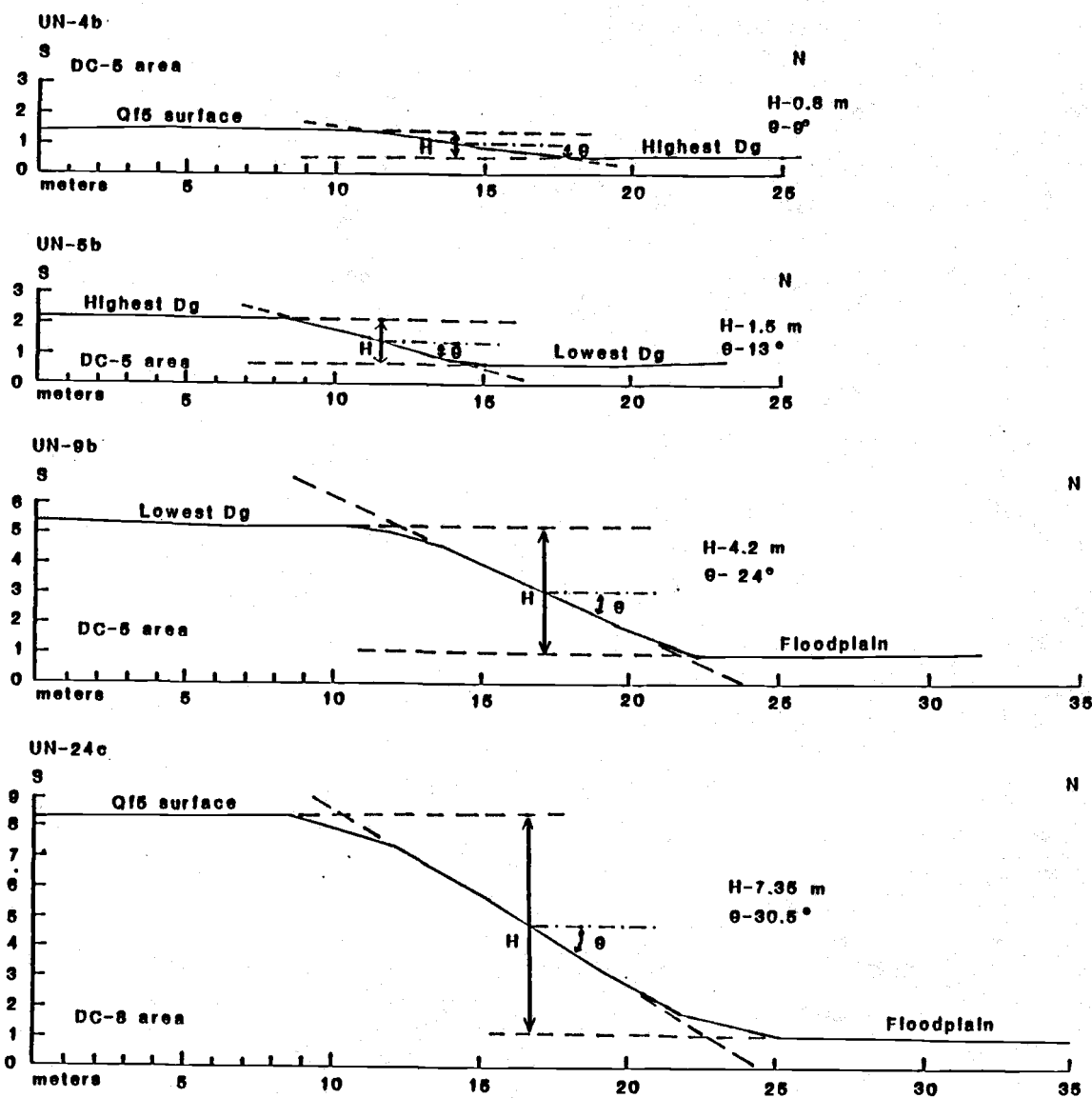


FIGURE 54 - Representative river-cut terrace scarp profiles, Upper Nevis Basin.

TABLE 4 - SCARP MORPHOLOGY DATA FOR SINGLE EVENT FAULT SCARPS

PROFILE NUMBER	LOCALITY	SURFACE DISPLACED BY FAULT	Hs (m)	$\theta$ (°)	$\alpha$ (°)	D (m)	$c\tau$ $\theta_0=28^\circ$	$c\tau$ $\theta_0=30^\circ$
UN-1	DC-5	Highest Dg	0.4	7	1	-	1.10	1.11
UN-2	DC-5	Lowest Dg	-	-	2	0.3	-	-
UN-8	DC-5	Qf5	0.6	9	2	-	1.76	1.78
UN-10a	DC-7	Qf5	0.5	7	2	-	2.50	2.51
UN-10b	DC-7	Qf5	0.6	12	2	-	0.79	0.81
UN-15a	DC-6	Qf5	0.9	8	1	-	4.01	4.05
UN-15b	DC-6	Qf5	1.1	10	2	-	4.43	4.49
UN-17	DC-6	Qf5	1.0	6	1	-	10.06	10.10
UN-19a	DC-8	Qf5	0.8	7	1	-	4.40	4.43
UN-19b	DC-8	Qf5	0.4	6	1.5	-	1.99	2.00
UN-22	DC-8	Qf5	0.5	11	2	-	0.70	0.71
UN-25a	DC-9	Qf5	0.5	9	1	-	0.93	0.94
UN-25b	DC-9	Qf5	0.9	7	2	-	8.09	8.13
UN-13	DC-7	Qf4	1.8	20	2	-	1.34	1.51
UN-18	DC-6	Qf3	2.2	16	1.5	-	4.17	4.41
UN-20	DC-8	Qf3	2.6	15	3	-	9.24	9.63

Average Values:  $H_s = 0.99$  m  
 $\theta = 10^\circ$   
 $c\tau(\theta_0=28^\circ) = 3.70$   
 $c\tau(\theta_0=30^\circ) = 3.77$

Locality DC-5 (etc.) is the area within 0.5 km of the DC-5 (etc.) trench site.  
Trench sites are located on Plate 1.

Dg - Degraded Qf5 surface  
Hs - Height of a single event fault scarp  
 $\theta$  - Maximum scarp slope angle  
 $\alpha$  - Original fan surface slope angle  
D - Vertical surface offset  
 $c\tau$  - Diffusion coefficient x time  
 $\theta_0$  - Angle of repose of unconsolidated fan alluvium (see section B-8.0)

TABLE 5 - SCARP MORPHOLOGY DATA FOR MULTIPLE EVENT FAULT SCARPS

PROFILE NUMBER	LOCALITY	SURFACE DISPLACED BY FAULT	Hm (m)	$\theta$ (°)	$\alpha$ (°)	D (m)	COMMENTS
UN-12a	DC-7	Floodplain	-	-	1.5	0.6	Profile disrupted by meander channel.
UN-12b	DC-7	Floodplain	1.3	12	0	1.3	
UN-7	DC-5	Middle Dg	0.6	7	1	0.5	
UN-1	DC-5	Highest Dg	1.3	7	1	1.0	
UN-3	DC-5	Qf5	-	-	2	1.6	Profile disrupted by water race.
UN-8	DC-5	Qf5	1.1	9	2	0.9	
UN-10a	DC-7	Qf5	2.0	7	2	1.5	
UN-10b	DC-7	Qf5	1.5	12	2	1.4	
UN-15a	DC-6	Qf5	1.8	8	1	1.5	
UN-15b	DC-6	Qf5	2.0	10	2	1.8	
UN-17	DC-6	Qf5	2.0	6	1	1.5	
UN-19a	DC-8	Qf5	3.0	7	1	2.2	
UN-19b	DC-8	Qf5	2.8	6	1.5	1.6	
UN-22	DC-8	Qf5	2.2	7	2	1.6	
UN-25a	DC-9	Qf5	1.9	7	1	1.5	
UN-25b	DC-9	Qf5	1.8	7	2	1.4	
UN-13	DC-7	Qf4	6.6	20	2	6.0	
UN-18	DC-6	Qf3	12.6	16	1.5	11.5	
UN-20	DC-8	Qf3	15.6	15	3	12.9	

Locality DC-5 (etc.) is the area within 0.5 km of the DC-5 (etc.) trench site.  
Trench sites are located on Plate 1.

Dg - Degraded Qf5 surface  
Hm - Height of a multiple event fault scarp.  
 $\theta$  - Maximum scarp slope angle  
 $\alpha$  - Original fan surface slope angle  
D - Vertical surface offset

TABLE 6 - SCARP MORPHOLOGY DATA FOR RIVER-CUT TERRACE SCARPS

PROFILE NUMBER	LOCALITY	SURFACE AT BASE OF SCARP	SURFACE AT TOP OF SCARP	H (m)	$\theta$ (°)	$\alpha$ (°)	D (m)	$c\tau$ $\theta=28^\circ$	$c\tau$ $\theta=30^\circ$
UN-14a	DC-7	Qf5	Qf4	3.7	17	0	3.1	5.48	5.89
UN-16	DC-6	Qf5	Qf3	8.9	22	0	8.3	14.19	17.14
UN-21a	DC-8	Qf5*	Qf3	16.8	23	0	16.5	43.61	55.25
UN-21b	DC-8	Qf5*	Qf3	12.2	23	0	11.6	21.55	27.31
UN-4a	DC-5	Highest Dg	Qf5	1.2	10	0	1.2	3.28	3.34
UN-4b	DC-5	Highest Dg	Qf5	0.8	9	0	0.8	1.85	1.88
UN-4c	DC-5	Highest Dg	Qf5	0.3	9	0	0.3	0.26	0.26
UN-11a	DC-7	Highest Dg*	Qf5	1.0	12	0	1.0	1.48	1.52
UN-11b	DC-7	Highest Dg*	Qf5	1.6	22	0	1.6	0.53	0.64
UN-14a	DC-7	Highest Dg*	Qf5	0.8	17	0	0.8	0.36	0.39
UN-14b	DC-7	Highest Dg*	Qf4	4.8	24	0	4.7	2.65	3.59
UN-6	DC-5	Lowest Dg	Qf5	2.5	18	0	2.5	2.95	3.22
UN-24a	DC-8	Lowest Dg	Qf5	4.9	19	0	4.5	7.89	8.76
UN-24b	DC-8	Lowest Dg	Qf5	7.1	27	0	7.1	1.26	3.42
UN-23b	DC-8	Lowest Dg	Qf5	3.8	23	0	3.7	2.19	2.78
UN-5a	DC-5	Lowest Dg	Highest Dg	1.5	14	0	1.5	2.25	2.34
UN-5b	DC-5	Lowest Dg	Highest Dg	1.5	13	0	1.5	2.73	2.82
UN-5c	DC-5	Lowest Dg	Highest Dg	2.7	23	0	2.7	1.17	1.48
UN-5d	DC-5	Lowest Dg	Qf5	1.3	20	0	1.3	0.54	0.61
UN-5e	DC-5	Lowest Dg	Qf5	0.9	12	0	0.9	1.20	1.23
UN-9a	DC-5	Floodplain	Lowest Dg	5.7	24	0	5.7	3.90	5.29
UN-9b	DC-5	Floodplain	Lowest Dg	4.2	24	0	4.2	2.12	2.87
UN-23a	DC-8	Floodplain	Qf5	6.7	24	0	6.7	5.39	7.30
UN-23b	DC-8	Floodplain	Lowest Dg	1.8	22	0	1.7	0.60	0.72
UN-23c	DC-8	Floodplain	Qf5	5.1	24	0	5.0	3.00	4.07
UN-24a	DC-8	Floodplain	Lowest Dg	0.6	13	0	0.6	0.44	0.45
UN-24b	DC-8	Floodplain	Lowest Dg	0.5	12	0	0.5	0.37	0.38
UN-24c	DC-8	Floodplain	Qf5	7.4	31	0	7.4	-	-
UN-26	DC-9	Floodplain	Qf5	4.1	21	0	4.1	4.35	5.07

\* - Surface at base of scarp is a floodplain, however these floodplain surfaces have been correlated with the surface in which they are grouped.

Locality DC-5 (etc.) is the area within 0.5 km of the DC-5 (etc.) trench site.  
Trench sites are located on Plate 1.

Dg - Degraded Qf5 surfaces

H - Terrace scarp height

$\theta$  - Maximum scarp slope angle

$\alpha$  - Original fan surface slope angle

$c\tau$  - Diffusion coefficient x time

$\theta_0$  - Angle of repose of unconsolidated alluvium (see section B-8.0)



TABLE 7 - REGRESSION EQUATIONS OF SCARP-SLOPE ANGLE ( $\theta$ )  
ON THE LOGARITHM OF SCARP HEIGHT (H)

TYPE OF SCARP	EQUATION	CORRELATION COEFFICIENT (r)	STANDARD DEVIATION OF ( $\theta$ )	NUMBER OF OBSERVATIONS
Single Event Fault Scarp	$\theta = 11.25 (\log H_s) + 10.96$	0.71	4.00	15
Multiple Event Fault Scarp	$\theta = 7.47 (\log H_m) + 6.82$	0.67	3.96	17
Qf5 Terrace Scarp	$\theta = 9.76 (\log H) + 11.90$	0.96	2.87	4
Highest Degraded Terrace Scarp	$\theta = 13.53 (\log H) + 14.24$	0.78	6.32	7
Lowest Degraded Terrace Scarp	$\theta = 13.94 (\log H) + 13.56$	0.81	5.09	9
Floodplain Scarp	$\theta = 12.24 (\log H) + 16.05$	0.92	5.89	9

B-7.0  $\theta$  versus Log H Model

Bucknam and Anderson (1979) recognized that a relationship exists between the scarp height (H), the maximum scarp-slope angle ( $\theta$ ) and the geomorphic age of a scarp. By plotting  $\theta$  versus the logarithm of scarp height ( $\log H$ ) they have found that for scarps of a given age, there is a linear relationship between  $\theta$  and  $\log H$  defined by the equation...

$$(1) \quad \theta = (\log H)x + y$$

In words, this equation says that for scarps of the same age, the slope angle is directly proportional to the logarithm of scarp height. For scarps of different ages which have the same height, the older scarp will have a lesser scarp-slope angle than the younger scarp. On a graph of  $\theta$  versus  $\log H$  (see Figure 55) older scarps will plot below younger scarps. The 5,000 and 15,000 year lines in Figures 55, 56 and 57 show this relationship. The 5,000 year line is a regression line through data collected by Machette (1982) from the Cox Ranch Fault and the La Jencia Fault, New Mexico which are dated as 4,000 to 5,000 years since the most recent movement. The 15,000 year regression line is from data collected by Bucknam and Anderson (1979) for the highest wave-cut shoreline scarp of Lake Bonneville, Utah which was abandoned about 15,000 years ago.

Machette (1982) noted that scarp morphology data should not be over-interpreted. For example, scarps that plot above the 5,000 year line are not necessarily less than 5,000 years old. He suggested that 1) scarps with data lying above the 5,000 year line indicate a Holocene age, 2) scarps with data lying between the 5,000 and 15,000 year lines indicate either a Holocene or latest Pleistocene age and 3) scarps with

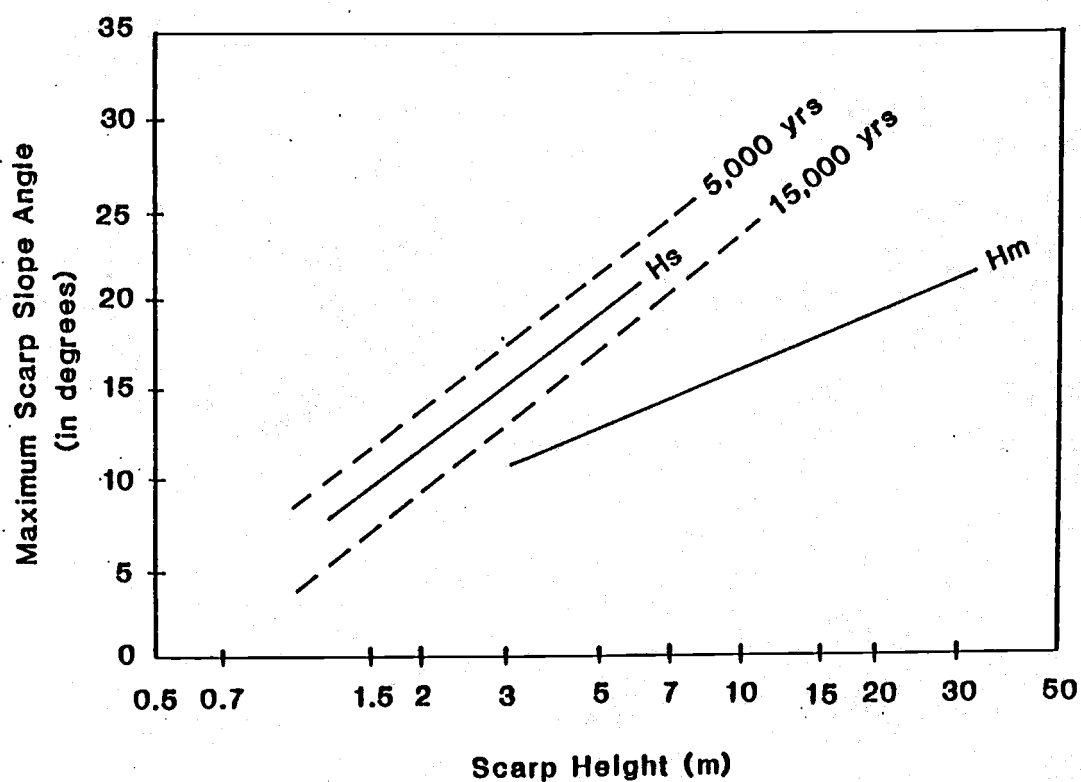


FIGURE 55 - Plot of maximum scarp slope angle ( $\theta$ ) against single-event scarp height ( $H_s$ ) and multiple-event scarp height ( $H_m$ ) for a multiple-event fault scarp. Figure is from Machette, 1982, Fig. 5.

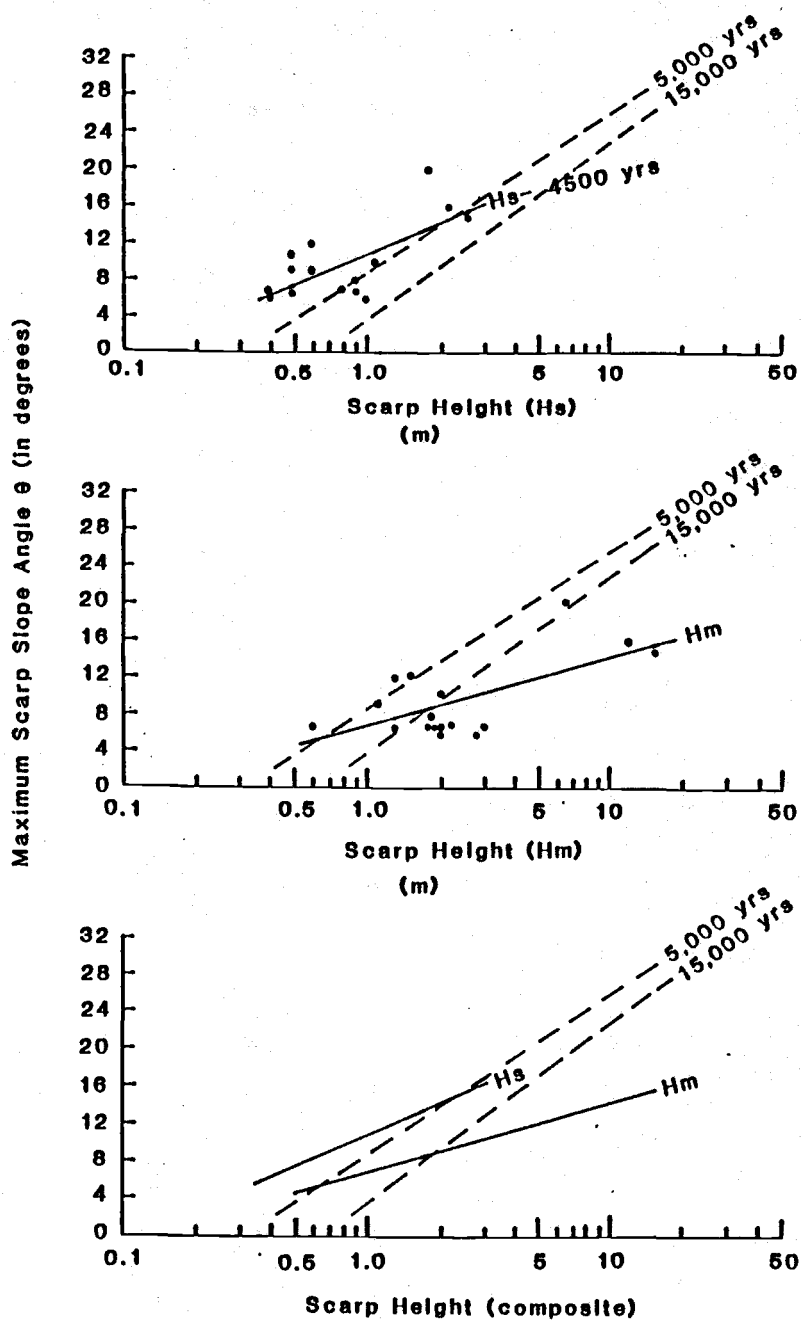


FIGURE 56 -  $\theta$  versus  $\log H$  for single and multiple event fault scarps, Nevis Fault. 5000 year regression line from Machette (1982), 15,000 year regression line from Bucknam and Anderson (1979).

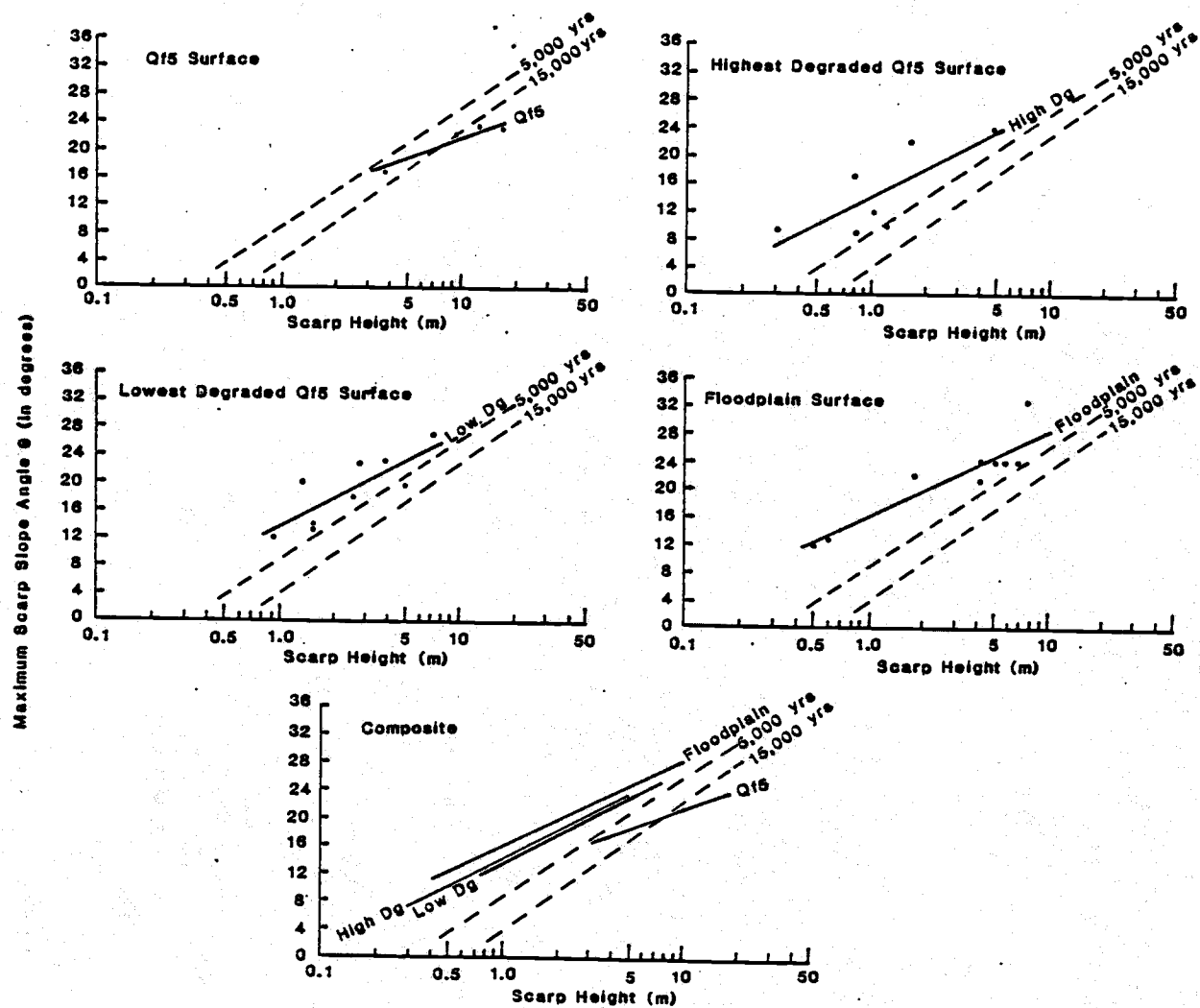


FIGURE 57 -  $\theta$  versus  $\log H$  for terrace scarps, Upper Nevis Basin. 5,000 year regression line from Machette (1982), 15,000 year line from Bucknam and Anderson (1979).

data lying below the 15,000 year line indicate a late Pleistocene age (10,000-150,000 years). Machette (1982) plotted  $\theta$  versus  $\log H$  for multiple event scarp heights ( $H_m$ ) and compared it to a plot of single event scarp heights ( $H_s$ ) that were measured off of the profiles of the multiple event scarps. Figure 55 shows that the  $H_s$  data plotted above the  $H_m$  data indicating a younger age for the single event.

#### B-7.1 Results from the Upper Nevis Basin

Figure 56 shows a plot of  $\theta$  versus  $\log H$  for single event scarp heights ( $H_s$ ) and multiple event scarp heights ( $H_m$ ) measured from data collected along the active trace of the Nevis Fault. Table 7 presents the regression equations for lines of best fit through these data. The regression line through the  $H_m$  data clearly plots older (below) than the regression line through the  $H_s$  data, supporting Machette's (1982) results as discussed above. The  $H_s$  line plots above the 5,000 year line of Machette (1982) suggesting a Holocene age for the most recent faulting event on the Nevis Fault. This agrees with geologic evidence for the age of the most recent faulting as discussed in Section 5.7.2.5.

Figure 57 shows a plot of  $\theta$  versus  $\log H$  for terrace scarps measured in the Upper Nevis Basin and Table 7 presents the regression equations for the lines of best fit through these data. The regression line for the scarps that have floodplains at their base (floodplain scarps) plots above the regression lines for the scarps which have Qf5 surfaces and degraded Qf5 surfaces at their base (Qf5 scarps and degraded Qf5 scarps, respectively). This indicates that the floodplain scarps are the youngest scarps and the floodplains at their base are

the youngest surfaces. The Qf5 scarps plot below the other scarps, and this indicates that the Qf5 surface is older than the floodplain and degraded Qf5 surfaces. The high and low degraded Qf5 scarps plot nearly on the same line. This is probably because their ages are so close in time that the  $\theta$  versus  $\log H$  technique cannot accurately resolve them. The degraded Qf5 scarps fall between the floodplain scarps and the Qf5 scarps on the graph indicating the degraded Qf5 surfaces are intermediate in age between the floodplain and Qf5 surfaces. The floodplain and degraded Qf5 scarp regression lines lie above the 5,000 year line of Machette (1982). This suggests a Holocene age for them. The Qf5 scarp regression line lies below both the 5,000 and 15,000 year lines. This suggests a late Pleistocene age for the Qf5 surface. These ages agree quite well with ages based on geologic criteria as discussed in Section 4.5.4.

In comparing Figures 56 and 57, all of the terrace scarps plot above (younger than) the single event (Hs) fault scarp regression line. This makes geologic sense for the floodplain scarps since the age of the floodplain surface is younger than the age of most recent faulting. The floodplain surfaces of tributary streams in the Upper Nevis Basin are not faulted except at Wrights Creek and at Wrights Creek, the floodplain surface is considered to be a degraded Qf5 surface that has only recently been rejuvenated by a modern stream (see Section 5.7.2. 3). The degraded Qf5 scarps and Qf5 scarps intuitively should not plot above (younger than) the single event fault scarp since the fault crosses the Qf5 and degraded Qf5 surfaces and should therefore be younger. Comparing the single event fault scarp data with the terrace scarp data using the  $\theta$  versus  $\log H$  model appears to be marginally useful.

## B-8.0 Diffusion Equation Model

Nash (1980), Hanks et al. (1983), and Colman and Watson (1983) have taken a more analytical approach to the degradation of scarps. Their individual techniques are similar and are based on a diffusion equation model for scarp degradation. The diffusion equation has been used in analyses of conductive heat flow, viscous flow through porous media, and chemical dispersion. It has also been applied to landform modification by several investigators including Culling (1960; 1963; 1965), Hirano (1968; 1972; 1975), and the workers mentioned above.

The first and most basic assumption underlying the diffusion equation model is that mass transport due to erosional processes proceeds in the downhill direction at a rate proportional to the local topographic gradient (Hanks et al., 1983)...

$$(2) \quad R = c \frac{dy}{dx}$$

$R$  = rate of downslope transport  
 $c$  = diffusion coefficient (rate constant)  
 $x$  = horizontal distance  
 $y$  = vertical distance  
 $\frac{dy}{dx}$  = topographic gradient perpendicular to the elevation contour

This equation applies only to wash-controlled processes such as soil creep, raindrop impact, and slopewash (Colman and Watson, 1983). It does not apply to gravitational processes such as spalling or slumping.

The second assumption is that conservation of mass holds on a local scale (no removal or addition of material) and there is no change in density of the surficial material. This requires that the change in elevation of a point (x,y) be equal to the difference between the amount of material transported to the point and the amount of material transported away from it. (Colman and Watson, 1983)...



$$(3) \quad \frac{dy}{dx} = \frac{dR}{dx}$$

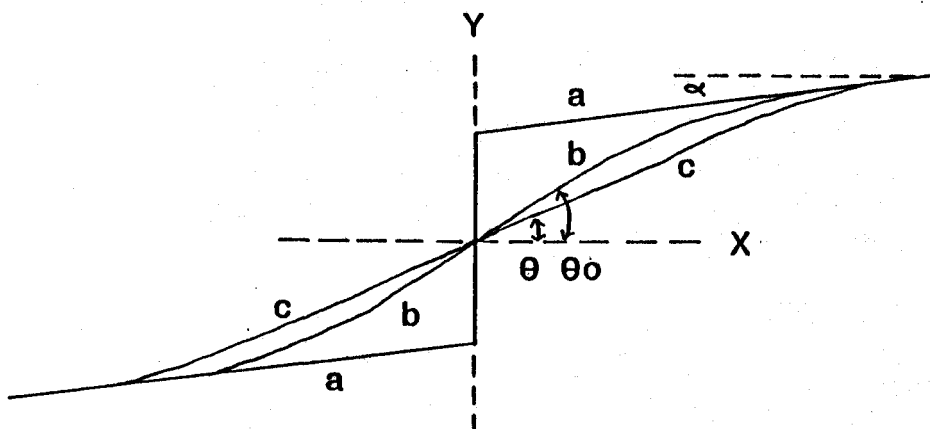
Combining equations (2) and (3) yields the diffusion equation:

$$(4) \quad \frac{dy}{dt} = \frac{d^2y}{dx^2}$$

In words, this equation says that the rate of change in elevation,  $\frac{dy}{dt}$ , at a point (x,y) on a slope profile is proportional to the curvature of the profile at that point,  $\frac{d^2y}{dx^2}$ . Where the profile is concave upward (ie, the base of a scarp), there is a positive curvature and through time the profile will increase in elevation. Where the profile is convex upward (ie, the crest of a scarp) the curvature is negative and through time the profile will decrease in elevation. With time, the crest and the base of the scarp become rounder while the scarp-slope angle,  $\theta$ , decreases.

Several assumptions have to be made for the diffusion equation model to be appropriate: 1) The trace of the scarp must be locally straight in map view and the scarp profile must be perpendicular to the trace. 2) The scarp must be composed of cohesionless material (this excludes scarps occurring in bedrock). 3) There has been no overall lowering of the landscape and a constant base level. 4) The scarps are formed by a single event and then left to degrade under constant conditions.

Colman and Watson (1983) have derived a solution to the diffusion equation based on the assumption that the initial scarp configuration is in the style of profile a on Figure 58; a vertical scarp displacing a gently sloping original surface. The solution is...



**Profile a – Vertical initial scarp with "free face"**

**Profile b – Degraded scarp with angle  $\theta_0$  at time  $t_0$  when the diffusion equation model begins to apply**

**Profile c – Degraded scarp observed at present with angle  $\theta$  at time  $t$**

FIGURE 58 - Scarp morphology progression of forms. Figure is from Colman and Watson, 1983, Fig. 1.

$$(5) \quad c\tau = \frac{D^2}{4\pi} \frac{1}{(g-g_1)^2} - \frac{1}{(g_0-g_1)^2}$$

where  $c$  = diffusion coefficient (rate constant)

$\tau$  = time

$D$  = vertical offset of original surface

$g = \tan \theta$ : present scarp slope ( $\theta$  = present scarp-slope angle), see profile c, Figure 58

$g_1 = \tan \alpha$ : slope of original surface ( $\alpha$  = slope angle of original surface)

$g_0 = \tan \theta_0$ : scarp slope at time  $t_0$  when diffusion equation begins to apply,  $\theta_0$  is approx. equal to the angle of repose, see profile b, Figure 58

Equation (5) says that for each scarp profile, the product of the diffusion coefficient and time ( $c\tau$ ) can be calculated from the initial and final configurations of the scarp (assuming the initial scarp profile was vertical). The desired solution, time, is dependent on the diffusion coefficient ( $c$ ).

Colman and Watson (1983) point out the fact that the diffusion equation model is not appropriate during the time that the free face is being eroded. The gravitational processes that remove the free face do not satisfy the basic assumption upon which the diffusion model is based; that the rate of mass transport due to erosional processes is proportional to the topographic gradient. This assumption only applies to wash controlled processes such as soil creep, raindrop impact, and slope wash. Hence, the diffusion equation model is only applicable to scarp degradation after the free face has been removed (as in profile b, Figure 58). According to Wallace's (1977) observations of fault scarps in Nevada, he suggested that the amount of time required to remove the free face is on the order of tens of years to hundreds of years (a short time relative to the elapsed time since scarp formation). Therefore, Colman and Watson (1983) have divided the age of the scarp ( $t$ ) into two segments  $t_0$  and  $\tau$  where...

- $t$  = the total age of the scarp.  
 $t_0$  = the time required to remove the free face from an initially vertical profile to a sloping profile at approximately the angle of repose,  $\theta_0$ , (a few tens to hundreds of years), profile a to b, Figure 58.  
 $\tau$  = the time required to modify the scarp from the angle  $\theta_0$  to the angle of the scarp observed today, profile b to c, Figure 58.

The time required to remove the free face ( $t_0$ ) must be added to the time ( $\tau$ ), which is derived from equation (5), to obtain a value ( $t$ ) for the true age of the scarp.

From their study of scarps in western Utah, Colman and Watson have determined  $\theta_0$  to be slightly lower than one might expect for the angle of repose for unconsolidated alluvium. They have therefore modified the definition of  $\theta_0$  to be the angle at which the diffusion equation applies to the degradation of the scarp rather than as the angle of repose. They determined that values for  $\theta_0$  of  $28^\circ$  and  $30^\circ$  gave better results than higher values of  $\theta_0$  ( $34^\circ$ - $37^\circ$ ) which are closer to the true angle of repose of unconsolidated coarse alluvium (Wallace, 1977).

Colman and Watson applied the diffusion equation model to the data from the wavecut shoreline scarp of Lake Bonneville, Utah and calculated a  $c\tau$  value of  $13.5 \pm 5.9$ . The age of abandonment of the Bonneville shoreline is radiocarbon dated at 15,000 years. To this age must be added  $t_0$ , the time required to remove a free face (possibly a hundred years). Substituting 15,100 years for  $\tau$  yields a  $c$  value of  $9.0 \times 10^{-4} \frac{m^2}{yr}$ . Hanks et al. (1983) have calculated a  $c$  value of  $1.0 \times 10^{-3} \frac{m^2}{yr}$  which is on the same order of magnitude as the  $c$  value calculated by Colman and Watson.



This age is assessed to be...

$$\begin{aligned}\tau &= 2800 \text{ years where } \theta_0 = 28^\circ, c\tau = 2.52, c = 9.0 \times 10^{-4} \text{ m}^2/\text{yr.} \\ \tau &= 3600 \text{ years where } \theta_0 = 30^\circ, c\tau = 3.27, c = \text{"}\end{aligned}$$

If several hundred years are added for the removal of a free face, then an estimate of the true age of the floodplain (t) is 3100-3900 years. These values are in good agreement with constraints placed on the age of the floodplain surface by a radiocarbon date of  $9670 \pm 130$  years which was obtained from a buried peat located c. 1 m above the floodplain surface of Whittens Creek. This peat represents an older stand of the floodplain surface. Therefore, the age of the modern floodplain surface should be less than 9670 years. The above values for (t) are consistent with this radiometric age.

The age of the Qf5 scarps yields the age of the Qf5 surface. The age is assessed to be...

$$\begin{aligned}\tau &= 23,600 \text{ years where } \theta_0 = 28^\circ, c\tau = 21.21, c = 9.0 \times 10^{-4} \text{ m}^2/\text{yr} \\ \tau &= 29,300 \text{ years where } \theta_0 = 30^\circ, c\tau = 26.40, c = \text{"}\end{aligned}$$

If several hundred years are added for the removal of a free face, the resulting values of (t) are 23,900-29,600 years. These values are slightly older, but correlate well with the age of 23,000 years assessed using geologic constraints (see Section 4.5.4).

The age of the degraded Qf5 scarps yields the age of the degraded Qf5 surfaces. The age of the highest degraded Qf5 surface is assessed to be...

$$\begin{aligned}\tau &= 1700 \text{ years where } \theta_0 = 28^\circ, c\tau = 1.49, c = 9.0 \times 10^{-4} \text{ m}^2/\text{yr} \\ \tau &= 1800 \text{ years where } \theta_0 = 30^\circ, c\tau = 1.66, c = \text{"}\end{aligned}$$

The age of the lowest degraded Qf5 surface is assessed to be...

$$\begin{aligned}\tau &= 2700 \text{ years where } \theta_0 = 28^\circ, c\tau = 2.46, c = 9.0 \times 10^{-4} \text{ m}^2/\text{yr} \\ \tau &= 3300 \text{ years where } \theta_0 = 30^\circ, c\tau = 2.96, c = \text{"}\end{aligned}$$

After several hundred years have been added for the removal of a free face, the resulting values of (t) are 2000-2100 years for the highest degraded Qf5 surface and 3000-3600 years for lowest degraded Qf5 surface. These values do not realistically relatively date the two surfaces with respect to each other or the floodplain surface, nor do they correlate well with geologic constraints on the age of the degraded Qf5 surfaces. The ages are too young.

### B-9.0 Conclusions

The  $\theta$  versus  $\log H$  method suggests that the most recent event on the Nevis Fault occurred in the Holocene. The diffusion equation dates this event at 4400-4500 years ago. These ages are consistent with each other, with geologic constraints, and with the data of Machette (1982).

The  $\theta$  versus  $\log H$  method suggests that the floodplain surface is Holocene in age and is the youngest surface studied in the Upper Nevis Basin. The diffusion equation dates the floodplain surface at 3100-3900 years. The results of both methods agree with each other and with constraints placed on the age of the floodplain by a radiocarbon date.

The  $\theta$  versus  $\log H$  method suggests that the degraded Qf5 surfaces are Holocene in age. The diffusion equation dates the highest degraded Qf5 surface at 2000-2100 years and the lowest degraded Qf5 surface at 3000-3600 years. The Holocene age is consistent with geologic constraints but the absolute ages are too young and do not provide a realistic relative age. The highest degraded Qf5 surface should be older than the lowest degraded Qf5 surface.

The  $\theta$  versus  $\log H$  method suggests that the Qf5 surface is late

Pleistocene in age. The diffusion equation model yields a date for the Qf5 surface of 23,900-29,600 years. The absolute ages are slightly older but agree fairly well with geologic constraints placed on the age of the Qf5 surface.

Both methods are found to be useful for dating the most recent faulting event on a reverse fault. The  $\theta$  versus  $\log H$  technique is useful for relatively dating the terrace scarps and comparing the Upper Nevis Basin scarp data with data from the western United States. This method is not useful for relatively dating the single event fault scarp ( $H_s$ ) with respect to the terrace scarps.

In conclusion, this study has determined that scarp morphology techniques give consistent results for dating reverse fault scarps and river-cut terrace scarps. The results of this study should be accepted with caution as the ages assessed have only one absolute age date in the Upper Nevis Basin as a reference and are derived by comparison with studies done in the western United States in regions of more arid climate. The ultimate effects of different climates on scarp degradation rates are presently unknown, but were assumed to be negligible in this study.



## Appendix C - SOIL DEVELOPMENT

### C-1.0 Introduction

Soil profiles are often used as a means of relatively dating landforms and surficial deposits. By comparing the degree of soil horizonation on surfaces of different ages, a soil chronosequence can be developed. The chief factors influencing the kind and thickness of soil formed are the climate, nature of the parent material, local topography, biota, and the length of time that a soil has been forming on a particular land surface. The time factor is of great importance, for the longer the soil forming processes operate, the greater their effect will be. According to McCalpin (1982), the most prominent age-dependent factors in the formation of non-calcareous soils are depth of oxidization and B-horizon development. For non-calcareous soils, differences in B-horizon thickness, structure and soil color are most diagnostic of age.

### C-2.0 Upper Nevis Soil Profiles

In the Upper Nevis Basin, soil profiles were studied in order to assess their usefulness as a relative dating tool. Soil pits (1.0 m long x 0.5 m wide x 1.0 m deep) were dug on Qf1 to Qf5 fan surfaces and degraded Qf5 surfaces. All pits were dug on planar surfaces away from slope influences. The soil pits are located on Plate 1 and descriptions of the measured profiles are presented in Figure 59 and Table 8.

The parent materials in which the soils have developed are schist

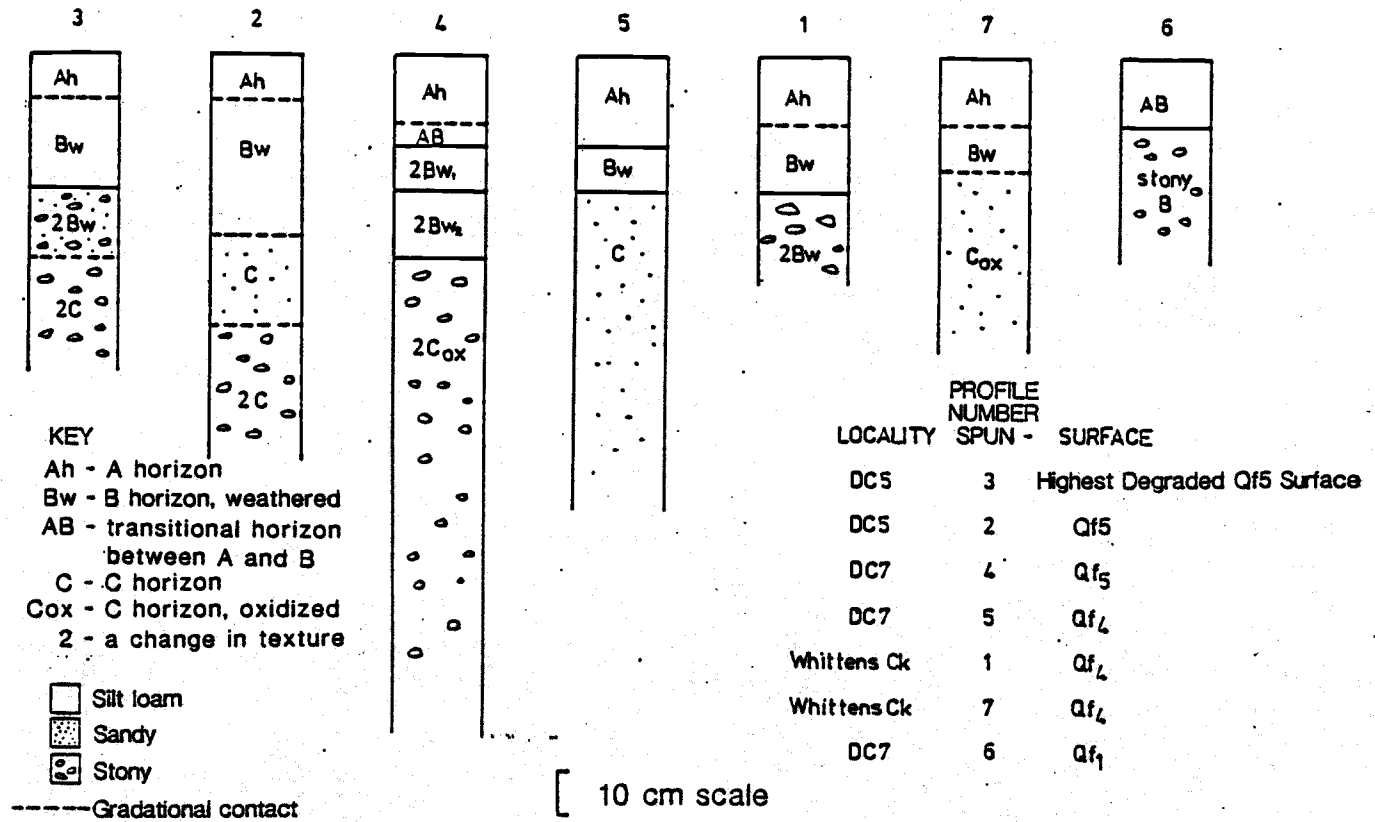


FIGURE 59 - Soil Profiles, Upper Nevis Basin

TABLE 8 - SOIL PROFILE DESCRIPTIONS, UPPER NEVIS BASIN

SURFACE	PROFILE NUMBER	A-HORIZON THICKNESS (cm)	STRUCTURE	B-HORIZON THICKNESS (cm)	STRUCTURE	GENERAL HORIZON	MAX. SOIL COLOR	DEPTH OF OXIDIZA- TION (m)
Highest Dg	SPUN-3	10	Weak, fine & medium nut with fine crumb	35	Moderate, medium & fine nut	A B C	10YR 3/2 2.5Y 4/4 11thchromic	
Qf5	SPUN-2	10	Weak, fine & medium crumb	30	Weak, coarse blocky, break- ing to medium & fine nut	A B C	10YR 3/2 2.5Y 5/4 2.5Y 4/4 to 5Y 4/3	
Qf5	SPUN-4	A=15	A= Moderate medium & fine nut with fine crumb	25	Weak, compact in place	A AB B C	10YR 3/2 2.5Y 4/2 5Y 5/4 to 10YR 4/6	0.45+
		AB=5	AB= Moderate medium fine nut					
Qf4	SPUN-5	20	Moderate medium nut & fine crumb	10	Weakly devel- oped coarse, blocky, break- ing to moder- ately devel- oped medium to fine nut	A B C	10YR 3/2 2.5Y 5/4 5Y 5/4	
Qf4	SPUN-1	15	Moderately developed fine & medium nut	25+	Weak, coarse blocky, break- ing to medium & fine nut	A B	10YR 3/3 2.5Y 4/4	
Qf4	SPUN-7	15	Weak	10	Moderately well devel- oped nut	A B C	10YR 4/3 2.5Y 5/4 5Y 6/3	0.45+
Qf1	SPUN-6	AB=15	Weak	30+	Moderate	AB	Dark yellow brown	

derived fan alluvium and loess. The vegetation is similar on all the surfaces and consists of speargrass and tussock grasses. The overall climate affecting soil development on the fan surfaces should be similar throughout the basin since the elevation difference between the surfaces is not great; however, rainfall may increase from north to south. The variability of loess distribution suggests that wind has been a significant environmental factor through time (Beanland and Barrow, 1984b).

To relatively date the fan surfaces, a progressive increase in soil development should be seen from younger, lower surfaces to older, higher surfaces. The soils in the Upper Nevis Basin were found to be weakly developed on all of the surfaces and have probably formed during the Holocene ( $\leq 10,000$  years; Basher, L., pers. comm., 1984). Figure 59 and Table 8 show that the B-horizon is 5-25 cm thicker than the A-horizon, in most cases, and structures within the A- and B-horizons are weakly to moderately developed. There is no systematic increase in B-horizon thickness or soil structure development with expected increase in age of fan surface. There is a distinct color difference between the A- and B-horizon in all profiles but there is no systematic change in soil color with increase in age of the surfaces. Therefore, a soil chronosequence can not be developed to relatively date the fan surfaces. The Upper Nevis soils can be compared with soils in the nearby Upper Clutha Valley where a soil chronosequence has been developed by Leamy and Saunders (1967). Table 9 shows the soil characteristics for different stages of soil development on progressively older surfaces in the Upper Clutha Valley. The Upper Nevis soil profiles can be correlated with the subhumid to humid yellow-brown earths and the

TABLE 9 - SOILS OF THE UPPER CLUTHA VALLEY  
From Leamy and Saunders (1967)

STAGE OF DEVELOPMENT	SOIL CHARACTERISTICS			AGE OF SURFACE
	YELLOW BROWN EARTHS (SUBHUMID HUMID ZONE)	YELLOW GREY EARTHS (SUBHUMID ZONE)	BROWN GREY EARTHS (SEMI ARID ZONE)	
Very weakly developed	Weak nutty structures; Indistinct color difference between topsoil and subsoil (pale brown/pale yellowish brown); Pale subsoil color. (Maungarewa soils)	Weakly to moderately developed nutty structures; Indistinct topsoil/subsoil color difference; Weakly compact subsoil. (Pigburn soils)	Weak platy structures; Indistinct topsoil/subsoil color differences; No subsoil clay accumulation. (Waenga soils)	Younger than Hawea
Weakly developed	Weak to moderate and moderate nutty and blocky structures; Crumb structure in topsoil; Distinct topsoil/subsoil color difference (dark greyish brown/brownish yellow); No textural B horizon. (Dublin soils)	Strong nutty structures; Distinct topsoil/subsoil color difference; Weak fragipan. (Cluden soils)	Weak platy structures; Distinct topsoil/subsoil color difference; Weak claypan, distinct carbonate accumulation. (Molyneux soils)	Hawea
Moderately developed	Moderate crumb and nutty structure; Textural B horizon; Brownish yellow subsoil colors. (Bourke soils)	Strong blocky and nutty structures; Moderately to strongly developed fragipan. (Lindis soils)	Moderate platy structures; Moderately to strongly developed claypan; Marked carbonate accumulation. (Lowburn soils)	Albert Town and Luggate
Strongly developed	Not mapped	Moderate blocky structures; Strong fragipan; Clay accumulation in subsoil. (Not mapped separately)	Moderate platy structures; Strong claypan; Marked carbonate accumulation. (Clyde soils)	Lindis

subhumid yellow-grey earths of Hawea to younger than Hawea age ( $\leq 23,000$  years).

An explanation for the youthfulness of the Upper Nevis soils is that soil development has not been a function of time only but has been modified through time by wind erosion and/or loess deposition. Removing or adding material to a soil system will cause a change in the equilibrium of the system and keep a soil youthful as the system readjusts to the new conditions. The eroded topsoil found in profile SPUN-6 (located on Plate 1 and described in Figure 59 and Table 8) on a remnant of the highest fan (Qf1) shows that erosion has occurred at some localities while the occurrence of thick loess in profiles SPUN-5 and SPUN-7 (on Qf4 surfaces) may indicate that their soil profiles have been modified by loess deposition since the formation of the surfaces.

In conclusion, this study found that a soil chronosequence could not be developed to relatively date the Quaternary fan surfaces in the Upper Nevis Basin. All of the soils are youthful and may have been modified by wind erosion and/or loess deposition.